NTNU – Trondheim
Norwegian University of
Science and Technology

The Effect of Blasting in Layered Soils, Example from Finneidfjord, Norway

Bruck Haile Woldeselassie

Geotechnics and Geohazards
Submission date: June 2012
Supervisor: Lars Olav Grande, BAT

Norwegian University of Science and Technology
Department of Civil and Transport Engineering

NORWEGIAN UNIVERSITY OF SCIENCE AND TECHNOLOGY
DEPARTMENT OF CIVIL AND TRANSPORT ENGINEERING

Title of the thesis: *The effect of blasting in layered soils, example from Finneidfjord, Norway*	**Date:** June 11 2012 **Number of pages** (incl. appendices): 114			
	Master Thesis	**X**	**Project Work**	

Name: *Bruck Haile Woldeselassie*

Professor in charge/supervisor: *Professor Lars Grande*

Other external professional contacts/supervisors: *Jean-Sebastian L'Heureux*

Abstract:
A case study on the role of blast vibration on the 1996 Finneidfjord landslide was carried out. This catastrophic landslide which claimed four lives has been under investigation during the past decade. The study area has been developed as natural laboratory and different field and lab investigation have been carried out in the process of understanding the event bed. The mechanically weak layer that the landslide used as a slip surface is found 2.8-3.1m below the sea bed and is composed of loose sand layer sandwiched between two very low permeable clay layers. The main focus herein is the effect that the vibration had on the sand layer and see if the energy from it was able to generate an excess pore water pressure or even liquefaction.

Literature review on different models for calculating energy from vibration and liquefaction susceptibility is done. The energy calculation models require inputs that involve laboratory test therefore they are to be referred for the future work. As for the liquefaction susceptibility; data from the field and laboratory investigation are utilized and are used for the simple liquefaction susceptibility analysis.

Utilizing a FEM software QUAKE/W, part of the GeoStudio software suite, the amount of excess pore water pressure generated due to the dynamic loading from the blast is analyzed. Keeping the parameters of the other materials in the model constant and changing the damping ratio of the sand layer ranging from 1% to 33%, and by changing the geometry of the model an excess PWP in the range of 0.4KPa to 6KPa is obtained. As for the liquefaction susceptibility analysis using the cyclic stress ratio, a factor of safety of 2.3 was obtained leading to the conclusion that liquefaction was not the cause of the landslide.
With the excess PWP obtained from the dynamic analysis plus a reading from a piezometer installed close to the landslide scar, slope stability analysis is done with a software tool called SLOPE/W which again is part of the GeoStudio software suite. The initial stability condition of the slope, only considering the excess PWP from the piezometer reading, was on the verge of failure. The analysis carried out, considering the result from the dynamic analysis, gave a factor of safety less than 1. Based on the results one might conclude that the excess PWP caused the landslide but given the fact that some very important parameters which should be obtained from a lab investigation are lacking, the study can only show that there is a possibility for generation of an excess PWP and for a slope already on the verge of failure, reduction in the effective stress caused by the excess PWP could lead an incidence like in Finneidfjord.

Future work for improving the study and some recommendations that could help in dissipating excess pore pressure in such a condition are also forwarded.

Keywords:

1. Landslide
2. Excess pore water pressure
3. Liquefaction
4. GeoStudio

(Signature)

NTNU
Fakultet for ingeniørvitenskap og teknologi
Institutt for bygg, anlegg og transport
Faggruppe for Geoteknikk

MASTER THESIS
SPRING 2012
For
Bruck Haile
Title

The effect of blasting in layered soils, example from Finneidfjord, Norway

Background

Landslides along Norwegian fjords occur periodically and pose a constant threat to coastal communities. In June 1996, a catastrophic near-shore landslide claimed 4 human lives and destroyed the E6 highway near the village of Finneidfjord, northern Norway. Since then, several failures have taken place in different parts of the fjord, implying the need for a better understanding of this type of natural hazard.

The International center for Geohazards (ICG) has since 2004 developed the Finneidfjord site as a natural laboratory. Ongoing multi-disciplinary research activities (geophysics, geotechnics, geology, and geochemistry) aim at knowledge-building for offshore geohazards and will contribute to mitigation measures for coastal communities as well as for the offshore industry. The thesis will therefore provide the student with a solid introduction to offshore and coastal geohazards with relevance to the industry, which has partly funded the data collection.

Objective

The MSc. thesis shall incorporate a combination of the following tasks:

- Literature review of models for calculation of excess pore water pressure and liquefaction potential due to blasting.
- Geotechnical characterization of the failure plane of the 1996 landslide at Finneidfjord from available laboratory data (fall-cone, DSS and triaxial tests) and in-situ tests results (CPTU).
- Numerical modeling and back-analysis of the 1996 Finneidfjord landslide with GeoSlope. The results shall be used to discuss if blasting was a possible triggering mechanism.
- A discussion on the present stability of slopes along the shoreline of Finneidfjord and recommendations based on the findings.

Lars Grande
Professor, NTNU

Preface and Acknowledgements

This master's thesis was undertaken at the Geotechnical Division of the Norwegian University of Science and Technology (NTNU). The study is based on the ongoing multi-disciplinary research at ICG aiming at knowledge building for offshore geohazards and mitigation measures for coastal communities as well as for the offshore industry. A case study on blast related land slide at Finneidfjord is the main aim of this study.

I am truly indebted and thankful to my advisor Dr. Jean-Sebastien L'Heureux for the support and guidance he gave me throughout the study. His wide knowledge on the study area and his welcoming attitude have kept me going and made the study process exciting. It was particularly kind of him to allow me work at his office and made himself accessible at all times. My heartfelt thanks goes to my supervisor Professor Lars Grande for making himself available when I needed his help and for giving me ideas that helped me understand the subject better.

I owe sincere and earnest thankfulness to NGI staffs particularly to Dr. Finn Løvholt for providing me data I needed for the analysis carried out in this study. It would not have been possible to carry out the analysis without the data he provided.

I am highly grateful for the financial support I got from the International Centre for Geohazards, ICG. My entire two years stay in Norway would not have been possible without ICG's help. It also gives me so much pleasure to forward my thankfulness to the department of Geotechnics and the staffs for helping me during the past two years.

My classmates and the Ethiopian community in Trondheim have made my experience in Norway worthwhile and I would like to thank everyone for that. I owe it all to my family for guiding me to be the man I am today. I will always stay true to the values my parents taught me. But above all I would like to thank the one GOD who has given me everything I have today.

Bruck H. Woldeselassie

Trondheim, June 2012

Abstract

A case study on the role of blast vibration on the 1996 Finneidfjord landslide was carried out. This catastrophic landslide which claimed four lives has been under investigation during the past decade. The study area has been developed as natural laboratory and different field and lab investigation have been carried out in the process of understanding the event bed. The mechanically weak layer that the landslide used as a slip surface is found 2.8-3.1m below the sea bed and is composed of loose sand layer sandwiched between two very low permeable clay layers. The main focus herein is the effect that the vibration had on the sand layer and see if the energy from it was able to generate an excess pore water pressure or even liquefaction.

Literature review on different models for calculating energy from vibration and liquefaction susceptibility is done. The energy calculation models require inputs that involve laboratory test therefore they are to be referred for the future work. As for the liquefaction susceptibility; data from the field and laboratory investigation are utilized and are used for the simple liquefaction susceptibility analysis.

Utilizing a FEM software QUAKE/W, part of the GeoStudio software suite, the amount of excess pore water pressure generated due to the dynamic loading from the blast is analyzed. Keeping the parameters of the other materials in the model constant and changing the damping ratio of the sand layer ranging from 1% to 33%, and by changing the geometry of the model an excess PWP in the range of 0.4KPa to 6KPa is obtained. As for the liquefaction susceptibility analysis using the cyclic stress ratio, a factor of safety of 2.3 was obtained leading to the conclusion that liquefaction was not the cause of the landslide.

With the excess PWP obtained from the dynamic analysis plus a reading from a piezometer installed close to the slide scar, slope stability analysis is done with a software tool called SLOPE/W which again is part of the GeoStudio software suite. The initial stability condition of the slope, only considering the excess PWP from the piezometer reading, was on the verge of failure. The analysis carried out, considering the result from the dynamic analysis, gave a factor of safety less than one. Based on the results one might conclude that the excess PWP caused the landslide but given the fact that some very important parameters which should be obtained from a lab investigation are lacking, the study can only show that there is a possibility for generation of an excess PWP and for a slope already on the verge of failure, reduction in the effective stress caused by the excess PWP could lead an incidence like in Finneidfjord.

Future work for improving the study and some recommendations that could help in dissipating excess pore pressure in such a condition are also forwarded.

Contents

List of Figures

List of Tables

Notations

ρ unit weight

ϕ Angle of friction

D_r Relative density

G_{max} Shear modulus

υ Poisson's ratio

ξ Damping ratio

C Cohesion

I_p Plasticity index

I_L Liquidity index

σ Confining stress

r_u Excess pore pressure ratio

e void ratio

Abbreviations

PWP Pore water pressure

CSR Cyclic stress ratio

CRR Cyclic resistance ratio

PEC Pseudoenergy capacity

MSF Magnitude scaling factor

FOS Factor of safety

1. Introduction

1.1 Background

Landslides caused by anthropological activity have been an issue for a long time now. Vibration from blasting, pile driving and traffic are some of the activities that have been the cause for a number of slides. Some historical events are mentioned in table 1.1. Especially if the profile of the slope incorporates weak layers that are close to failure, as the case to be discussed in this thesis, then even a small scale human activity could cause the instability. The sole role of these anthropological activities in causing instability is poorly understood even if it is inevitable that they are capable of triggering a landslide.

Experience from Finneidfjord case study shows that mechanically weak layer in marine deposit is mostly an event bed for submarine landslide. An increased attention is being given in identifying this weak layers and characterizing them in order to understand their contribution to mass wasting processes and to perform geohazard assessment.

Table 1-1 Lists of registered landslides due to anthropological activities

Locality	**Country**	**Date**	**Trigger**	**Time frame**	Referance(s)
Trondheim	Norway	04.25.1990	Blasting	3hrs&21min	Emdal et al. 1996, L'Heureux et al. 2007
Finneidfjord	Norway	06.20,1996	Blasting	2 or 3hrs ?	Longva et. al. 2003, L'Heureux et al. 2007
Finneidfjord	Norway	08' 2006	Blasting	?	L'Heureux et al. 2007
Finneidfjord	Norway	1978	Blasting	?	L'Heureux et al. 2010
Kattmarka	Norway	03.13.2009	Blasting	30sec	Nordal et al. 2009
La Romain, Basse Côte-Nord	Canada	08.01.2009	Blasting	?	Locat et. al., 2010

? Unknown or uncertain data

In this thesis it is tried to study the effect of blasting on the stability of the shallow weak layer that is thought to be the event bed for the 1996 landslide around Finneidfjord, Norway. This catastrophic landslide took four human lives and mobilized $1x10^6$ m^3 of sediment. The landslide started as a local failure below the sea level and the creation of this failure surface spread outwards in a progressive manner with the initial failure contributing to the instability of the remainder of the landslide mass. Due to its retrogressive behavior 100 to 150m of the inland near to the shore was taken. Three houses close to the shore and 250m long of the E6 road were destroyed.

Chapter 1: Introduction

The initial landslide started below sea level some time before midnight. Eye witnesses saw waves, bubbles and whirls moving away from the shore around midnight. About 25 minutes after midnight a driver felt his car and the road were shaking and stopped. At that moment the beach below the road was gone. Minutes later he saw part of the E6 road breaking in three parts and slumping into the sea. Shortly after this, the nearest houses started to move and then sank in to the mud and disappeared. Three people in the house couldn't escape. A car with one person also disappeared (Longva et. al., 2003).

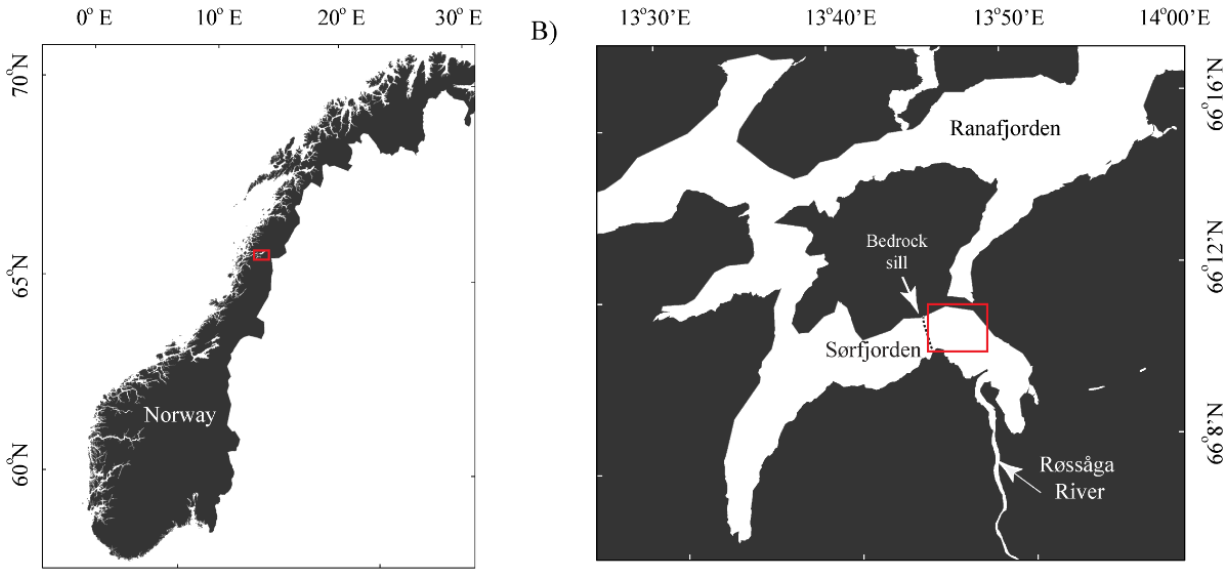

Figure 1-1 Location of the study area (from Verdy et. al., 2012)

The study of the weak layer was done using geotechnical and geophysical investigation in the past decade. The international center for Geohazards (ICG) has since 2004 developed the finneidfjord site as a natural laboratory. Ongoing multi-disciplinary research activities (geophysics, geotechnics, geology, and geochemistry) aim at knowledge-building for offshore geohazards and will contribute to mitigation measures for coastal communities as well as for the offshore industry. There were number of different investigations carried out under the ICG project to study the morphology, lithology, and geotechnical properties of this weak layer. For example Very-high-resolution swath bathymetry and 2D seismic profiles, a decimeter-resolution 3D seismic volume, numerous short cores, two long cores, and free fall cone penetrometer (FF-CPTu) profiles were some of them. And according to the finding, at 3,1m b.s.f. there is a 15 to 20cm thick sand layer which is sandwiched between a very low permeable clay layers. And this layer is thought to be the slide plane (L'Heureux et al. 2012).

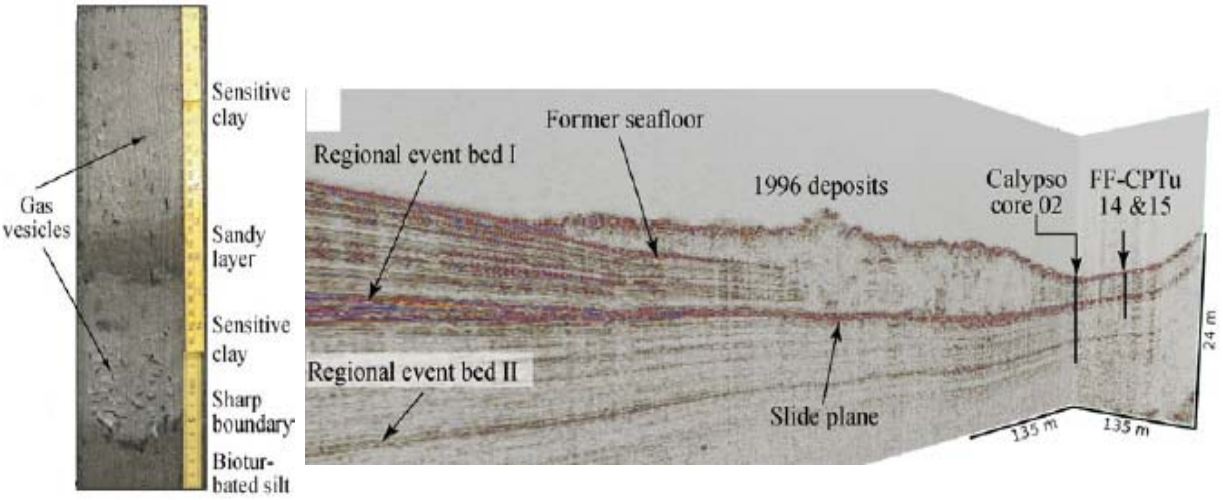

Figure 1-2 left side: Gravity core showing layering of the event bed, Right side: 3D seismic cube showing the landslide deposit and slide plane (from L'Heureux et al. 2012)

There have been different suggestions for the factors that have contributed to the failure by different studies. Gas-generated pore pressure (Morgan et al., 2010), heavy rainfall prior to the slide being cause for formation of artesian groundwater pressure(L'Heureux et al. 2012), increase in overburden stress due to alongshore dumping of material (Gregersen,1999) and excess pore pressure as a result of climatic and anthropogenic factor (e.g. blasting; Janbu, 1996) are some of the suggestions. The later suggestion, anthropologic factor, is the main focus herein.

There was a tunnel construction prior to the slide in June 1996. For this purpose Statens vegvesen was undertaking rock blasting. According to the testimony of an eye witness the landslide took place couple of hours after the blast. Statens Vegvesen, in collaboration with NGI, carried out an investigation in 1999 to see whether the vibration from the blasting was the sole reason for the landslide. Two different trial blasting were made to measure the response of the ground to the vibration and one additional measurement was taken from a blasting carried out for road construction which was taking place during the investigation. It was possible to get these measurements from NGI and carry out dynamic analysis to check whether the blasting had energy enough to generate an excess pore water pressure or even further create liquefaction. Based on the dynamic analysis result it was also possible to carryout slope stability analysis. The main tool for the analysis herein is a software package called GeoStudio. GeoStudio is a product suite for geotechnical and geo-environmental modeling with a broad range of capacity from a simple limit equilibrium modeling to a complex finite element method modeling. Apart from the software based analysis different simple models that do not require the use of software are also studied in the literature review herein. While using these types of

models it's basically quite crucial to run laboratory tests because much of the models require a specific site oriented inputs. Given the scope of the thesis and time restriction it was not possible to carry out the required laboratory investigation to make use of them. But they are mentioned for any one with the required input to make use of them.

When the investigation was carried out in 1999, the main focus was to see the effect of the vibration in the clay. Most of the measurements were taken in the clay and in a rock mass. The existence of the event bed, which is the mechanically weak layer, was not realized at the time. Geological, geotechnical and geophysical observations after the 1999 investigation have shown that the mechanically weak layer is a thin, very loose sand layer sandwiched between two impervious clay layers (L'Heureux et al. 2012; Verdy et. al., 2012). The effect of the vibration on the thin sand layer is the main focus of this thesis.

1.2 Motivation of the study

There is an increasing interest in identifying weak layers and their role for stability of shallow near-shore slopes. These interests are leading to the observation of similar beds in fjords around Norway and Canada and the layers are identified to be an event bed for quick-clay landslides (table 1.1). In relation to these weak layers, the understanding of the effect of different human activities on these layers is quite limited. The motivation of this study is basically to study the role of the blasting on the 1996 catastrophic landslide at Finneidfjord, Norway.

The Finneidfjord case has been under study for an over a decade now but it is still not clear how or if the vibration from the blasting contributed to the initiation of failure. Trying to understand the effect of the blasting in relation to these weak layers could give additional information to the Finneidfjord case and also be an addition to a remedial measure before undergoing projects incorporating blasting.

1.3 Objective of the study

The objective and scope of the study is basically generalized in four points and they are listed below.

- Literature review of models for calculation of excess pore water pressure and liquefaction potential due to blasting.
- Geotechnical characterization of the failure planes at Finneidfjord from available laboratory data (fall-cone, DSS and triaxial tests) and in-situ tests results (CPTU).
- Numerical modeling and back-analysis of the 1996 Finneidfjord landslide with GeoSlope. The results will be used to discuss the effect of blasting on the stability of the shoreline slope in 1996.
- A discussion on the present stability of slopes along the shoreline of Finneidfjord and recommendations based on the findings.

1.4 Structure of the thesis

The organization of the remaining chapters of this thesis is briefed below:

Chapter 2: Models used for calculation of excess pore pressure and analyzing potential of liquefaction are reviewed. Empirical relations based on insitu tests for liquefaction analysis is also presented.

Chapter 3: Finneidfjord regional geology, landslide description and morphology and the characteristics of the event bed is discussed.

Chapter 4: Data gathered from previous study and method of analysis is presented.

Chapter 5: Numerical Modeling and Back Analysis using the vibration data from the 1999 investigation is carried out. Some simple analytical calculations using the empirical relations are also part of this chapter

Chapter 6: Discussion based on the result from the analysis is presented.

Chapter 7: Conclusion, Recommendation and future work are forwarded.

Appendices: Calculations to get some parameters used in the analysis are presented. The calculations are based on the relations and field investigation results discussed in chapter two and three. Measurement of pick particle velocity and shear wave velocity are attached. The MATLAB Code used to change the measured vibration data file, *.sgy to *.txt file and to plot curves is also included.

Chapter 1: Introduction

2. Literature Review

2.1 Introduction

Before going deep in to the models used for the calculation of excess pore press and analyzing potential of liquefaction, a brief discussion on behavior of loose sand is presented.

Many researchers have shown that loose sandy soils are susceptible to liquefaction (Kramer, 1996; Youd et. al., 2001; Groot et. al., 2006). Many factors related to the property of the soil can influence liquefaction potential. The two most prominent factors are the density and the stress state (Kokusho, 2003). Different initial stress states can have a profound effect on the soil behavior when subjected to monotonic or cyclic loading. This phenomenon is well described in figure 2.1.

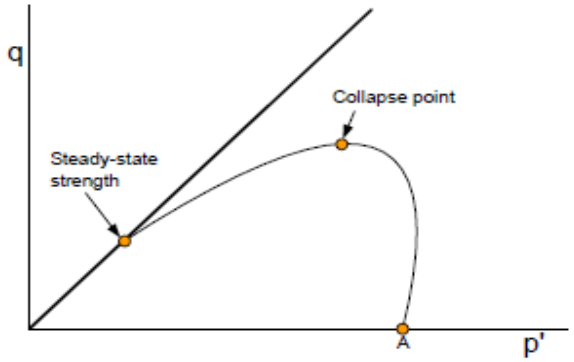

Figure 2-1 Effective stress path for loose sand under monotonic loading, (from QUAKE/W 2007 manual)

Figure 2.1 shows a sample consolidated isotropically. Under an undrained monotonic loading, the effective stress path for sample at point A tends to follow the curve shown in figure 2.1. Before reaching the collapse point, the shear stress rises. But once it reaches its maximum point the soil grain structure will collapse. After the collapse there will be a sudden increase in pore pressure and the strength will decrease to the steady-state strength. Since this pore pressure is an extra to the hydrostatic pore pressure, it is called excess pore pressure. At this sudden stage where excess pore pressure is generated, liquefaction is initiated.

For a series of triaxial tests at the same initial void ratio but consolidated under different confining pressure, figure 2.2 illustrates the collapse surface.

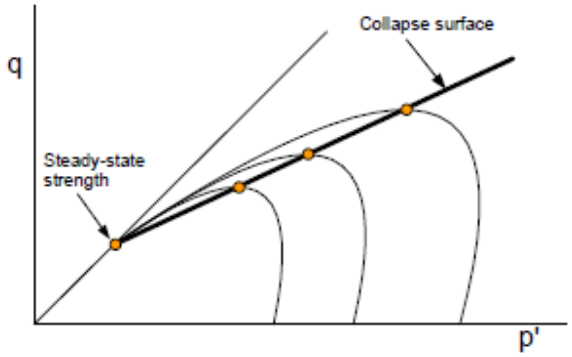

Figure 2-2 Collapse surface illustration

The straight line drawn from the steady-state strength point through the peaks or collapse points is called a collapse surface (Sladen et. al., 1985). The laboratory test done by Skopek et al. (1994) shows the relation between the sudden loss in strength with the collapse of the soil grain. The results from the test are plotted in figure 2.3.

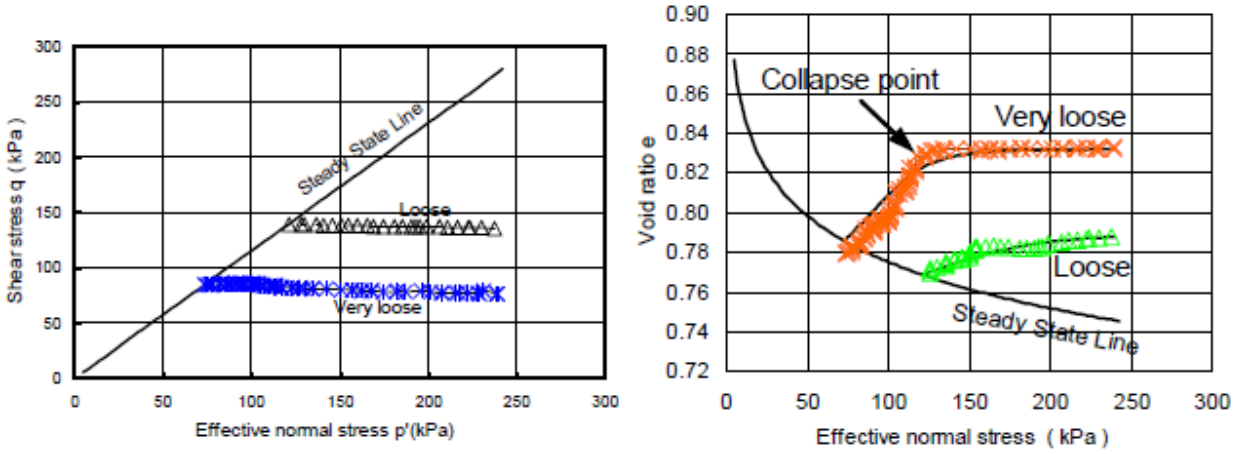

Figure 2-3 Test on dry sand

At the beginning the void ratio remained relatively constant, but then a dramatic decrease was observed when the soil-grain structure collapsed. The point of significance is that this behavior occurred for dry sand that is the volumetric compression occurred in the absence of any pore-pressure. The only logical reason then for the compression is that the grain-structure changed.

The main thing to focus here is that the sudden loss in strength and the resulting liquefaction can occur under monotonic load, not just cyclic loading.

Cyclic loading is probably the most known factor for being the cause for liquefaction. This phenomenon is described in figure 2.4.

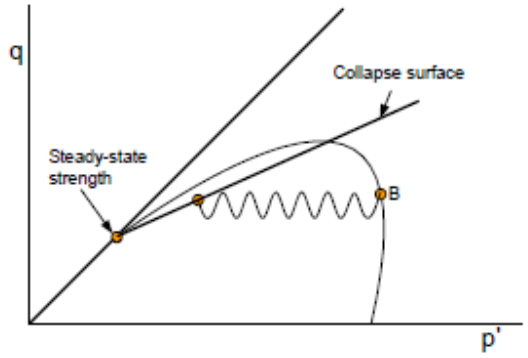

Figure 2-4 Cyclic stress path

Consider a sample at a stress state represented by point B. when a cyclic loading is applied at this state, the pore pressure will continue to increase until the stress cyclic path reaches the collapse surface. After reaching the collapse surface the soil will liquefy and the strength will suddenly fall along the collapse surface to the steady state point.

Dense dilative sands

Excess pore –pressure can also be generated in dilative sand if subjected to cyclic loading. The situation how this happens is described in figure 2.5. Under a cyclic loading, for a sample at point B, the pore pressure will increase until the effective stress state reaches point C. thereafter, point C will simply move up and down along the stress path between point A and the steady-state point. If the cyclic loading ends at point C and then there is further static loading, the soil will dilate and increase in strength until the stress state reaches the steady-state point. The strain associated with the cyclic loading from point B to C is known as mobility.

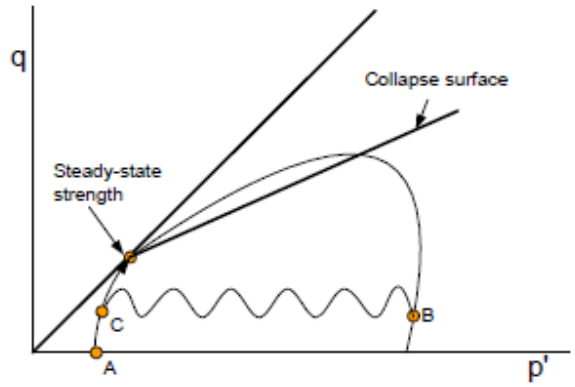

Figure 2-5 Stress path for cyclic loading with starting static stress state below steady-state strength.

This is just a brief overview of the behavior of sand susceptible to liquefaction in response to static and dynamic loading. In the previous chapter it is mentioned that the vibration from the blasting carried out in 1996 could have generated an excess pore pressure and might even initiated liquefaction. Since it's the aim of this study to investigate the effect of the vibration on the sand layer, it will be an addition to the knowledge to study what different people have done in relation to liquefaction and excess pore pressure generation models.

When it comes to the different models and basically excess pore pressure generation related to cyclic lading, earth quake is the first thing that comes to people's mind. This of course is logical since most of the registered cases related to liquefaction are caused by earth quake. Most of the models developed to get the effect of dynamic loading on soils base earth quake as their starting discussion point. The models discussed herein base the same thinking as well thought the source of loading might be different. The premise for doing so is that, the physical process of inducing liquefaction is the same irrespective of whether the input energy is from earth quake shaking or other human activity like remedial ground densification or in our case blasting (QUAKE/W 2007 manual).

2.2 Theory on liquefaction

When a soil body is under a certain load, the stress coming to it is divided into two. That is Normal stress and shear stress. In water saturated soil the normal stress is carried by the soil skeleton and the pore water. As for the shear stress, it's carried by the intergranular contact between the soil grains, since water cannot take shear stress. Under any circumstances if this intergranular contact is lost, then this soil cannot sustain the coming normal stress which in turn means it can't also take shear stress. In such a condition the soil is said to be liquefied. This phenomenon occurs when pore pressure increases and total stress remains constant or pore pressure remains constant and total stress decreases to a level where the normal effective stress becomes zero(Kramer, 1996). Figure 2-6 shows intergranular contact before and after liquefaction.

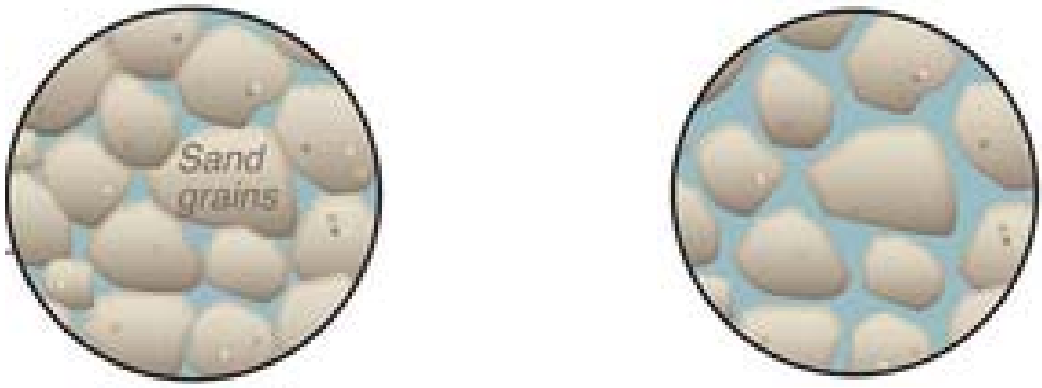

Soil grains before liquefaction Soil grains after liquefaction

Figure 2-6 Intergranular contact before and after liquefaction

The study only deals with noncohesive soils, like sand or silt, usually described as "sandy soil". This restriction is partly for reasons of shortage of time, and partly because sandy soils are generally the most sensitive materials to liquefaction. It should be realized that certain clays show similar behavior under certain circumstances like very sensitive clays or quick clays.

"In cohesionless soils, the transformation is from a solid state to a liquefied state as a consequence of increased pore pressure and reduced effective stress.''(Groot, 2006)

For such situation to happen, liquefaction, an excess pore pressure is required. This excess pore pressure is the difference between the actual pore pressure and the hydrostatic pore pressure.

Excess pore pressure that leads to liquefaction can be caused;

- When loose granular soil's grains are rearranged and densely packed due to shearing.
- When dense granular soils are sheared, the grains tend to compress before dilating.

Densification of sandy soil is nearly always a result of cyclic shearing and dilation does not seem to play a role in most cases of cyclic shearing, but experience shows that severe vibration can induce loosening (Groot, 2006).

Liquefaction phenomena is influenced by different factors like

Grain size distribution: grain size distribution can say a lot about a given soil's density and void ratio. A well graded granular soil, where smaller grains fill voids created by larger grains, will have a denser packing compared to a uniformly graded granular soil where it contains a narrow range of particle size. The latter is quite susceptible to liquefaction.

Relative density: This property of a soil gives a rough indication on the type of response a soil has upon loading. Table 2.1 shows classification according to AS1726.

Table 2-1 AS1726 classification of coarse grained soils relative density

Relative Density (%)	0-15	15-35	35-65	65-85	85-100
Classification	**Very loose**	**Loose**	**Medium dense**	**Dense**	**Very dense**

Loose granular soils are more susceptible to liquefaction than dense once (Kramer, 1996).

Degree of saturation: Liquefaction resistance is highly affected by the degree of saturation. Many researches show that as the degree of liquefaction increases the susceptibility of the soil to liquefaction will also increase (Kokusho, 2002; Ashford, 2004). Most liquefaction related studies that have been performed were on highly saturated soils.

2.3 Excess pore pressure generation models

Excess pore pressure generation related with cyclic loading like earthquake or pile driving induced loading has been studied by different people for so many years now and is still being studied (Ashford, 2004). Excess pore pressure generated by blasting and ultimately leading to liquefaction is not a common issue or is not an area that has been investigated in depth. But with the idea that the physical process of inducing liquefaction is the same with any type of cyclic loading we can proceed with calculating excess pore pressure using models that has already been developed (Russell A. Green, 2004).

The excess pore pressures generated in a soil during cyclic loading can be separated into two components: transient and residual. In saturated soils, the transient pore pressures are equal to the changes in the applied mean normal stresses resulting from the dynamic loading. Because the generated pore pressures are equal to the change in total stress acting on the soil, the transient excess pore pressures will have little influence on the effective stresses acting on the soil. On the other hand, the residual excess pore pressures result from the progressive collapse of the soil skeleton i.e., plastic deformations and, thus, alter the effective stresses acting on the soil. Consequently, the residual excess pore pressures directly influence the strength and stiffness of the soil. During stress-controlled cyclic tests, the residual pore pressures are those present at the time when the applied deviator stress is equal to zero. Residual excess pore pressures are often quantified in terms of residual excess pore pressure ratio. The pore pressure ratio, r_u is defined as the ratio of the residual excess pore pressure, u to the initial effective confining stress, σ_o' acting on the soil (i.e., r_u=u/ σ_o'). This ratio varies from zero, no residual excess pore pressures, to unity, complete transfer of the load to the pore water or "liquefaction", and, therefore, provides more insight than the magnitude of the residual excess pore pressure alone (Polito et. al. 2008). The section proceeding discusses some models for predicting r_u in soils subjected to cyclic loading.

2.3.1 Stress-Based Model

Two types of pore pressures are generated in soils during seismic shaking called transient and residual. The transient pore pressure is equal to the mean normal stress during the earth quake excitation and its influence is little on the soil's effective stress. The residual pore pressure result from the progressive collapse of the soil skeleton (i.e. plastic deformation) and has a major influence on the strength and stiffness of the sand. If stress controlled cyclic test is run, the residual pore pressure is the one when the applied deviator stress equal zero. The residual pore pressure is often quantified in terms of excess pore pressure ratio. This excess pore pressure ratio is defined as the ratio between the residual excess pore pressures, U_{xs} and the initial effective confining stress, σ_o acting on the soil. This ratio varies between zero meaning no residual excess pore pressure to unity meaning liquefaction. An empirical equation has been developed for the residual excess pore pressure ratio, r_u in 1975 by Seed et al. and was again modified by Booker et al. in 1976.

$$\mathbf{r_u}=\frac{2}{\Pi}\sin^{-1}\left(\left(\frac{N}{Nliq}\right)^{\frac{1}{2\theta}}\right) \qquad 2\text{-}1$$

Where N_{liq} is number of loading cycles in a stress-controlled cyclic test required to cause initial liquefaction also known as the point where r_u is equal to zero. And θ is an empirical constant

that depend on the soil type and test condition. Both are calibration parameters determined from stress controlled cyclic triaxial test. N is number of loading cycles in a stress-controlled cyclic test. For a given soil, N_{liq} increase with increase in relative density and decrease with increase in magnitude of loading. The biggest disadvantage of using this model is that the seismic motion should be converted to an equivalent number of uniform cycles and it can only be applied to liquefiable soils. But it should be noted that the so called ¨nonliquefiable¨ soils like dense sand soils with plastic fines, can still undergo significant pore pressure increase and deformation as a result of softening.

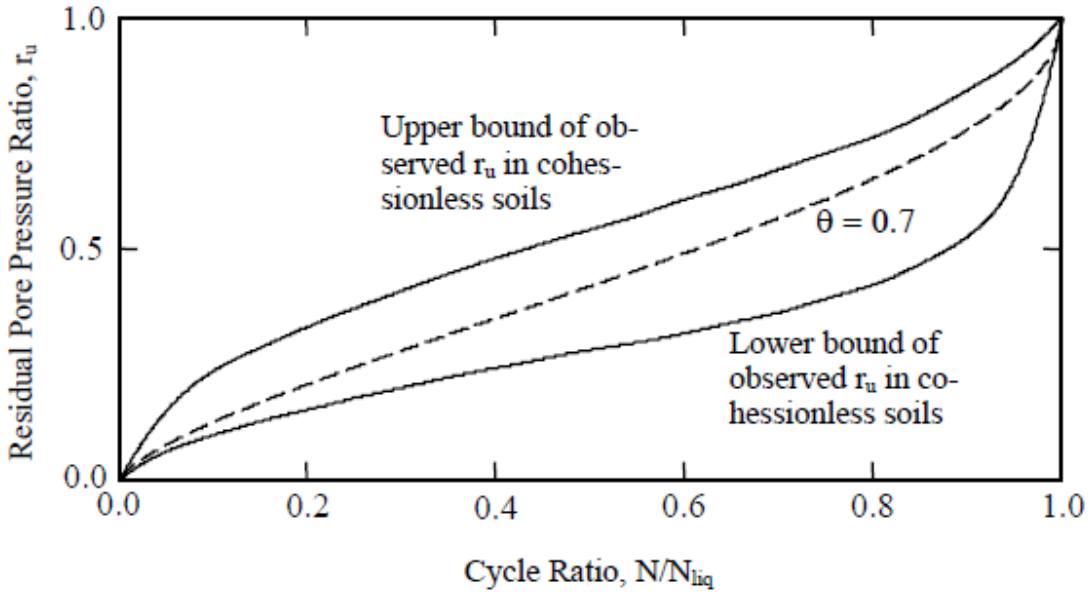

Figure 2-7 Observed bounds of excess pore pressure generation as a function of cyclic ratio, (from Seed et al. 1975b)

Figure 2.7 shows recommendation from Lee and Albaisa of the upper and lower bounds of residual pore pressure ratio for cohessionless soils. The broken line represents the approximate average of bounds given by equation 2.1 when θ is 0.7.

2.3.2 Energy–Based Model

The motivation for development of an energy based model is for application to projects and problems involving liquefaction for soil densification and ground improvement purposes. There are several energy based excess pore pressure generation models. Some of the published once

are presented in this section. Most of the presented models are relating excess pore pressure generation and dissipated energy and are empirical curve fit equations of laboratory data. Unlike the pore pressure ratio, r_u way of presentations, some models relate dissipated energy per unit volume of material, ΔW to the residual excess pore pressure u_{xs}. And in some cases the models are presented in terms of pore pressure ratio, r_u which is defined earlier.

MH Model (Mostaghel and Habibaghi 1978, 1979)

$$r_u = \frac{1}{e_o}\frac{\Delta W}{\sigma'_{vo}} \qquad 2\text{-}2$$

Where: ΔW is dissipated energy per unit volume of material.

e_o is initial void ratio.

σ'_{vo} is initial vertical effective stress.

DBI Model (Davis and Berrill 1982)

$$r_u = \alpha\frac{\Delta W}{\sigma'_{vo}} \qquad 2\text{-}3$$

Where: ΔW is dissipated energy per unit volume of material.

σ'_{vo} is initial vertical effective stress.

α is dimensionless calibration parameter and it's between $50 \leq \alpha \leq 80$

BD Model (Berrill and Davis 1985)

$$r_u = \alpha'^{\left(\frac{\Delta W}{\sigma'_{vo}}\right)^{\beta}} \qquad 2\text{-}4$$

Where: ΔW is dissipated energy per unit volume of material.

σ'_{vo} is initial vertical effective stress.

α' and β are dimensionless calibration parameters.

(α', β): (0.8,0.6), (0.65,0.5), and (0.5,0.5) for β=0.5 appears to be optimal.

DB2 Model (Davis and Berrill 2001)

$$r_u = 1 - \exp\left(-\alpha\frac{\Delta W}{\sigma'_{vo}}\right) \qquad 2\text{-}5$$

Where: ΔW is dissipated energy per unit volume of material.

σ'_{vo} is initial vertical effective stress.

α is dimensionless calibration parameter and it's between $50 \leq \alpha \leq 80$

Hsu Model (Hsu 1995)

$$r_u = \alpha \left(\frac{\Delta W}{\sigma'_{vo}}\right)^b \qquad 2\text{-}6$$

Where: ΔW is dissipated energy per unit volume of material.

σ'_{vo} is initial vertical effective stress.

a and b are dimensionless calibration parameters.

$a=(400\text{-}420Dr)CSR^2$

$b=(1.9\text{-}1.25Dr)CSR^{1/2}$

CSR= Cyclic stress ratio

Dr= Relative Density.

OAY Model (Ogawa, Abe, and Yoshitsugu 1995)

$$U_{xs} = \Delta W^{0.5} \qquad 2\text{-}7$$

Where ΔW is dissipated energy per unit volume of material.

U_{xs} is pore pressure ratio.

FSKL Model (Figueroa, Saada, Kern, and Liang 1997)

$$r_u = -A\Delta W(A\Delta W - 2) \qquad 2\text{-}8$$

Where ΔW is dissipated energy per unit volume of material (KPa).

A is calibration parameter.

Calibration Parameters: $A= 151.52\text{-}1.10Dr\text{-}27.89\gamma\text{-}0.016\sigma'_o$ (Kern 1996)

A=165.6-1.44Dr-9.09γ (Figueroa et al. 1997)

Where Dr is relative Density (%)

γ is Shear strain (%)

σ'_o initial effective confining stress (KPa).

Some commentaries were given by Green based on his research done in 2000. For example the MH model seems to predict that more energy is required to liquefy loose sand than dense sand, which is not what reality shows. This can be seen when the formula is rearranged to

$\Delta W = r_u e_o \sigma'_{vo}$.

The DBI model tends to over predict the increase in pore pressure as the cumulative dissipated energy increases.

GMP Model

This model was developed by Green et al. (2000) and the motivation for the development was to enable the use of dissipated energy as a measure of soil liquefaction resistance and for development of energy based methods for design of grounds improvement by soil densification. The empirical expression was developed after analyzing numerous cyclic triaxial tests. It provides a relationship between residual excess pore pressure generation and energy dissipated per unit volume of soil. The model is easy to implement and calibrate since it has a simple mathematical form and a single calibration parameter.

$$r_u = \sqrt{\frac{W_s}{PEC}} \qquad 2\text{-}9$$

Where W_s is the dissipated energy per unit volume of soil normalized by the initial effective confining pressure.

PEC, pseudoenergy capacity is a calibration parameter.

For general loading, increment in W_s can be related to stress condition and increments in strain by

$$dW_s = (\sigma'_v d\varepsilon_v + 2\sigma'_h d\varepsilon_h + \tau_{vh} d\gamma_{vh} + \tau_{hv} d\gamma_{hv}) \frac{1}{\sigma'_o} \qquad 2\text{-}10$$

Where dWs = incremental dissipated energy normalized by the initial effective mean stress

σ'_v= effective vertical stress

$d\varepsilon_v$= incremental vertical strain

σ'_h= effective horizontal stress

$d\varepsilon_h$= incremental horizontal strain

τ_{vh}= horizontal shear stress acting on a plane having a vertical normal vector

$d\gamma_{vh}$= incremental shear strain resulting from τ_{vh}

τ_{hv}= vertical shear stress acting on a plane having a horizontal normal vector

$d\gamma_{hv}$= = incremental shear strain resulting from τhv, and

σ'_o= initial effective stress.

For undrained cyclic triaxial and cyclic simple shear loading Ws in the above equation can be solved numerically by

$$Ws = \frac{1}{2\sigma'_o}\sum_{i=1}^{n-1}\left(\sigma_{d,i+1} + \sigma_{d,i}\right)\left(\varepsilon_{a,i+1} + \varepsilon_{a,i}\right) \qquad 2\text{-}11$$

Where n= number of load increment to liquefaction.

$\sigma_{d,i}$ and $\sigma_{d,i+1}$= applied deviator stress at load increment i and i+1 respectively.

$\varepsilon_{a,i}$, $\varepsilon_{a,i+1}$= axial strain at load increment i and i+1, respectively.

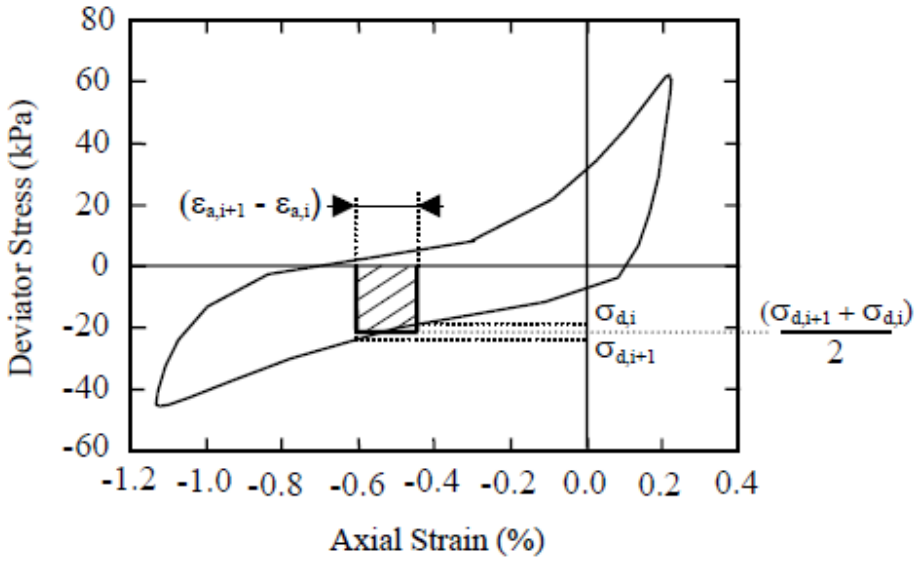

Figure 2-8 Application of equation 2.10, (from Green et al. 2000)

Figure 2.8 shows the dissipated energy per unit volume for a soil sample in cycle triaxial is the area bounded by the stress-strain hysteresis loops.

The pseudoenergy capacity, PEC can be determined from cyclic test data by plotting r_u versus the square root of W_s. The process of determining PEC is illustrated graphically in the figure below.

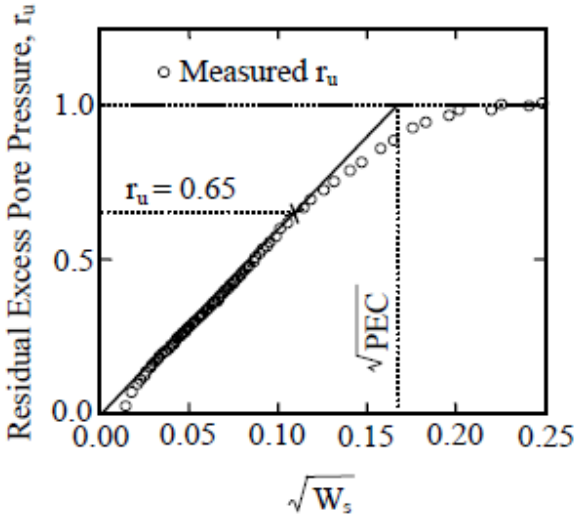

Figure 2-9 Determination of PEC from cyclic test done on clean sand, (from Green et al. 2000)

The square root of PEC is the value on the horizontal axis where a vertical line meets the horizontal axis starting from a point where a diagonal line that pass through the origin and r_u =0.65 and a horizontal line that pass through r_u=1 meet. It can also be simplified by the formula:

$$PEC = \frac{W_{s,r_u=0.65}}{0.4225} \qquad 2\text{-}12$$

Where $W_{s,ru=0.65}$ is the value of Ws at r_u=0,65.

Green did some comparison between the measured and the calculated residual pore pressure. One of the graphical comparisons is presented on figure 2-10.

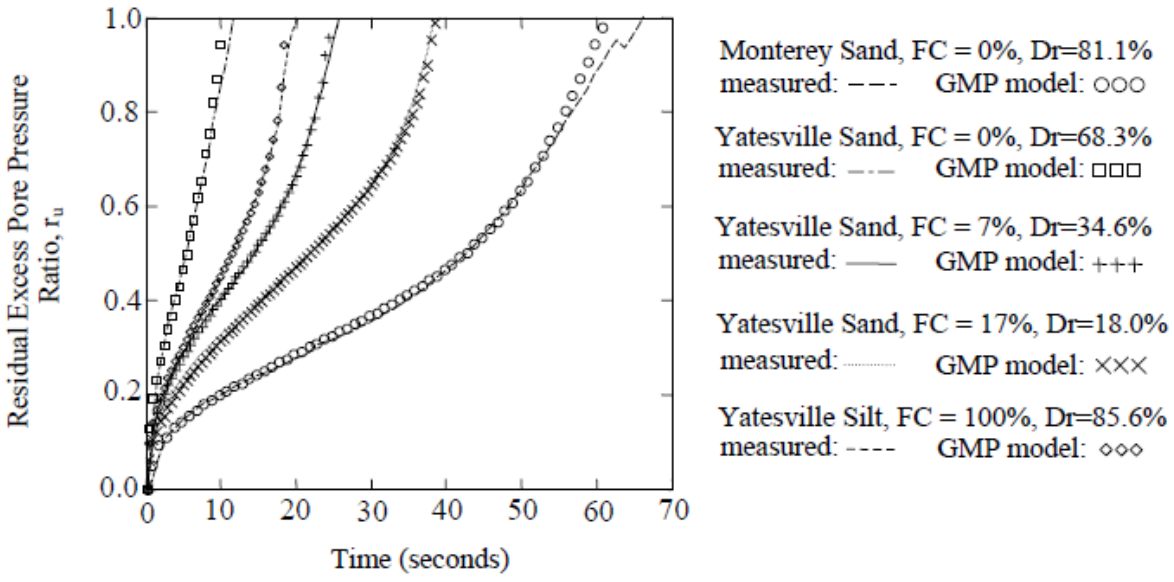

Figure 2-10 Comparison between measures and computed residual pore pressure, (from Green et al. 2000)

Figure 2-10 shows the accuracy of the GMP model. Apart from the fact that GMP model does not require the seismic loading to be converted to an equivalent number of uniform cycles unlike the stress-based model, both models seem to give a decent result compared to the measured value. Figure 2-11 shows the comparison done by Green (2000) GMP and Booker's stress based model and the measured values.

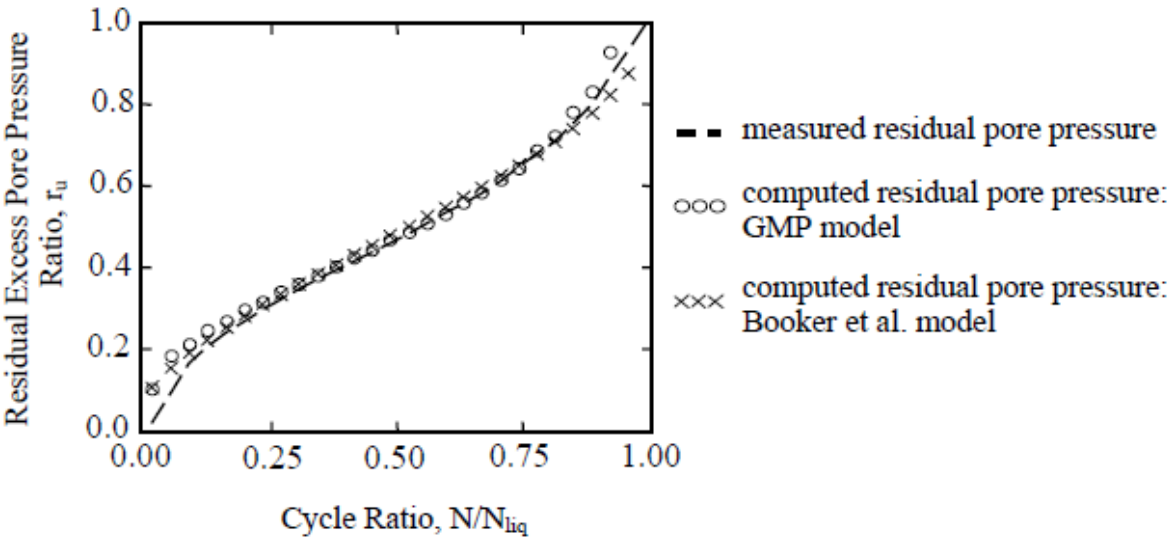

Figure 2-11 Comparison between computed and measured residual pore pressure, (from Green et al. 2000)

The above comparison is based on over 200 cyclic tests.

In order to make use of the proposed models it's quite mandatory to run a laboratory test. But unfortunately running a laboratory test is not the scope of this study. Therefore the next best thing to do will be referring to a test done on a different sample which has a closer property as the one under consideration or make use of correlation developed between a particular soil property and one of the model parameter, PEC for example.

Correlation between Relative density and PEC has been done on Yatesville fine sand-silt mixture by Green et al. (2000). Though running a test gives a rather accurate result, this correlation can be used for fine sand-silt mixtures (Green 2000).

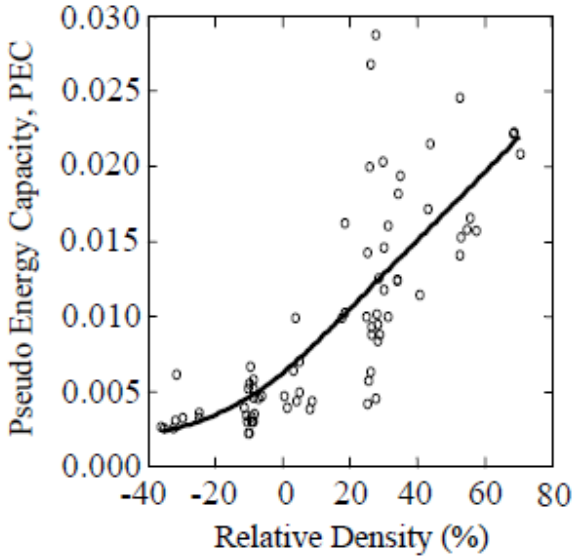

Figure 2-12 Correlation between PEC with relative density, (from Green 2000)

The negative relative density on figure 2-12 result from the specimens being prepared to void ratios larger than the maximum index void ratio determined using the ASTM standard.

2.4 Yield Strength Ratio and Liquefaction Analysis

In this section an approach by Olson et al. (2003) to evaluating the triggering of liquefaction in sloping grounds using yield strength ratio, $S_u(yield)/\sigma'_{vo}$, is discussed. Yield shear strength, $S_u(yield)$, is defined as the peak shear strength available during undrained loading (Terzaghi et al. 1996). The short term strength, $S_{u,}$ is mobilized during undrained or short term loading. This short term loading can be caused by static or dynamic loading. The short term yield strength is

presented as a function of vertical effective stress and the ration between the yield strength and the vertical effective stress is nearly equivalent to the yield strength envelop.

$$\frac{S_u(yield)}{\sigma'_{vo}} \sim \tan \varphi_y \qquad 2\text{-}13$$

Where φ_y is mobilized yield friction angle.

The mobilization of the S_u yield or simply the response of saturated contractive sandy soils is shown in the figure below.

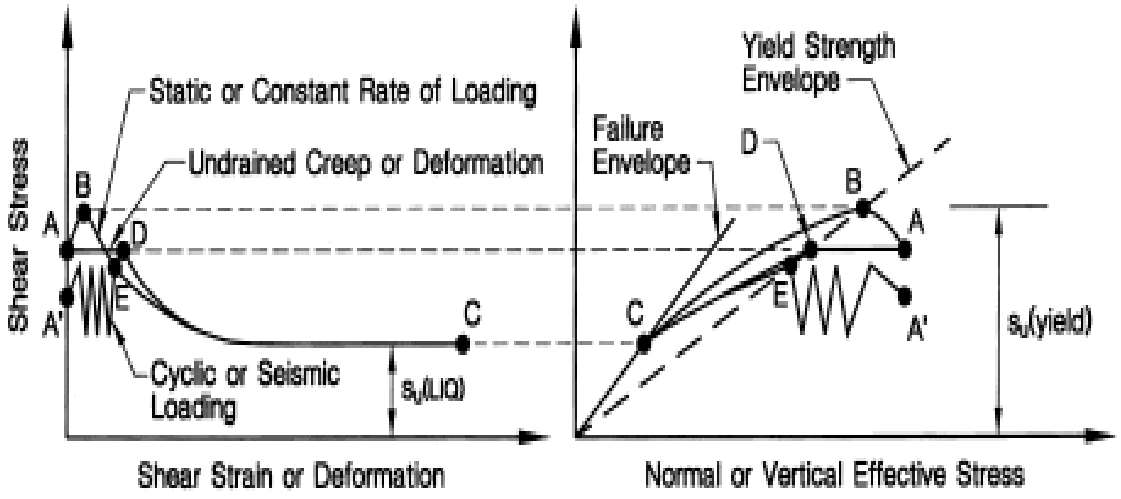

Figure 2-13 Undrained response of saturated, contractive sandy soil (from Olson et. al., 2003)

Figure 2-13 shows three categories of flow failure mechanism in an element scale. The mechanisms are static loading-induced failure, deformation-induced failure and seismically induced failures. For static loading induced failure, given an element at point A, during undrained loading, embankment construction for example, it moves to point B, located at the yield strength envelope. This path considers the drainage boundaries and permeability of the element causing temporary undrained condition. But as the shear stress tends to increase the loose sand skeleton yields and will collapse. The collapse will in turn trigger liquefaction. Right after the liquefaction the element will go to point C where it meets its liquefied shear strength.

For deformation induced failure, given a stress condition at point A, when static shear stress resulting from embankment for example, is able to cause shear strain or creep and if point A is undrained, the element will move to point D. Point D is located on the yield strength envelope.

After reaching point D liquefaction is triggered and the element will move to the liquefied shear strength, point C.

For seismically induced liquefaction, given a stress condition at point A' on figure 2-13, if point A is subjected to seismic or dynamic loading with an intensity to cause pore water buildup, it will move to point E. After reaching point E liquefaction will be triggered and the element will move to point C, the liquefied shear strength.

Olson (2001) evaluated effect of static loading, deformation instability and seismic loading on over 30 real cases. The discussion for the first two loadings is found on Olson (2003). As for the seismic loading, Olson used a relation that basis cyclic stress method proposed by Seed and Idriss (1971) for level ground to calculate average sustained seismic shear stress and stress ratio.

$$\tau_{ave,seismic} = \left(0{,}65\frac{\alpha_{max}}{g}.\sigma_{vo}\,(avg).\,r_d\right)/C_m \qquad 2\text{-}14$$

$$\frac{\tau_{ave,seismic}}{\sigma'_{vo}\,(avg)} = (0{,}65\frac{\alpha_{max}}{g}.\frac{\sigma_{vo}\,(avg)}{\sigma'_{vo}\,(avg)}.\,r_d)/C_m \qquad 2\text{-}15$$

Where α_{max}=peak free field surface acceleration. This is introduced to characterize the intensity of the ground shaking.

g = acceleration of gravity

r_d = depth reduction factor

r_d=1.0-0.00765*Z for Z≤9.15m

r_d=1.0-0.0267*Z for 9.15m≤ Z≤23m Youd and Idriss (1997)

Cm= lower bound of the range of magnitude scaling factor (refer table 2.2)

Table 2-2 Magnitude scaling factor, Youd and Noble, 1997

Magnitude, M	Cm		
	P_L<20%	PL<32%	PL<50%
5.5	2.86	3.42	4.44
6.0	1.93	2.35	2.92
6.5	1.34	1.66	1.99
7.0	1.00	1.20	1.39
7.5	-	-	1.00
8.0	-	-	0.73?
8.5	-	-	0.56?

Note:? = Very uncertain value.

The average seismic shear stress is then taken in to a relation, along with other destabilizing forces, that gives the safety factor against triggering liquefaction. But before going to the factor of safety the yield shear strength is discussed.

According to the research by Olson, (2003) the data collected had a trend showing increase in yield strength as penetration resistance increased. With this, an average relation was proposed considering the upper and lower bound of the trend. The relation is given by:

$$\frac{S_u(\text{yield})}{\sigma'_{vo}} = 0.205 + 0.0143(qc) \pm 0.04 \text{ for } q_c \leq 6.5\text{Mpa} \qquad 2\text{-}16$$

Where q_c is the penetration resistance.

The yield strength calculated should generally be corrected for the amount of the fine with in the sample. As the fine content increase the penetration resistance will decrease. The need for fine content adjustment for the sand under study will be disused later in the report.

Generally liquefaction analysis based on the yield strength ratio, according to Olson and Stark (2001), is briefly described below.

- Slope stability analysis is conducted for the prefailure geometry to establish the static shear stress in the liquefiable layer. The assigned shear strength for this layer is altered until a factor of safety of 1 is reached. For the rest of the layer around the liquefiable layer, fully mobilized drained or undrained shear strength is assigned. Bot circular and noncircular potential failure surfaces should be considered.

- Divide the critical slip surface into some number of segments. Ten to fifteen divisions will be optimum.
- Calculate the average static shear stress ratio, $\tau_{driving}/\sigma_{vo}'$ based on the weighte average value of σ_{vo}' along the critical slip surface.
- Calculate the average seismic shear stress, $\tau_{ave,\ seismic}$, using equation 2.14 or site response analysis.
- If, in case, there is an additional shear stress to be considered, τ_{other}, calculate using an appropriate analysis.
- Estimate the yield strength ratio using equation 2.16.
- Calculate the values of $S_{u(yield)}$ and $\tau_{driving}$ for all the segments in the critical slip surface by multiplying the values of the ratios by the weighted average σ_{vo}'.
- At last the safety factor against the triggering of liquefaction in each segment can be calculated as,

$$FS_{triggering} = \frac{S_u(yield)}{\tau_{driving} + \tau_{ave,seismic} + \tau_{other}} \qquad 2\text{-}17$$

Segments with a factor of safety less than one are likely to liquefy and vice versa. If all the segments have FS>1 then post-triggering stability analysis is unnecessary. On the other hand if there are some segments with a FS<1, then for the post-triggering stability analysis these segments should be assigned the liquefied shear strength, as can be calculated in equation 2.17, and for those with FS>1 they should be assigned their yield shear strength.

$$\frac{S_u(LIQ)}{\sigma'_{vo}} = 0.03 + 0.0143(q_{c1}) \pm 0.03 \text{ for } q_{c1} \leq 6.5\text{MPa} \qquad 218$$

Post-triggering analysis or flow failure stability analysis is done to determine whether the static shear force is greater than the available shear resistance including the liquefied shear strength. If the $FS_{flow,}$ after assigning the liquefied shear strength for the appropriate segments, is less than one flow failure of the entire structure is likely to occur and if between 1 and 1.1 some deformation is expected therefore segments which had a $FS_{triggering}$ between 1 and 1.1 should be assigned their liquefied shear strength and the overall stability against flow failure should be checked.

2.5 Insitu Tests

This section discusses the types of insitu tests that one could carry out to locate layers susceptible to liquefaction. Layered sand deposits, if liquefied, form water film beneath less pervious sublayers due to the local migration of pore water, which serves as part of the sliding surface for post-liquefaction flow failure (Kokusho and Fujita, 2002). Standard penetration test, SPT and Cone penetration test are the two most widely used insitu tests. If one must evaluate the liquefaction resistance or cyclic resistance ratio, CRR in the lab, it's required to retrieve and test undisturbed samples. But in most cases it's almost impossible to reestablish insitu stress state in the lab unless and otherwise a specialized sampling technique like ground freezing is done. Therefore in undertaking the above mentioned field tests one can try to reduce the errors related to laboratory investigation.
The above mentioned field insitu tests will be described briefly and how their result is used in relation to liquefaction susceptibility analysis is discussed.

2.5.1 Standard Penetration Test, SPT

Apart from its robustness, SPT is relatively easy and cheap to use for evaluating liquefaction resistance. The criteria is based on the cyclic stress ratio (CSR) or cyclic resistance ratio (CRR) and Corrected blow count, $(N_1)_{60}$. The count is normalized to an over burden pressure of approximately 100KPa and a hammer energy ration or hammer efficiency of 60%. If the sample has a fine content more than 5%, $(N_1)_{60}$ should be corrected for the influence of fines content. Correlation of $(N_1)_{60}$ to an equivalent clean sand value, $(N_1)_{60cs}$ according to Youd and Idriss, (2001) is given by:

$$(\mathbf{N_1})_{\mathbf{60cs}} = \boldsymbol{\alpha} + \boldsymbol{\beta}(\mathbf{N_1})_{\mathbf{60}} \qquad 2\text{-}19$$

Where $\alpha=0$ for FC$\leq$5%

$\alpha=\exp(1.76-(190/FC^2))$ for 5 %< FC<35%

$\alpha=5$ for FC$\geq$35%

$\beta=1$ for FC$\geq$35%

$\beta=(0.99+(FC^{1.5}/1{,}000))$ for 5%<FC<35%

$\beta=1.2$ for FC$\geq$35%

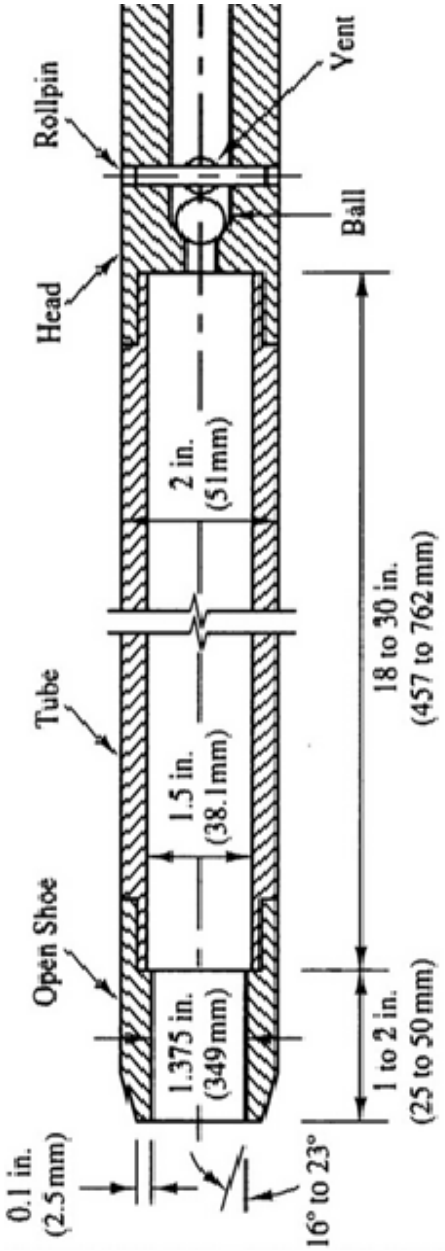

Figure 2-14 Typical SPT dimension

other factors also affect result from SPT other than fines content and the correction is given by:

$$(N_1)_{60} = N_m C_N C_E C_B C_R C_S \qquad 2\text{-}20$$

Where N_m = measured standard penetration resistance

C_N=normalize N_m to a common reference effective overburden stress.

C_E = correction for hammer energy ratio (ER).

C_B = correction factor for borehole dimension.

C_R = correction factor for rod length and

C_S = correction for samplers with or without liners.

For the values of the correction factors table by Robertson and Wride, 1998 can be referred. Based on clean-sand (FC<5%) A.F.Rauch at University of Texas has suggested a relation for the CRR.

$$CRR_{7.5} = \frac{1}{34-(N_1)_{60}} + \frac{(N_1)_{60}}{135} + \frac{50}{(10*(N_1)_{60}+45)^2} - \frac{1}{200} \qquad 2\text{-}21$$

The above equation is only for earthquake of magnitude 7.5. And only valid for $(N_1)_{60}$ <30, greater value of $(N_1)_{60}$ implies too dense to liquefy therefore if above 30 then the soil is classified as non-liquefiable. As for the magnitude there are scaling factors to adjust CRR values to other magnitudes. The different scaling factors can be referred on T.L.Youd and I.M.Idriss, 2001. Once we have the liquefaction resistance we can compare it with the cyclic stress ratio, CSR.

A relation to calculate the CSR was formulated by Seed and Idriss in 1971.

$$\mathrm{CSR} = \left(\frac{\tau_{av}}{\sigma'_{vo}}\right) = 0.65\left(\frac{a_{max}}{g}\right)\left(\frac{\sigma_{vo}}{\sigma'_{vo}}\right) r_d \qquad 2\text{-}22$$

Where a_{max}= pick horizontal acceleration at the ground surface

g=gravity

σ_{vo} and σ'_{vo} = total and effective vertical overburden stresses respectively.

r_d = stress reduction coefficient. It account for flexibility of the soil profile.

r_d=1.0-0.00765z for z≤9.15m

r_d=1.174-0.0267z for 9.15m<z≤23m

where z is depth below ground surface in meters.

The factor of safety against liquefaction will be

$$FS = \frac{CRR_{7.5}}{CSR} MSF \qquad 2\text{-}23$$

where MSF is the magnitude scaling factor to convert the $CRR_{7.5}$ to the design magnitude. Some values of MSF are listed on table 2.2.

It's also possible to check if the ground is contractive or dilative using the SPT blow count. The first step in liquefaction analysis for sloping ground should be to determine if the soil is contractive, i.e., susceptible to flow failure (Olson and Stark, 2003). Figure 2-15 shows the boundary between contractive and dilative condition constructed based on flow failure case histories and SPT blow counts. After deciding the soil condition, i.e. whether it is contractive or dilative, we can proceed to the triggering analysis.

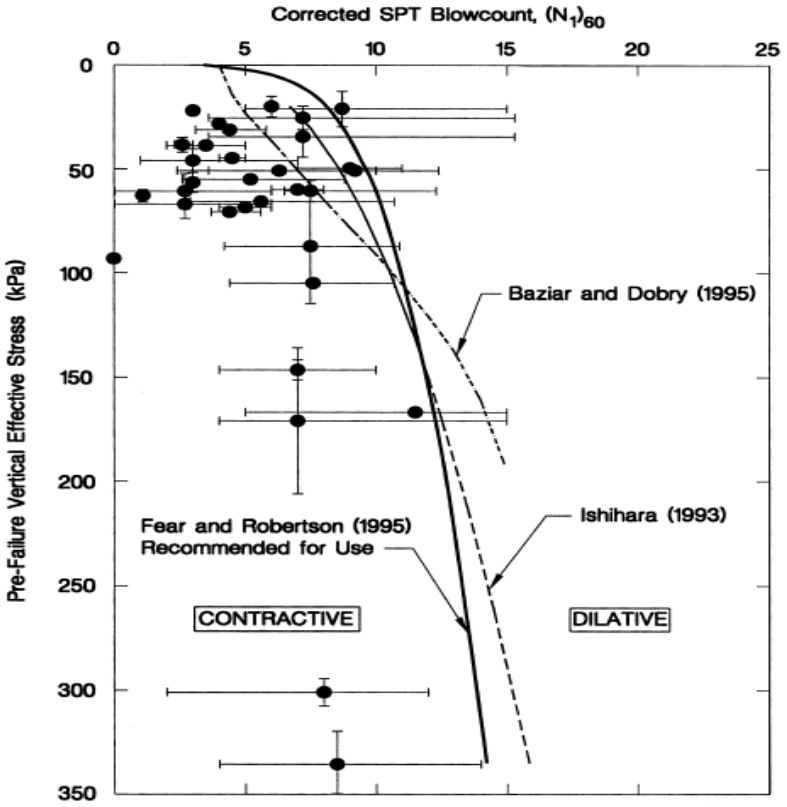

Figure 2-15 Boundary between contractive and dilative conditions using flow failure case histories and SPT blowcount, (from Olson et al., 2003)

2.5.2 Cone Penetration test, CPT

The CPT gains advantage over SPT for its simplicity, repeatability, accuracy and continuous record. Using electronic transducers, it's possible to record real time measurement of cone resistance (q_c), sleeve friction (f_s), and pore pressure (u) during penetration of the probe. Having a continuous soil profile allows for a more detailed definition of soil layer.

A simplified approach by Youd et. al., (2001) has been developed to calculate the cyclic resistance ratio, CRR. The approach is based on some conservative assumptions and sould be used for low to medium risk projects and for preliminary screening of high risk projects.

The recommended CPT correlation for sand is (Robertson, 2009):

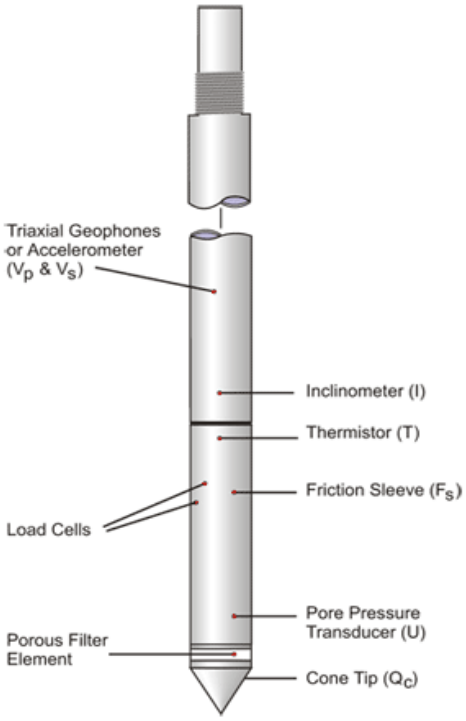

Figure 2-16 Typica CPTu equipment

$$\mathrm{CRR}_{7.5} = 93\left[\frac{(\mathrm{Q_{tn,cs}})}{1000}\right]^3 + 0.08 \qquad 2\text{-}24$$

If $50 \leq Q_{tn,cs} \leq 160$

$$\mathrm{CRR}_{7.5} = 0.833\left[\frac{(\mathrm{Q_{tn,cs}})}{1000}\right]^3 + 0.05 \qquad 2\text{-}25$$

If $Q_{tn,cs} < 50$

Where $CRR_{7.5}$= cyclic resistance ratio.

$Q_{tn,cs}$= equivalent clean sand cone penetration resistance.

Relations 2-24 and 2-25 are based on some specific factors like; the test was done on a clean sand and for magnitude M=7.5 earthquake. Therefore before proceeding to the factor of safety calculation we need to correct to the soil condition we have and adjust the magnitude of the stress.

Correlation to determine equivalent clean sand cone penetration resistance, $Q_{tn,cs}$ is based on the grain characteristics such as fins content and is given by:

$$(Q_{tn})_{cs} = K_c Q_{tn} \qquad 2\text{-}26$$

Where K_c = correction factor that is a function of grain characteristics.

This grain characteristic is estimated using the suggestion from Robertson and Wide (1998) and soil behavior type index, I_c given by:

$$I_c = [(3.47 - logQ_{tn})^2 + (logF + 1.22)^2]^{0.5}$$

$$Q_{tn} = \left(\frac{q_c - \sigma_{vo}}{\sigma'_{vo}}\right)$$

Where Q_{tn} =the normalized tip resistance (dimensionless)

F = is the normalized friction ratio, % and is given by:

$$F = \frac{fs}{[(q_c - \sigma_{vo})]} X100\%$$

f_s = CPT sleeve friction stress

P_a = reference pressure in the same unit as the effective vertical overburden stress and P_{a2} = reference pressure in the same unit as total vertical overburden stress.

The recommended relationship between I_c and the correction factor K_c is given by:

K_c=1 if $I_c \leq 1.64$

$K_c = 5.581I_c^3 - 0.403I_c^4 - 21.63I_c^2 + 33.75I_c - 17.88$ if $I_c > 1.64$

CRR7.5 can also be calculated from the shear wave velocity. And the relation is given by:

$$CRR_{7.5} = 0.022\left(\frac{V_{s1}}{100}\right)^2 + 2.8\left(1/(V_{slc} - V_{s1}) - \frac{1}{V_{slc}}\right) \qquad 227$$

Where V_{slc} is an upper limiting value of the shear wave velocity related to fines content (FC) and its given by V_{slc} = 215m/s if FC<5% and V_{slc} = 200m/s if FC>35%

The factor of safety against liquefaction will be

$$FS = \frac{CRR_{7.5}}{CSR} MSF \qquad 2\text{-}28$$

Where MSF is the magnitude scaling factor.

As was done for SPT, relationship separating contractive from dilative condition was developed based on flow failure case histories and CPT tip resistance. Identifying this can be a base for proceeding with liquefaction analysis. Figure 3.6 shows this relationship.

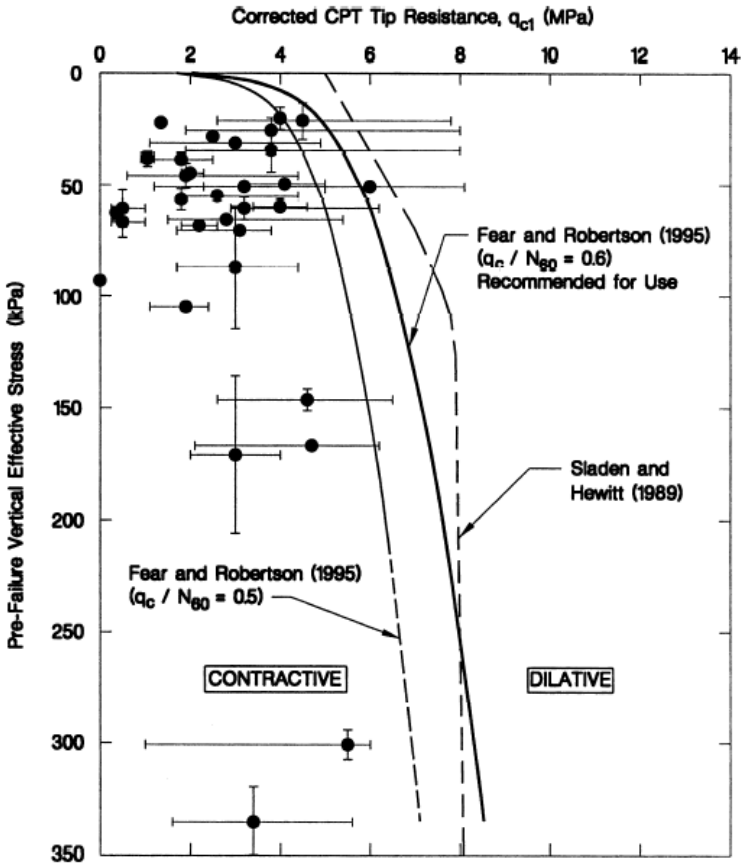

Figure 2-17 Boundary between contractive and dilative conditions using flow failure case histories and CPT tip resistance, (from Olson et al., 2003)

3. Case Study: Finneidfjord

3.1 Introduction

Under the ICG research activity numbers of investigations were carried out for a better understanding of the formation and stability of the submarine slope at Finneidfjord. To mention some, Very-high-resolution swath bathymetry data, side-scan sonar or backscatter data, high to very high resolution 2D seismic and very high resolution 3D chirp seismic, sediment sampled by shallow gravity and Calypso piston cores (including X-ray imaging, X-ray fluorescence data, lithology, water content, multi-sensor core logging results, fall cone shear strength, AMS ^{14}C dating), high quality soil sampling for advanced geotechnical laboratory tests, in-situ cone penetration tests using a free-fall piezocone penetrometer and long-term double-sensor in-situ pore pressure measurement were taken(Vardy et al., 2012).

From part of the above mentioned investigation data, which will be presented in the next chapter, its tried to discuss the regional setting, describe the landslide under study and the morphology and characterize the event bed of the landslide and their property.

3.2 Regional setting

The village of Finneidfjord is part of the 12Km long and 2Km wide fjord called Sørfjord which is situated in Northern Norway (Figure 3.1). Sørfjord is composed of two basins separated by ice-marginal deposits and a bed rock sill (Olsen et al., 2001). The western part of the basin is quite steep changing 30m in depth with in 200m of the shore. The fjord levels out beyond 200m due to the glacimarine and marine clay infill sediments derived from the Røssåga River. The eastern part near to the village of Finneidfjord is around 50m in depth but increase gradually to more than 150m at the western end (Vardy et al., 2001).

Most of the area surrounding Sørfjord was subjected to intense glacio-isostatic rebound after the last glacial period. As a result, glacio-marine and marine deposit took place which raised the marine limit to about 124m above sea level. The low lands around the study area are almost totally covered with marine deposits overlain locally by fluvial or littoral deposits. These marine deposits, after their emergence in the Holocene, were exposed to ground water flow and due to this leaching of salt resulted in the formation of very sensitive clays also known as quick clay.

Chapter 3: Case Study: Finneidfjord

Several quick clay landslides have occurred in this area during the Holocene and until present (L'Heureux et al., 2012). The debris from the slides during this period have occasionally deposited into the fjord forming thin laminated soft clay beds which are quite different from the normal homogeneous post-glacial sediments.

In addition to other speculations, anthropological activity (blasting) is thought to play a role in triggering the slide in 1978, 1996, 2006 and these layers are used as slip plane for the mass movement (Maarten Vanneste, 2012).

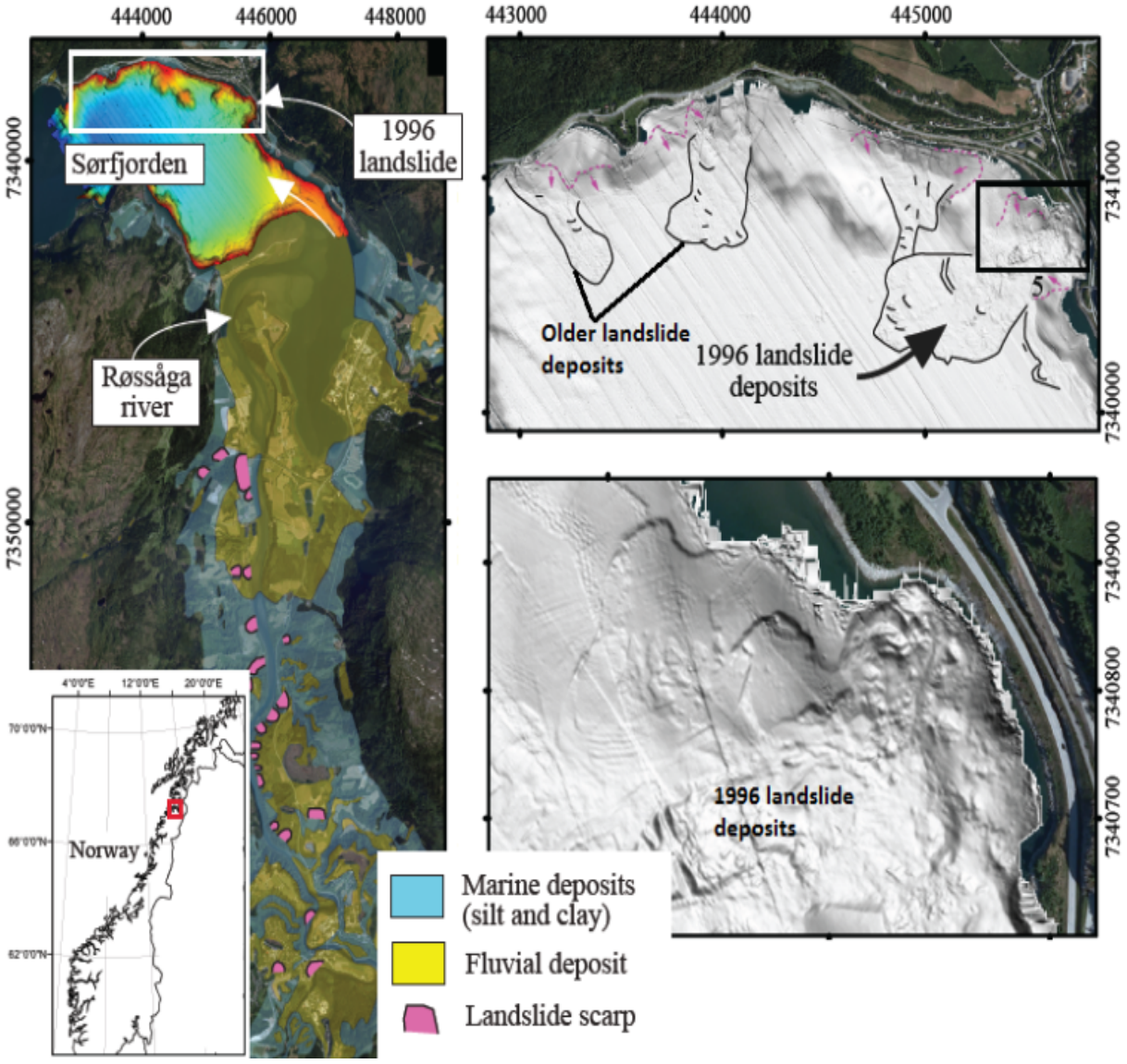

Figure 3-1 Overview of the study area (modified from L'Heureux et al. 2012)

The shore line of Finneidfjord and area close to the 1996 landslide is covered by beach deposit (sand and gravel). These coarser sediments rest on a thick sequence of clayey silts overlying on bed-rock. Pockets of quick clay are found at several locations along the shoreline and offshore.

3.3 Landslide description and Morphology

The catastrophic landslide at Finneidfjord mobilized 10^6 m^3 of sediment and due to its retrogressive behavior it was able to reach 100 to 150m inland. The landslide occurred shortly after a period (around 14 days) of intense rainfall, which is believed to contribute as a pre conditioning factor for the slope instability. In addition, during the same day the landslide occurred, there was a road construction underway where blasting was carried out for tunnel construction which further undermined the stability of the slope.

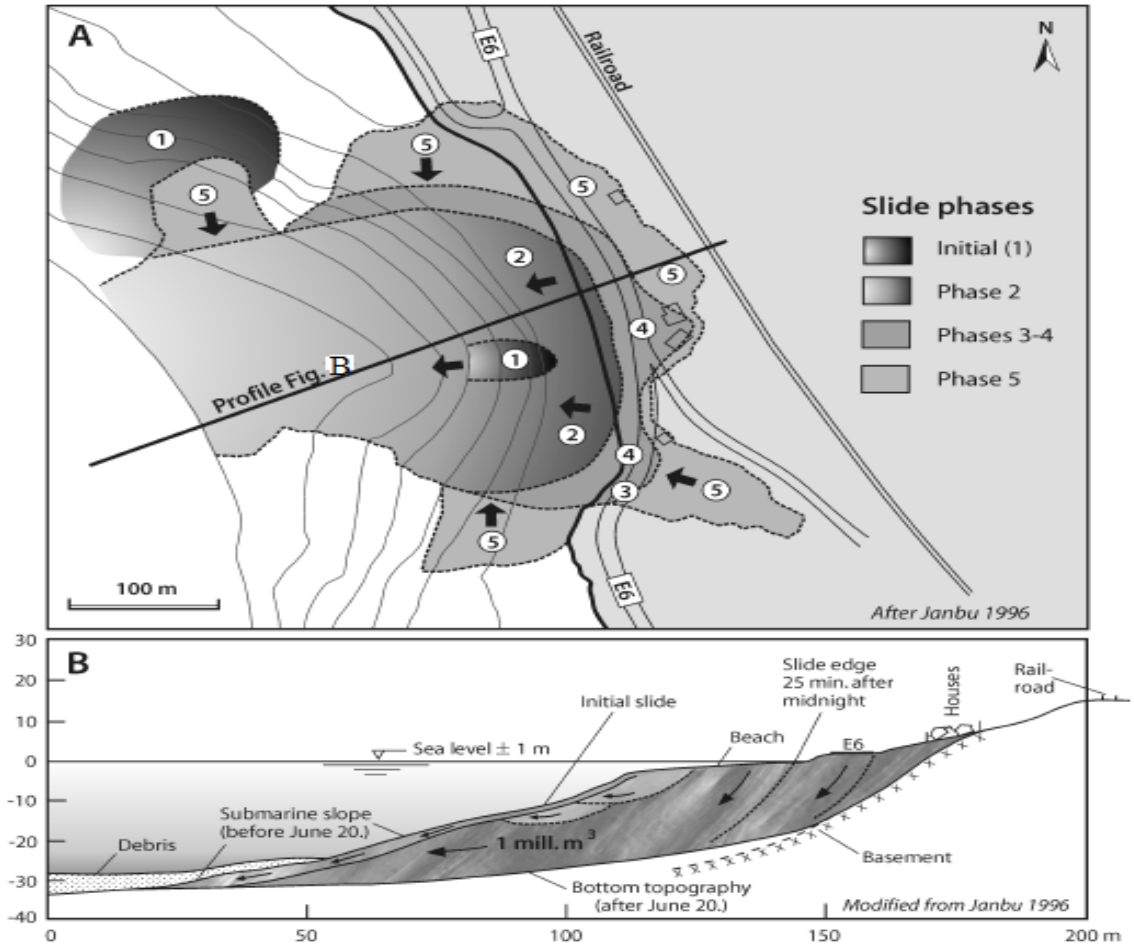

Figure 3-2 A: Janbu's slide development definition. B: Profile based on 1984 survey illustrating slide mechanism (from Longva et al., 2003)

Chapter 3: Case Study: Finneidfjord

Based on the swath bathymetry survey done in 1997 Janbu (1996) and Longva (2003) were able to define the different phases of the landslide. Figure 3.2 describes the definition given by Janbu.

Janbu (1996), Longva et al. (2003) and L'Heureux (2012) have discussed the different mechanism of the slide in a quite similar manner. According to Longva et al. (2003) the mechanism is generally dividing it into two main stages as shown in figure 3.3.

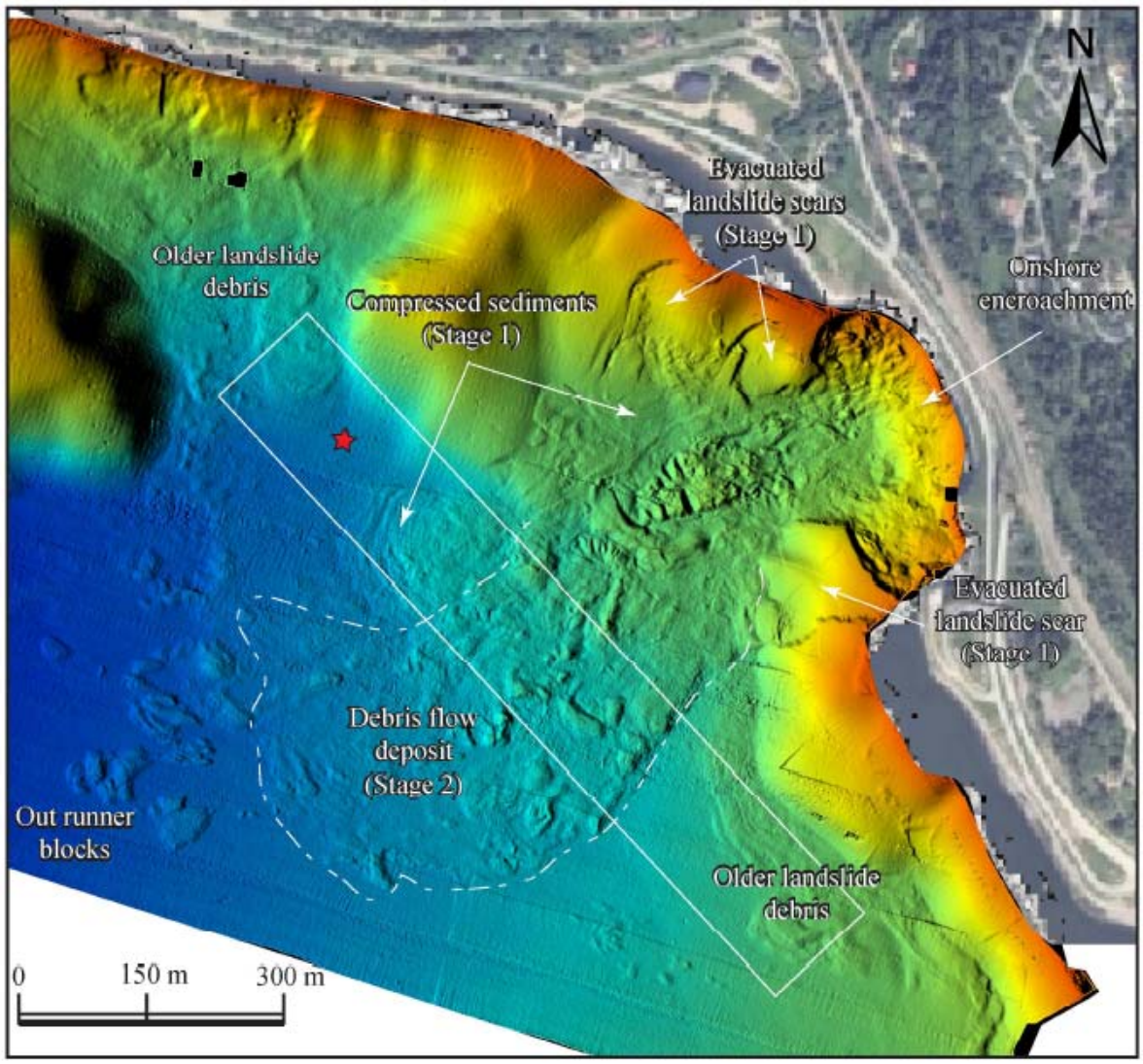

Figure 3-3 Surface morphology and the two phases of the 1996 landslide development identification by Longva et al., (2003). (From Verdy et al., 2012)

The initial phase involved translational movement of foreshore slope material on the event bed. The detachment along the weak layer is thought to represent the initial slide mechanism and has probably punctured the quick clay chamber either by unloading, overstepping or erosion

and triggered the retrogressive slide with development of typical “bottle neck“ slide (Longva et al., 2003). This phenomenon was followed by overlaying, blocky debris flow deposition as the headwall retrogressed to the palaeo-shoreline and 150m to 200m beyond.

Figure 3.3 shows the mass wasting process at several locations along the Sørfjorden shoreline and also shows two types of seafloor geomorphologies. L’Heureux (2012) describes these seafloor geomorphologies as smooth and rough. The smooth seafloor corresponds to evacuated landslide scars devoid of landslide debris. The surrounding intact slope varies between 13^{o}-21^{o} and it is believed that the evacuated landslide scar is usually similar to the surrounding. The height of the escarpment is about 2 to 3m.

The rough seafloor morphology corresponds to mass wasting deposit up to a few meters thick (see figure 3.4). The debris of the landslide is mainly concentrated around the central part of the fjord (see figure 3.1c) and comprises of blocks and slabs of compressed sediment from part of the fjord.

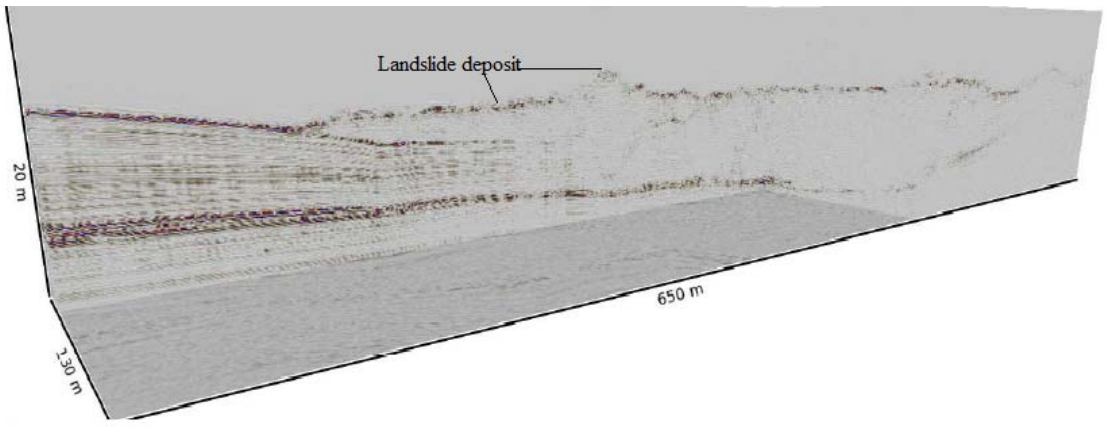

Figure 3-4 Landslide deposit (modified from Longva et al., 2003)

3.4 Event Beds and their Properties

It is tried to discuss the characteristics of the weak layer that is thought to be the event bed for the 1996 Finneidfjord landslide herein. Based on a range of investigations carried out on the study area different researchers have tried to explain the event bed and its properties (Longva et al., 2003; L'Heureux et al., 2012; Steiner et al., 2012).

The clay-slide activity in the catchment of the fjord resulted in the deposition of regional event beds with a distinct sedimentological and geotechnical signature in the fjord stratigraphy (L'Heureux et al., 2012, Steiner et al., 2012). Findings from the different swath bathymetry and high-resolution seismic cores data show that most of the underwater landslides in Sørfjorden initiate from a common weak layer. The landslide under under consideration is also in this category. The 1996 landslide initiated alone a weak layer which comprises a thin sand layer sandwiched between two soft clay layers. The clay layer is believed to exist due to the debris from the slides during Holocene period which has occasionally deposited into the fjord forming thin laminated soft clay beds. These layers are quite different from the normal homogeneous post-glacial sediments. The schematic description of the near shore setting is presented in figure 3.5.

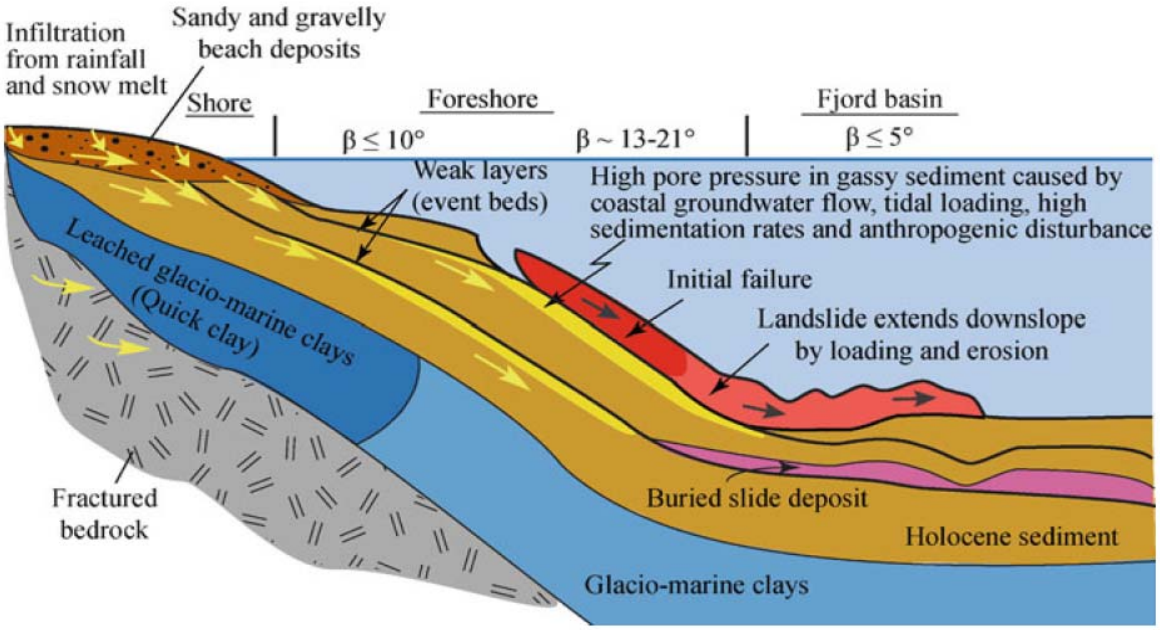

Figure 3-5 Schematic description of near–shore setting at Finneidfjord, (from L'Heureux et al., 2012)

The Kullenberg-Calypso piston core sample taken adjacent to the landslide deposit shows normally consolidated sediment dominated by homogenous, brownish, silty clay with some small fragment. As the depth increases this characteristics change and around a depth of 2.9m below the sea bed the thin layer mentioned earlier appears. The two soft clay layers confining the sand layer are about 10cm each and the sand layer is 15 to 20cm thick.

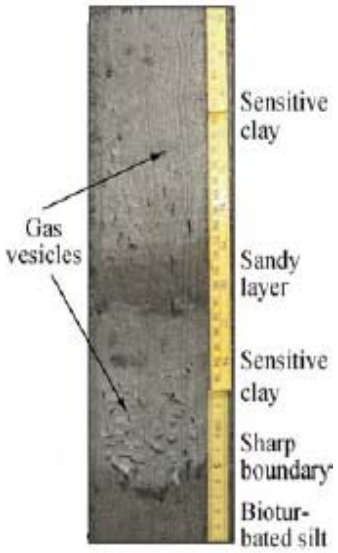

Figure 3-6 Gravity core showing layering of the event bed (from L'Heureux et al., 2012)

With the information that the different landslides that has happened at Finneidfjord including the one under study has translated using this weak layer, the following chapter will focus on presenting the soil property of the layer from the different investigation that are done in relation to the 1996 landslide and method used for the analysis carried out.

Chapter 3: Case Study: Finneidfjord

4. Data and Methods

4.1 Introduction

This chapter is dedicated for presenting insitu geotechnical data collected and laboratory test results in relation to the study area and methods used for caring out the analysis. The data are collected by NGU and ICG hoping that the finding will improve the understanding of the landslide at Finneidfjord and also to investigate whether or not intermittent landslide in the future will be an issue. It's also basing the results from the investigation that the dynamic and slope stability analysis are carried out in this study.

4.2 Data

4.2.1 Data from Calypso Core

The calypso corer is a giant piston corer (type kullenberg), and is considered one of the most useful and efficient coring system. The corer is designed in such a way that soil deformation is minimal. The CALYPSO corer weights 7 to 10 tons, and is equipped with a 40 to 60m iron lance (5 inches ½ diameter) and an internal high-pressure PVC liner (20cm diameter in Finneidfjord case), a mechanical trigger and a piston to ensure regular rising of the sediment within the lance during the final free fall from about 1m above the seabed. It can retrieve long sediment cores, of up to 25-30m beneath the seabed. Figure 4.1 shows the process of calypso coring.

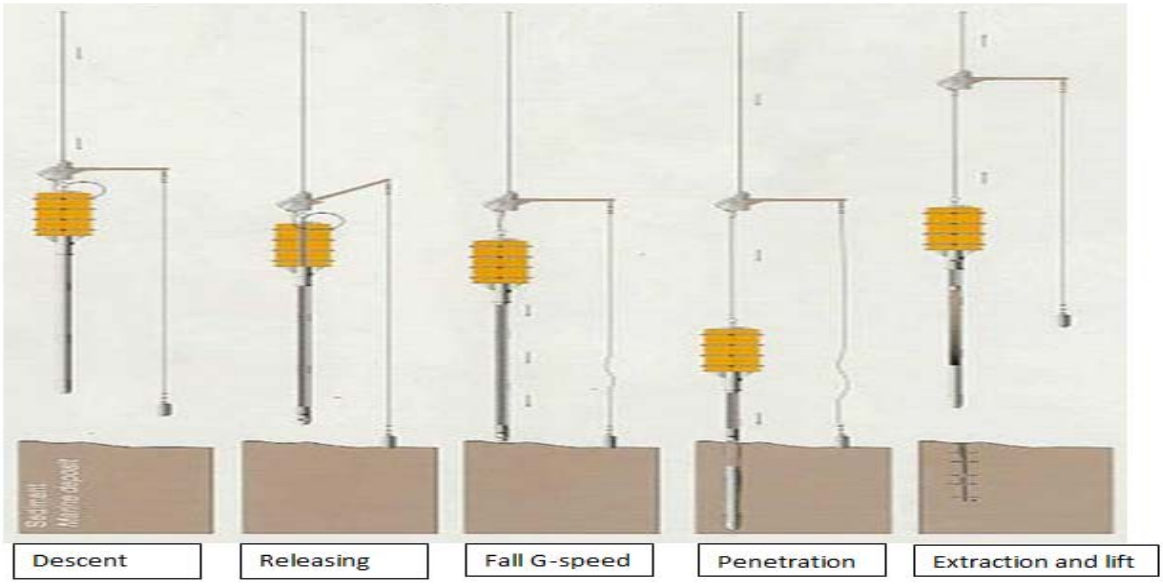

Figure 4-1 Process of Calypso coring

Calypso core samples were taken right outside the 1996 landslide in 2010. Multi-sensor core logging (MSCL), XRF core scanning, sedimentological description, gamma density, magnetic susceptibility measurement and geotechnical analysis are performed on the sample taken.

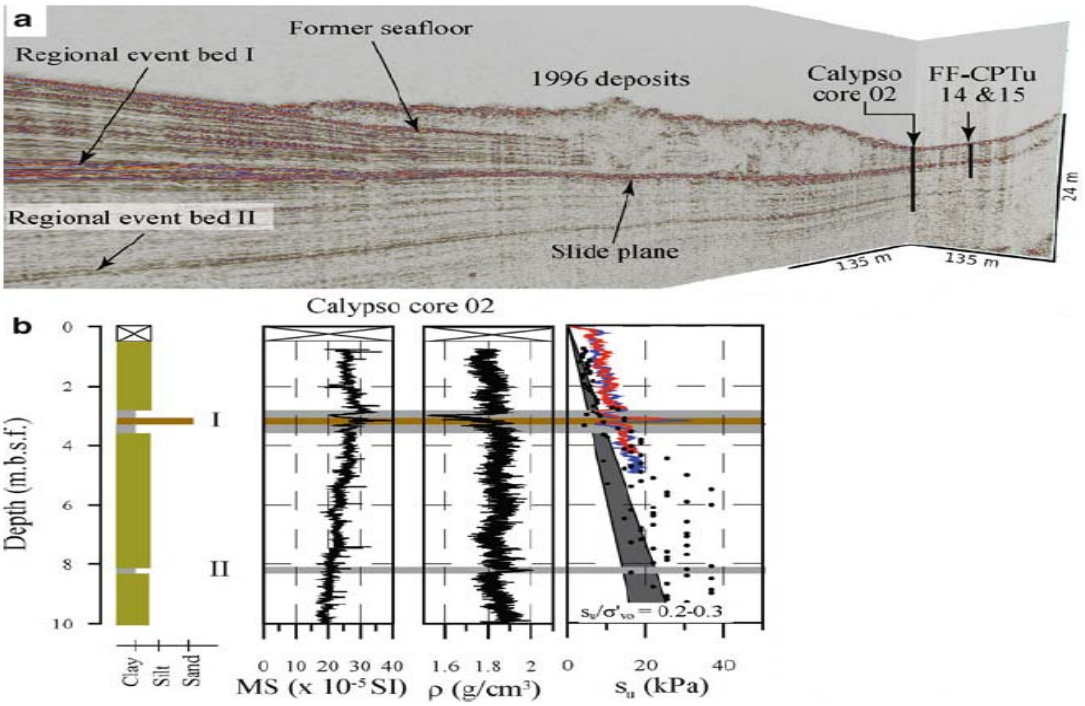

Figure 4-2 a: Fence diagram from 3D seismic cube showing the 1996 landslide deposit, b: geotechnical and sedimentological details from the calypso core, (from L'Heureux et al., 2012)

Until a depth of 2.8m below the sea floor, the sample from the calypso showed a homogenous, brownish, bioturbated, clayey silt with some shell fragments. At 2.8m below the sea bed, there is a 45cm distinct bed with a sand layer sandwiched between two clay layers. The sand layer is 15 to 20cm thick and it seats on 10 to 15cm thick gray clay and on top there is a 10cm clay layer.

The clay layers have low magnetic susceptibility and gamma density, refer figure 4.2. Whereas the sand layer sandwiched between the clay layers shows positive peak. The undrained shear strength ratio (S_u/σ'_{vo}) generally exceed 0.3 for the massive clayey silt, which is an indication for normally to slightly over-consolidated sediments. As for the weak layer, the undrained shear-strength ratio is lower between 0.2 and 0.3 which indicated that the layer is normally consolidated sediment.

4.2.2 In-situ Free-fall Piezocone Penetrometer Test

Characterizing weak layers is a key element in submarine landslide research and the MARUM (center for Marine Environmental Sciences and Faculty of geosciences) free-fall piezocone penetrometer (FF-CPTU) is a key tool for the research. Using such types of state-of-the-art measurement will have a great plus to our knowledge of initiation of submarine landslide and geohazards assessment. FF-CPTU is a light weight, modular, straightforward, cost effective and time effective technique to measure de/acceleration, tilt/temperature and CPTU parameters (q_c, f_s, u_2) with the 15cm^2 geomil subtraction piezocone (Alois Steiner et al. 2012). During investigation, its deployed from free-fall from a short distance, 10 to 15m above seabed. Figure 4-3 shows the instrument used.

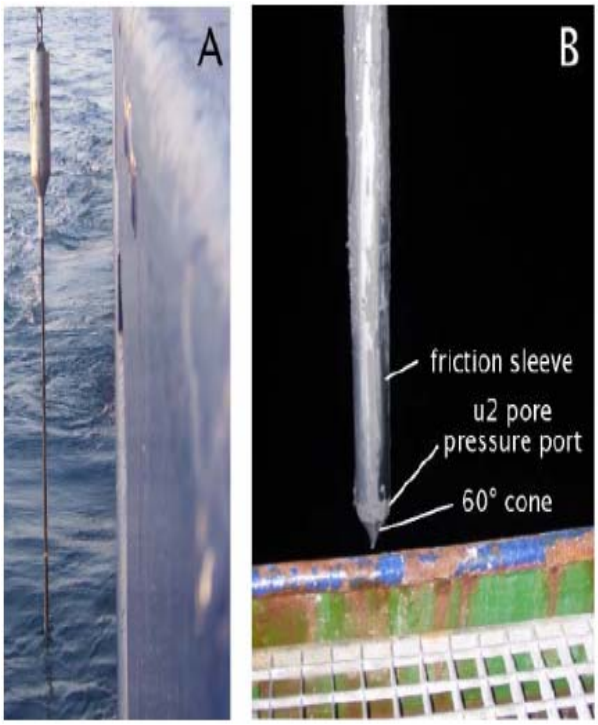

Figure 4-3 Shallow-water FF-CPTU instrument, A: probe detail B: as used in Finneidfjord target area (from Steiner et. al., 2011)

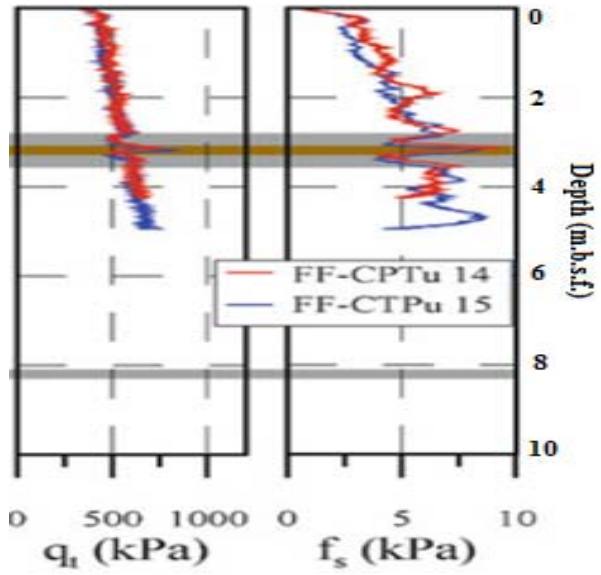

Figure 4-4 cone resistance and sleeve friction profiles from FF-CPTU test (from Steiner et al., 2011)

Results from the FF-CPTU (refer figure 4-4) shows a decrease in the undrained shear strength and sleeve friction in the weak layer. Compared to the surrounding sediments, the undrained shear strength is at least 1.8 to 2.2 times less. Same goes for the sleeve friction.

4.2.3 Pushed GOST CPTU Tests

The conventional CPTU equipment is pushed in to the soil with a quasi-static penetration velocity of 0.02m/s, unlike the FF-CPTU which is a free fall penetration. CPTU is a widely used and efficient measurement technique for geotechnical investigation. There is possibility of measuring cone resistance, sleeve friction and pore water pressure simultaneously. And from these datas it's possible to get information on lithology, soil stratification and geotechnical properties.

The type of CPTU used for the Finneidfjord project is called GOST (Geotechnical Offshore Seabed Tool). It was developed by MARUM and is used to collect in situ cone-penetration test with pore pressure measurement. It has the capacity of penetrating 50m below seabed soil. The penetration rate is 2cm/s, same as the conventional CPTU.

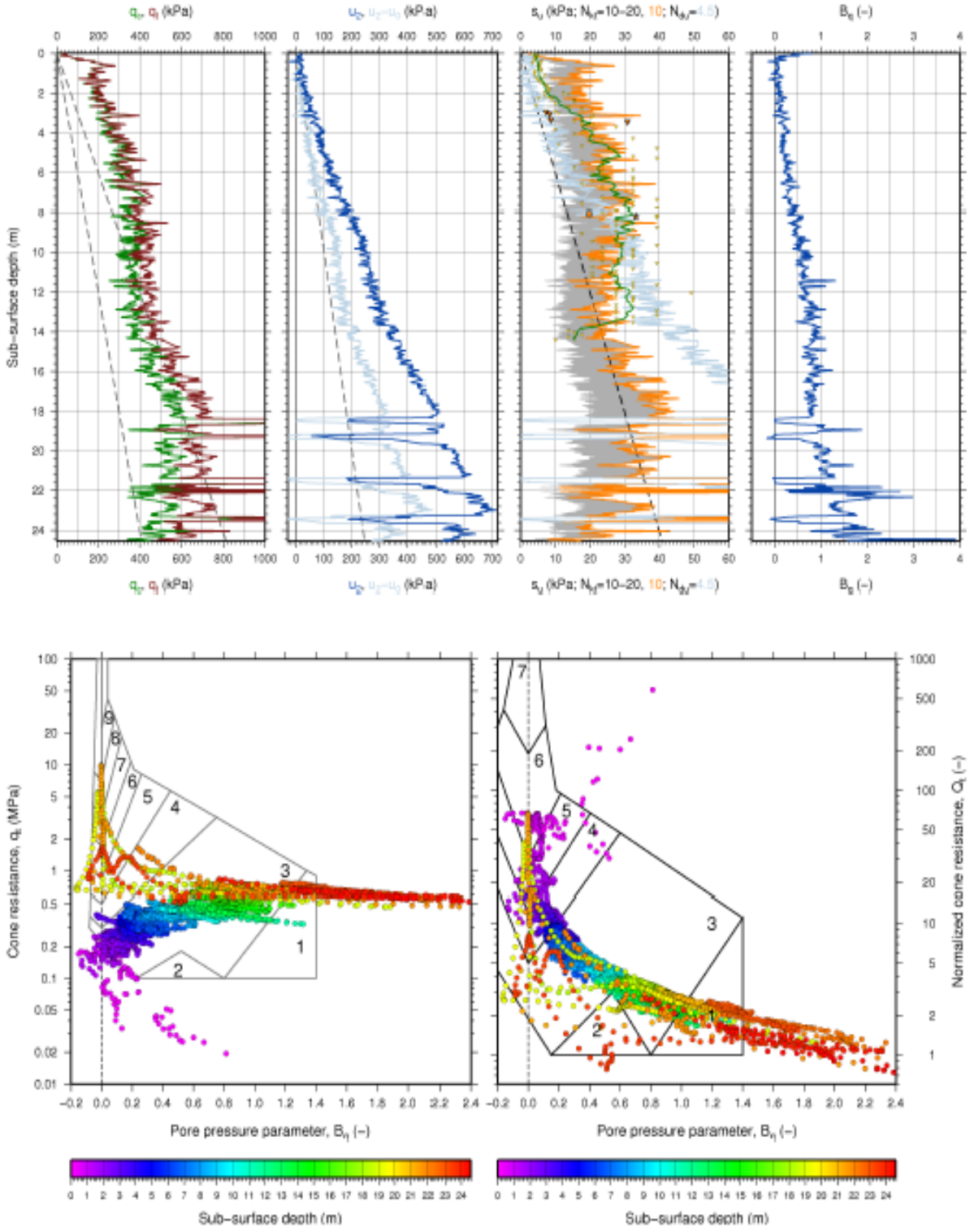

Figure 4-5 Result from the GOST-CPTU (top) and colour-coded soil classification (bottom), (ICG report, 2012)

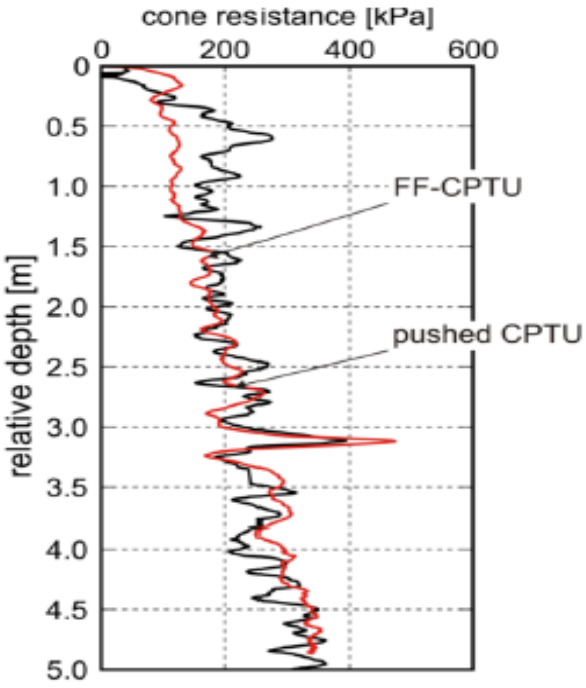

Figure 4-6 revels the layering condition at Finneidfjord. The cone resistance picks up when it reaches the sand layer and the pore pressure measurement drops. The tip resistance change is quite visible on Figure 4-6. It also shows that the result from the conventional CPTU and the FF- piezocone penetrometer agree on most of the layering, especially around 3,1m below sea bed, where the loose sand layer it thought to exist. The pore pressure parameter B_q, figure 4-5 (bottom), shows that the soil is generally silty-clays to clay with clay content diminishing with depth.

Figure 4-6 Comparison between GOST-CPTU (black) and FF- piezocone penetrometer (red) (from Steiner et al., 2012)

4.2.4 Geotechnical Laboratory Data

Varity of geotechnical tests were carried out focusing towards characterizing potential weaker layers. The test ranges from standard index test to more advanced strength test.

Table 4-1 Falling cone strength result, ICG report, 2012

Depth (mbsf)	Label	S_u (KPa)	$S_{u,\ rem}$ (KPa)	S_t (-)
2.94	1b	7.33±0.64(n=3)	1.97±0.06(n=3)	3.73±0.34
3.03	2b	8.33±0.45(n=4)	1.30±0.18(n=4)	6.40±0.96
3.33	4b	8.65±0.94(n=4)	2.35±0.19(n=4)	3.68±0.50
3.43	5b	30.75±6.18(n=4)	2.94±0.29(n=5)	10.46±2.34

The results shown on table 4.1 are obtained from a test done on a sample taken from around the event bed. Initial water content was measured to be 42.5%.

Direct simple test was also performed on 35cm^2 and 16mm high specimens. Rate of shearing was 5% shear strain/hour. The reason for choosing DSS instead of triaxial test is because the event bed is very thin and it was not possible to get a specimen that is sufficient to run triaxial test.

Table 4-2 DSS strength test result, (NGI report 2012)

Depth (mbsf)	Label	S_u^{DSS} (KPa)	U_f (KPa)	w_i (%)	w_f (%)	K (m/s)	Soil
2.98	1	6.7	12.6	37.3	32.6	$2.89e^{-9}$	CLAY, silty
3.03	2	7.2	9.7	68.4	67.5	$2.64e^{-8}$	CLAY, silty
3.10	3	8.7	7.7	50.5	47.8	$1.04e^{-7}$	SILT, sandy, clayey
3.18	4	15.4	-0.5	46.0	42.2	$6.67\ e^{-7}$	SAND, silty, clayey
3.26	5	9.5	8.6	47.5	38.8	$1.06\ e^{-8}$	CLAY, Silty

4.2.5 Grain Size Distribution

Grain size distribution was part of the laboratory investigation in characterizing the weak layer. The result is presented in figure 4-7.

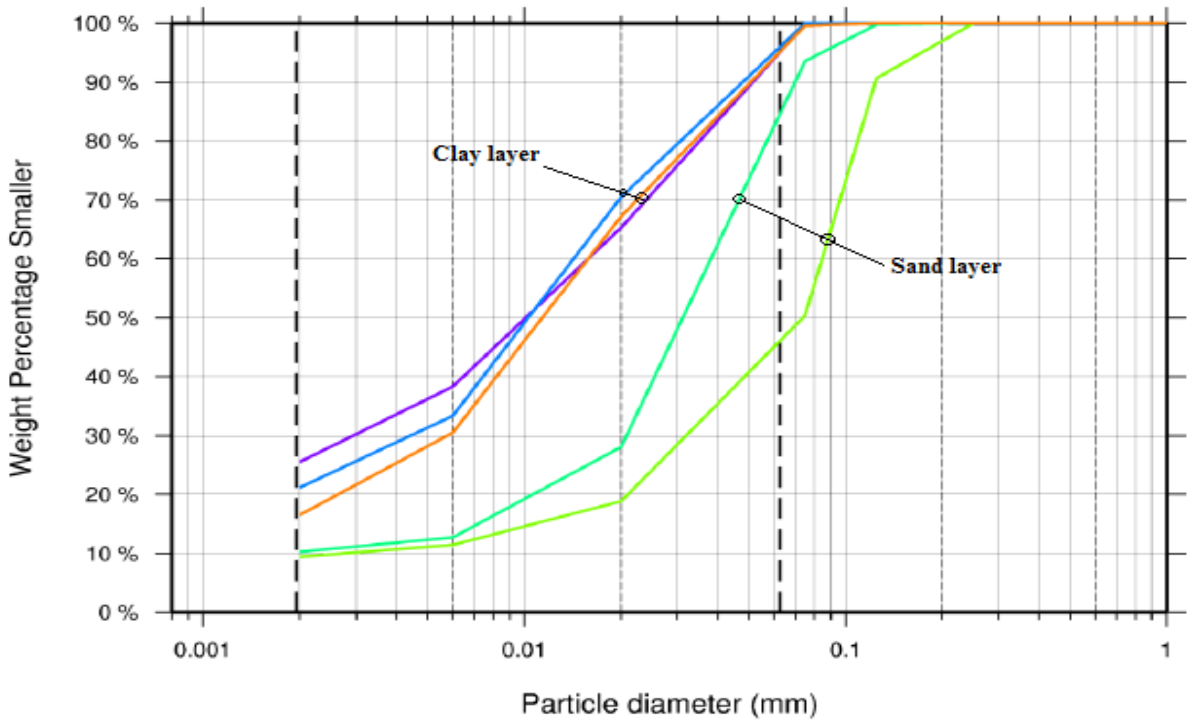

Figure 4-7 Grain size distribution curve, ICG data

The grain size distribution shows that the amount of fine content is approximately 10%. It was mentioned in the literature chapter that yield strength calculated using equation 2.15 should be corrected for the amount of fine with in the sample. The fine content of the sand under consideration is below 10% and low plastic. Therefore fine content adjustment is not required. This is because the amount of fine and the plasticity condition will only have a moderate influence on penetration resistance.

4.2.6 Geophysical Data, Very-High-Resolution 3D (VHR-3D) Seismic Data

VHR-3D seismic data was collected in order to identify the slip surface.

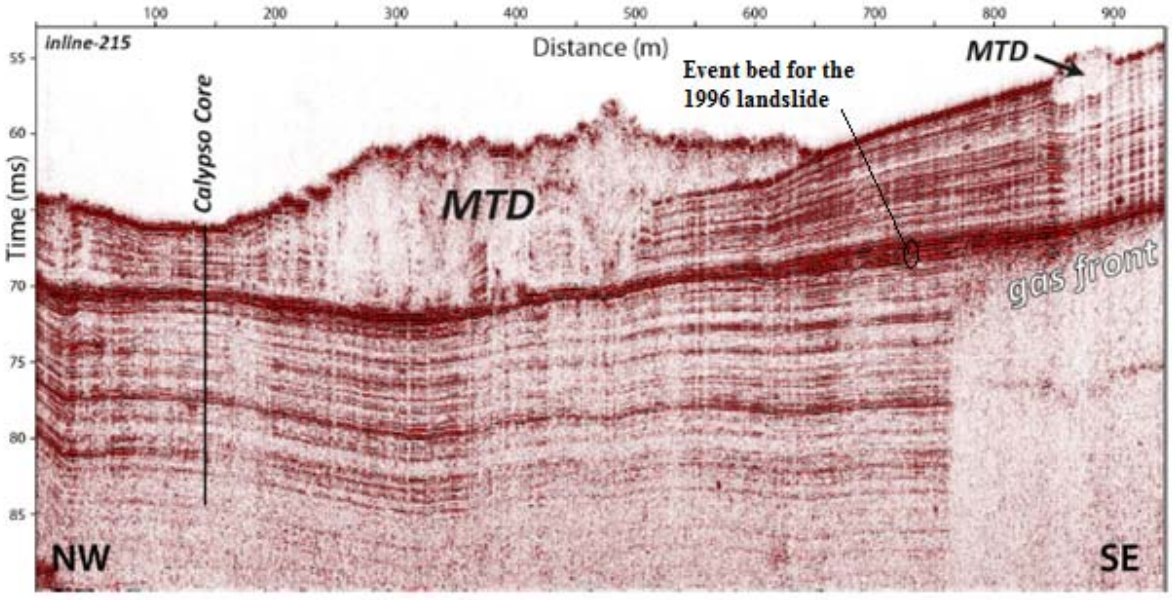

Figure 4-8 VHR-3D across the 1996 Finneidfjord landslide, (MTD = Mass transport deposit), ICG data

Figure 4-8 shows distinctly that the land slide has used the layer with the high amplitude reflection and the mass with a lower amplitude reflection is the mass transported during the landslide.

4.2.7 Existing Excess Pore Pressure

A piezometer was installed at a depth of 3.1m and 5.3m to gain information on the pore pressure regime in the shoreline slope.

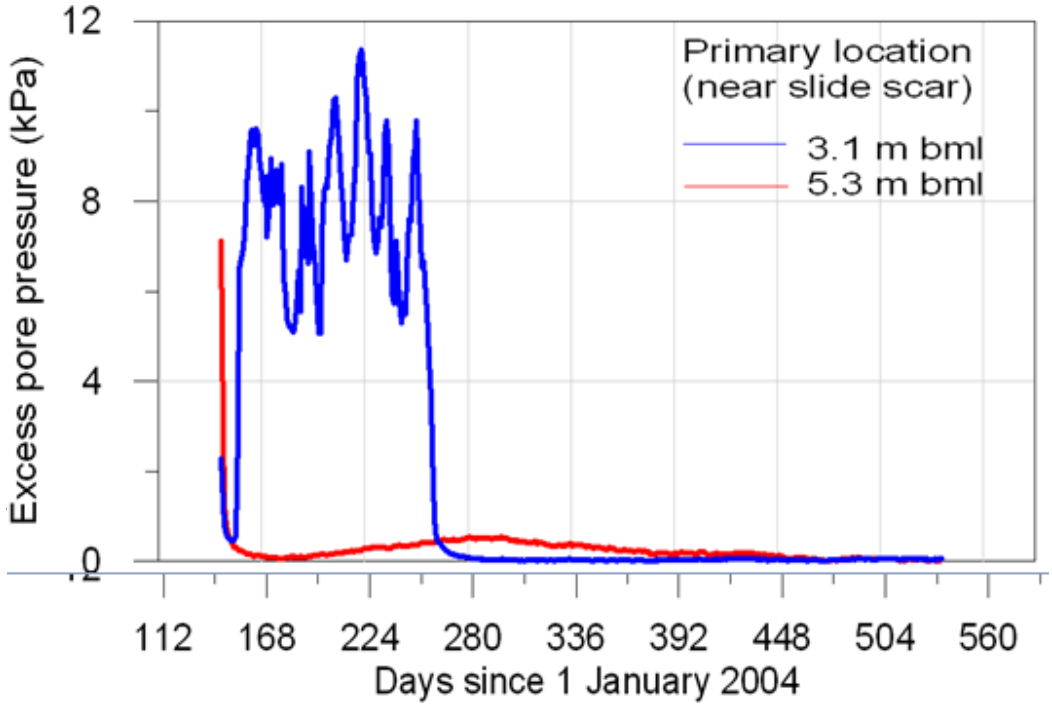

Figure 4-9 Piezometric reading (ICG data)

The installation of the piezometer was near the landslide scar. The data was collected for 4 months. Figure 4-9 shows the measurement at a depth of 3.1m and at 5.3m below sea floor. According to the measurement an average excess pore pressure of 8kPa was registered. This is equivalent about 26% higher than the hydrostatic pore pressure. This registered value in addition to the excess pore pressure from the dynamic analysis is to be an input for the slope stability analysis.

4.3 Method

'' The attraction of modeling is that it combines the subtlety of human judgment with the power of the digital computer.'' Anderson and Woessner (1992).

This section presents the method used for the dynamic analysis in order to study the influence of the blasting carried out prior to the landslide and the stability analysis using the output from the dynamic analysis and piezometric reading. The analysis was done using a software package called GeoStudio. This package incorporates different types of unique softwares that are integrated with one another. QUAKE/W, one of the finite element software and SLOPE/W, one of the limit equilibrium software are mainly used herein. All the individual softwares can be used as a stand-alone product and/or can be integrated with one another.

4.3.1 Numerical Modeling in Geotechnical Engineering: What and Why

A numerical model is a mathematical simulation of a real physical process. Unlike other engineering professions, in Geotechnical engineering it is not possible to choose a specific material type or geometry which one would like to work with. One has to face the fact that it is a must to work with what nature has to provide and make sure that it is well understood. For this reason it is wise to turn complex physical reality in to some mathematical systems and understand risk and uncertainties related. Therefor it is the role of numerical modeling to assist us in developing appropriate mathematical abstraction and make it possible for us to base our design.

The role of modeling in geotechnical engineering, as illustrated by Professor John Burland in 1987, is presented in the figure below. In his lecture in 1987, it was explained how geotechnical engineering is composed of three fundamental components: **1.** establishing the ground profile, insitu test and field measurement, **2.** defining ground behavior, defining and describing the site condition, and **3.** Modeling, can be conceptual, analytical or physical and all are interlinked and supported by experience consisting of empiricism and precedent.

If the question why model were to be raised, the first or rather most obvious answer would be to analyze the problem. But for a broader and a high level perspective the reason for modeling can be explained as follows:

Make quantitative predictions

Most engineers do modeling from the desire to say something about future behavior or performance. Quantitative predictions say a lot about the above reason. Making quantitative prediction is the most difficult part of modeling since it's directly related with the soil property. But with the proper site investigation and experience it's possible to predict the possible behavior of a given situation.

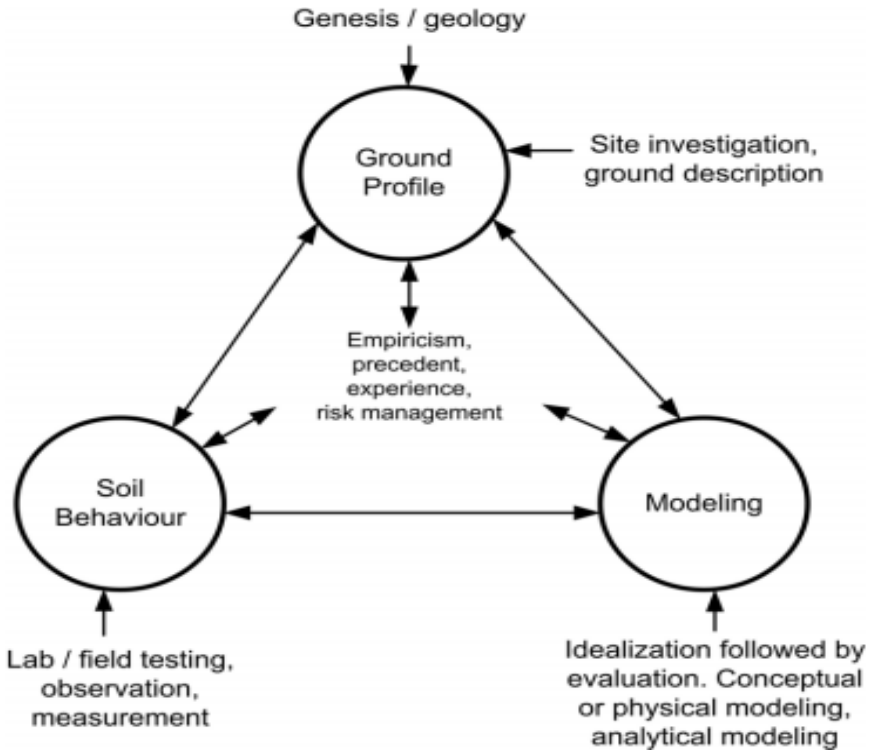

Figure 4-10 Expanded Burland triangle

Compare alternatives

Numerical modeling is useful for comparing alternatives. Keeping everything else the same and changing a single parameter makes it a powerful tool to evaluate the significance of individual parameters. For modeling alternatives and conducting sensitivity studies it's not all that important to accurately define some material properties. All that is of interest is the change between simulations (Dynamic Modeling with QUAKE/W 2007, 2010).

Identify governing parameters

Identifying critical parameters in design is one of the reasons we need numerical modeling. The identification can be done by changing a single parameter and keeping the other constant. Once

the key issue is identified, further modeling to refine a design can concentrate on the main issue, then effort can be made on what needs to be done for a better and safe design.

Understand physical process

The other and one of the most powerful aspects of numerical modeling is that it can help us understand physical processes and in turn helps us to train our mind. It can either confirm our thinking or help us to adjust our thinking if necessary. In the process of numerical modeling and analyzing the results we might end up discovering things new to us or even a completely new idea for the society.

In general modeling is a path we take in order to understand complex physical behavior, especially in the field of geotechnics, and discover new things. As a result this path will take as to a position where we can exercise our engineering judgment with a high confidence.

4.4 QUAKE/W and SLOPE/W

4.4.1 QUAKE/W

QUAKE/W is a geotechnical finite element CAD software product for the dynamic analysis of earth structures subjected to earthquake shaking and other sudden impact loadings like from a blast or pile driving. QUAKE/W determines the motion and excess pore-water pressures that arise due to shaking. QUAKE/W's comprehensive formulation makes it well suited to analyzing a wide range of problems.

QUAKE/W is part of GeoStudio, suite for geotechnical and geo-environmental modeling, which is fully integrated with other components of the suite such as SLOPE/W, used herein, SIGMA/W and more. It can be used as a stand-alone product, but one of its main attractions is the integration with other components of GeoStudio which enables users to run an expanded range of problems.

A generalized material property function allows using any laboratory or published data. Three constitutive models are supported in QUAKE/W: a Linear-Elastic model, an Equivalent Linear model, and an effective stress Non-Linear model. QUAKE/W uses the Direct Integration Method to compute the motion and excess pore-water pressures arising from inertial forces at user-defined time steps.

QUAKE/W can be used to analyze almost any dynamic earthquake problem one will encounter in one's geotechnical, civil, and mining engineering projects.

From the four types of analysis available in QUAKE/W Initial static and equivalent linear dynamic analysis are used. How these two analysis types work is presented below.

Initial static

In QUAKE/W the initial stress should be established first before proceeding with the dynamic analysis. The initial static analysis type is basically formulated to establish the initial stress condition. Material properties like shear modulus, G and variables like cyclic stress ratio are usually a function of effective stress in the ground. Therefore it's essential to know the initial state of stress in the ground before starting the dynamic analysis.

Initial pore-water pressure can be specified by 1) drawing an initial water table; 2) using the results of another finite element analysis; or 3) using a spatial function. The initial water table is assumed to be on the ground surface and using the first option series of points that are automatically connected to form the water table are drawn. The initial pore-water pressure is calculated by assuming a linear relationship between the pore-water pressure, unit weight of water and the depth below the water table. Therefore, pore-water pressure distribution is hydrostatic. The pore-water pressure condition in the weak layer is different from hydrostatic condition but this difference is considered in the slope stability analysis.

Dynamic analysis

Once the insitu static stresses have been established, the next step is to do the dynamic or shaking analysis making the initial static analysis the ¨Parent¨ analysis. The main reason for running QUAKE/W is for dynamic analysis. It models the response of an earth structure to some kind of osculating or sudden impulse force such as earthquake shaking or blasting. The main building blocks of this dynamic analysis are dynamic driving force, boundary conditions, material properties and temporal integration.

- Dynamic driving force – in any type of analysis related to dynamic analysis, the driving forces are associated with, for example, earthquake shaking or blasting. In QUAKE/W the force is specified by velocity time history. The velocity time history of the blast is applied to simulate the very sudden impulse load. This data, by use of numerical integration, can be converted into displacement versus time record. The displacement time history is then applied as a nodal boundary function.

- Boundary condition – Often most part of the boundary is specified as being fixed. For dynamic analysis the vertical movement is fixed but the ground is allowed to move laterally. For all QUAKE/W analysis, there must be at least some specified displacement

in order to compute a solution. It is numerically not possible to obtain a finite element solution if there are no specified displacements.

- Material properties – while working with dynamic analysis material model selected plays a great role than the behavior of the material itself. An equivalent linear model is chosen herein. This type of model is not recommended for real projects but for an educational analysis, it works just fine. With the equivalent linear model QUAKE/W starts a dynamic analysis with the specified soil stiffness. It steps through the entire blast record and identifies the peak shear strain at each gauss numerical integration point in each element. The shear modulus is then modified until the required modification is within a specified tolerance.

  Most of the material properties used herein are calculated based on CPTU and other field measurement data. The different material types used are presented in the next chapter.

- Time stepping – the vibration data from Finneidfjord shows that the blasting lasts only a fraction of seconds. Therefore it is very important to have a very small time step in order to capture all the characteristics of the motion. A typical value of two hundredths (0.02) of a second is recommended and is used herein. It's not a firm rule to use this step as long as the peaks and sudden changes are approximately captured.

4.4.2 SLOPE/W

SLOPE/W is one component in the complete suite of geotechnical product, GeoStudio. It is designed and developed to be a general software tool for the stability of earth structure. Dynamic loading like earthquake or impact loading from a blast or pile driving creates inertial forces that may affect the stability of structures. The loading may also generate excess pore-water pressures. Both the dynamic stress conditions and the generated pore-water pressures can be taken into SLOPE/W to study how the loading condition affects the earth structure stability and deformation. SLOPE/W can perform a Newmark-type of deformation analysis to determine the yield acceleration and estimate the permanent deformation of the earth structure.

Among the many limit equilibrium methods found in this package like Bishop's simplified or Janbu's simplified methods, the General limit equilibrium method (GLE) is used herein. The formulation was first developed by Fredlund at the University of Saskatchewan in the 1970's. The method incorporates most other limit equilibrium method's key elements found in SLOPE/W. The GLE method bases two types of equations. One of the equations gives a factor of safety with respect to moment equilibrium, F_M and the other gives a factor of safety with respect to horizontal force equilibrium, F_f.

$$F_m = \frac{\sum(c'\beta R+(N-u\beta)R\tan\varphi')}{\sum W_x-\sum Nf\pm\sum Dd} \qquad 4\text{-}1$$

$$F_f = \frac{\sum(c'\beta\cos\alpha+(N-u\beta)\tan\varphi'\cos\alpha)}{\sum N\sin\alpha-\sum D\cos\omega} \qquad 4\text{-}2$$

Where: c' = effective cohesion D = concentrated point load

ϕ' = effective angle of friction β, R, x, f, d, ω = geometric parameters

u = pore-water pressure α = inclination of slice base

N = slice base normal force, $N = \frac{W+(X_R-X_L)-\frac{(c'\beta\sin\alpha+u\beta\sin\alpha\tan\varphi')}{F}}{\cos\alpha+\frac{\sin\alpha\tan\varphi'}{F}}$

W = slice weight

There is one characteristic in the two factor of safety equations and the base normal equation that have a profound consequences. In the end of the analysis there is only one factor of safety for the overall slope. F_m and F_f are the same when both moment and force equilibrium are satisfied. This same value appears in the equation for the normal at the slice base. This means the factor of safety is the same for each and every slice.

The analysis carried out using the data and methods from this chapter and the corresponding results are presented in the next chapter.

Chapter 4: Data and Methods

5. Results and Interpretation

5.1 Introduction

Data from insitu and laboratory test and methods to be followed while carrying out the analysis were presented in the previous chapter. This chapter deals with parameters and assumptions taken for the advanced numerical analysis and also presents the result from the analysis. Some parameters are calculated based on the insitu and lab data. The calculation of these parameters was done by making use of approaches discussed in the literature review chapter.

5.2 Input Parameters and Assumptions

5.2.1 Geometry

In GeoStudio, the geometry of a model is defined in its entirety prior to consideration of the discretization or meshing. The geometry of the ground condition is developed based on the terrain condition shown on figure 5.1. The slope follows the yellow cross section line on this figure. While modeling soil regions were specified, geometry lines were drawn at the location where there is a change in soil property, soil material models were created and assigned onto the geometry objects and pre-defined boundary conditions were drawn on the region edge. Since the analysis incorporated finite element numerical method, the continuum is subdivided into finite elements. Herein the global element size is specified as 1.0 meters.

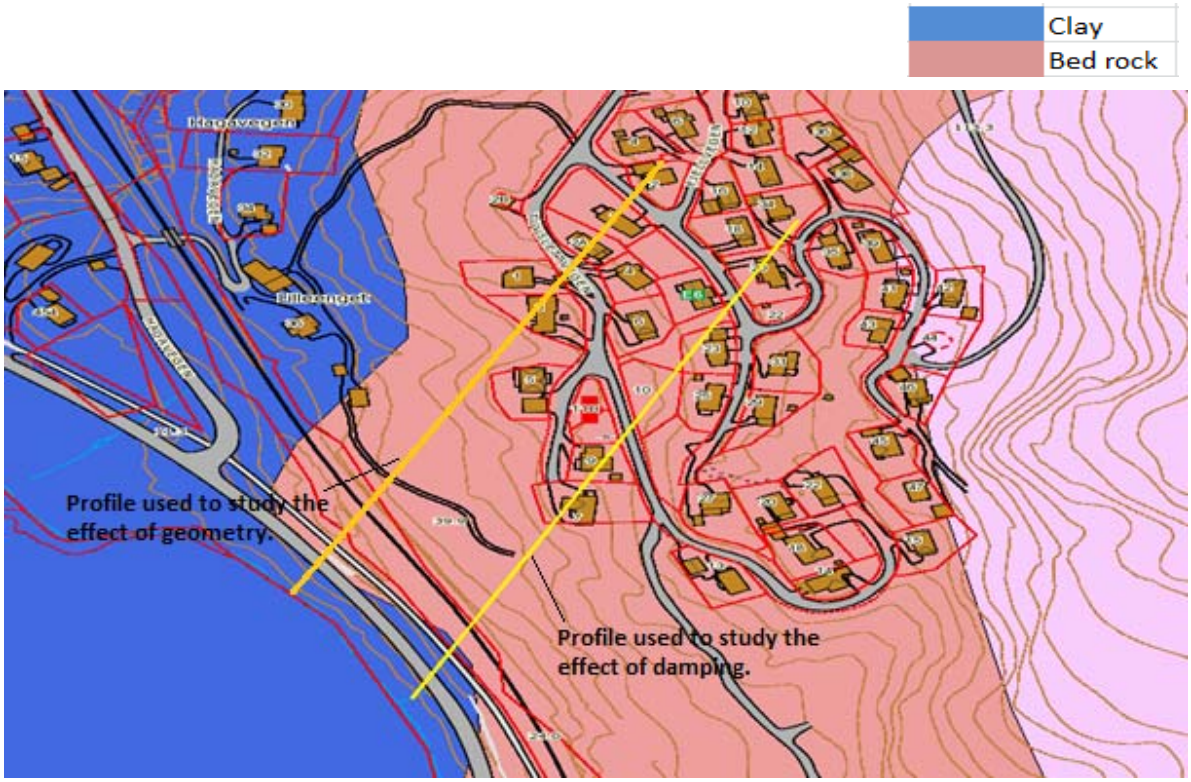

Figure 5-1 Plan view of the slope considered

The yellow cross section line crosses two types of ground condition. The blue region represents the clay layer and the orange coloured region shows where the bed rock is found. The orange colour region is also the location where the blasting was carried out for the tunnel construction in 1996.

Three kinds of models are created with a slope angle of approximately 17^{o} to see the effect of having a clay layer on top of the bed rock and without. Also a model to see the effect of the distance between the shore line and the end of the clay region is created.

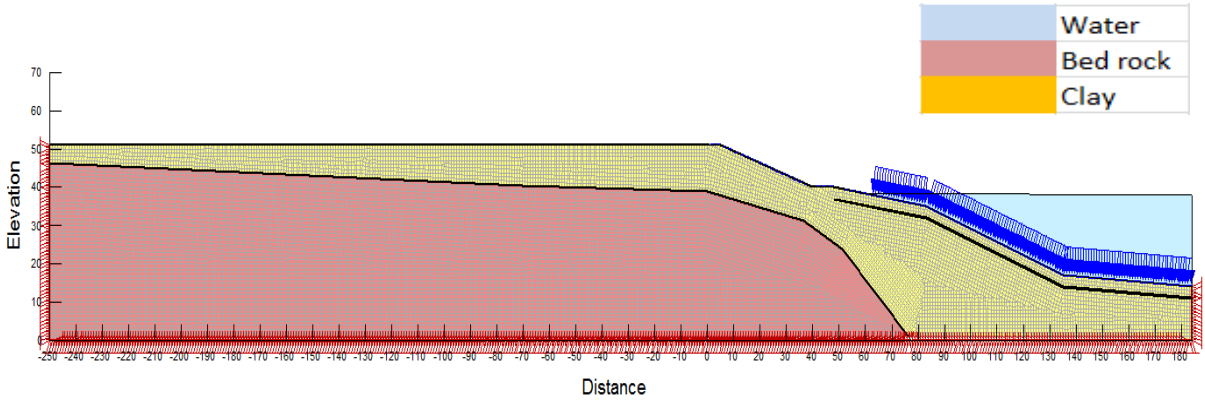

Figure 5-2 Model 1

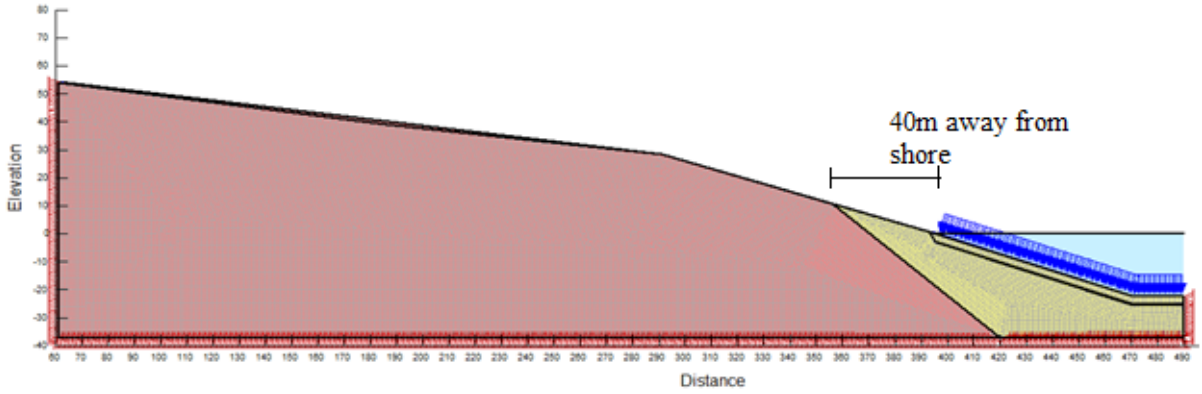

Figure 5-3 Model 2

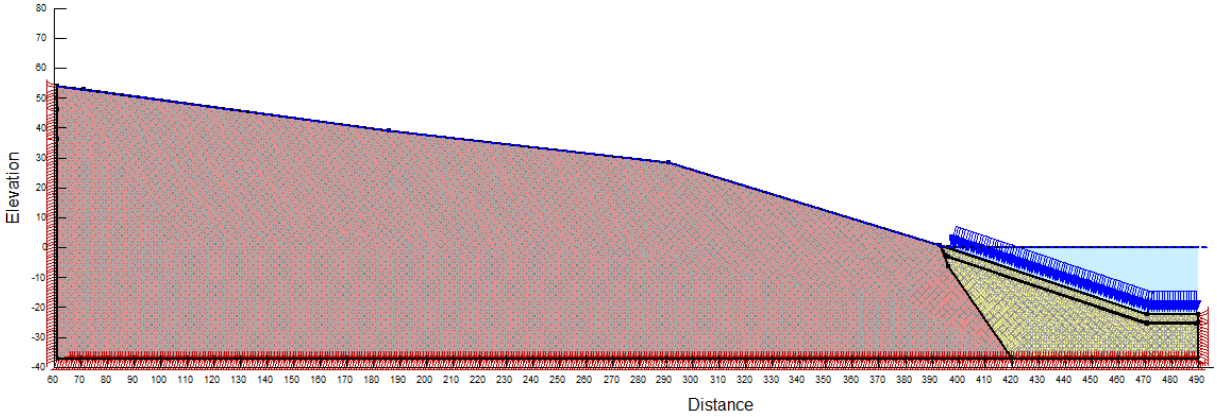

Figure 5-4 Model 3

Figure 5.2 shows the model created to see the effect of having a clay layer on top of the bed rock. Figure 5.3 and 5.4 are models to see the effect of not having the clay layer on top and also to see if the distance between the shore line and the clay region has any significance on the generation of excess pore pressure.

It is mentioned, in previous sections, that the thickness of the sand layer is between 15cm to 20cm. Compared to the other materials, the sand layer is very thin. The bold line below the sea floor on figures 5-2 to 5-4 is the thin sand layer. Figure 5.5 shows a closer look of this layer. The green thin layer represents the sand layer.

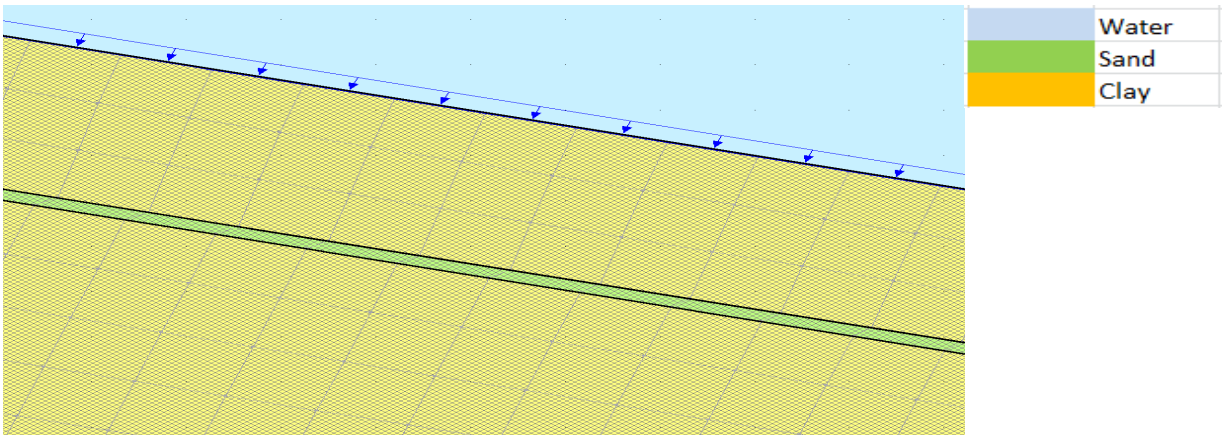

Figure 5-5 Thin sand layer

At the time when the slide occurred in 1996, the distance between the point of blasting and slide scar was approximately 400m (Statens vegvesen report). Based on this information the modeling is done in such a way that there will be a 400m difference between the application of the blast loading and the underwater slope.

QUAKE/W, like all other finite element products in GeoStudio, is a boundary valued analysis; i.e. the problem consists of only a small portion of the real domain and consequently it is necessary to specify conditions along the boundaries where the analysis section has been lifted out of the actual field domain. Apart from the fixities, horizontal and vertical fixities, the loading is also provided as a boundary condition. Figure 5.6 shows how the blast load is applied.

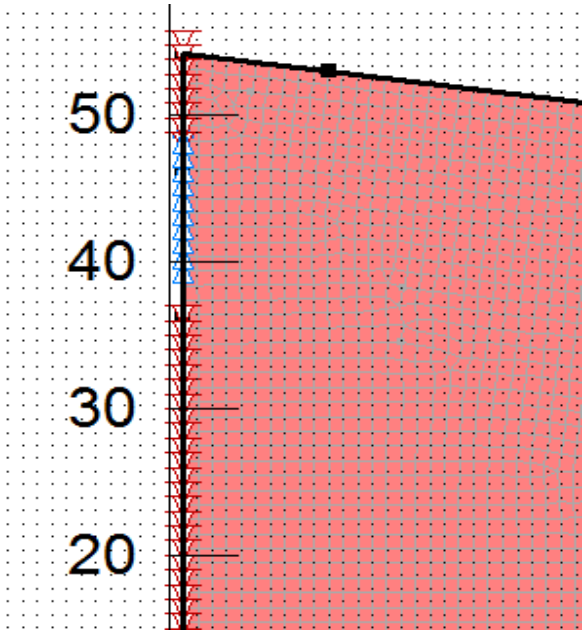

The blue arrow represents the blast loading. All boundary conditions are applied directly on geometry items such as region faces, region lines, free lines or free points. It's not possible to apply a boundary condition directly on an element edge or node. The advantage of connecting the boundary condition with the geometry is that it becomes independent of the mesh and the mesh can be changed if necessary without losing the boundary condition specification.

Figure 5-6 Boundary condition

For the slope stability analysis the same model in QUAKE/W is used on SLOPE/W. In addition to the previous model a fully specified slip surface is introduced. This 'fully specified slip surface' is one of the features of SLOPE/W where a slip surface can be specified with a series of data points. This allows for complete flexibility in the position and shape of the slip surface. This method is useful when large portion of the slip surface position is known from slope inclinometer field measurement, geological stratigraphic controls and surface observations. The slip surface of the Finneidfjord landslide is one of the given we have. Therefore based on previous studies it was possible to model the slip surface as shown on Figure 5.7.

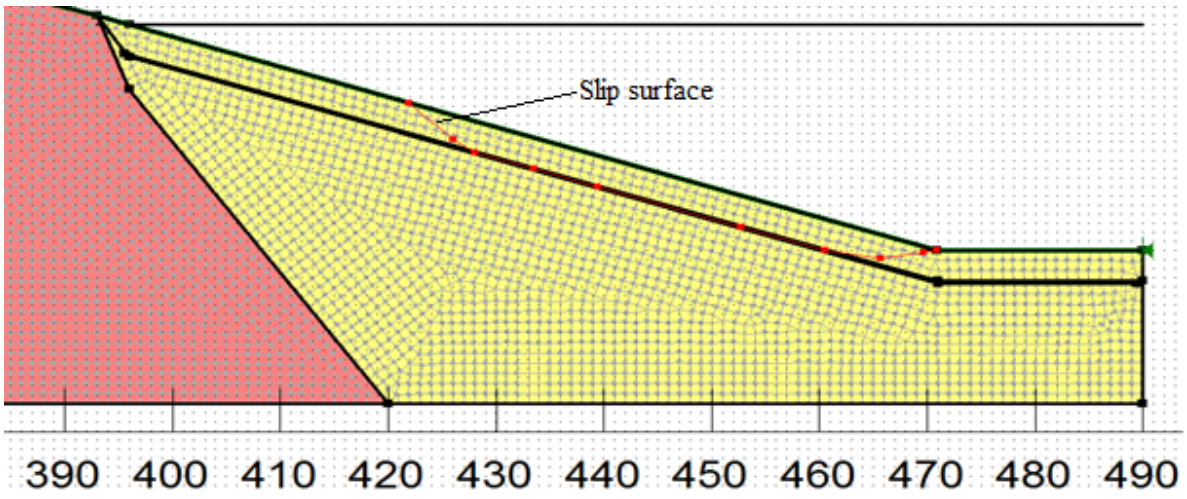

Figure 5-7 fully specified slip surface

5.2.2 Parameters

Gmax

The shear modulus, G=Gmax, at small strain amplitude, which is typically 10^{-6} (=0.00001%) or less, is considered as one of the basic soil parameters. This modulus is most adequately determined from shear wave velocity (Vs) which is measured directly in-situ, $V_s = \sqrt{G\max/\rho}$. According to the measurement done at Finneidfjord in 1999 the shear wave velocity was measured to be 115m/sec.

$$G_{\max(clay)} = V_s^2 * \rho_{clay}$$
$$= 115^2\, {}^{m}/_{sec} * 1900\, {}^{kg}/_{m^3}$$
$$= 25.13MPa$$

$$G_{\max(sand)} = V_s^2 * \rho_{sand}$$
$$= 115^2\, {}^{m}/_{sec} * 1700\, {}^{kg}/_{m^3}$$
$$= 22.5MPa$$

Angle of friction, Robertson and Campanella, 1983

The angle of friction of the sand layer is calculated by an empirical relation from Robertson and Campanella, 1983.

$$tan\varphi = \frac{1}{2.68}\left[log\left(\frac{q_c}{\sigma'_{vo}}\right) + 0.29\right]$$

Where q_c is cone resistance in the sand layer and σ'_{vo} is effective overburden stress.

$$tan\varphi = \frac{1}{2.68}\left[log\left(\frac{381.7KPa}{21.358KPa}\right) + 0.29\right]$$

$$tan\varphi = 0.575$$

$$\varphi = 30^o$$

Relative density, Baldi et al. 1986

The relative density is calculated from an empirical relation from Baldi et al. 1986.

$$D_r = \frac{1}{C_2} ln \frac{Q_{cn}}{C_o}$$

Where Q_{cn} is normalized CPT resistance, corrected for overburden pressure (more recently defined as Qtn, using net cone resistance, qn)

Co and C2 are soil constants.

$$Q_{cn} = \frac{q_c}{P_a} \Big/ \left(\frac{\sigma'_{vo}}{P_a}\right)^{0.5}$$

C_o=15.7

C_2=2.41

P_a=ref. Pressure 100Kpa

$$Q_{cn} = \frac{381.7KPa}{100KPa} \Big/ \left(\frac{21.36KPa}{100KPa}\right)^{0.5}$$

$$Q_{cn} = 8.26$$

$$D_r = \frac{1}{2.41} ln \frac{8.26}{15.7}$$

$$D_r = 22\%$$

According to table 2.1 in section 2.2 ¨ Theory of liquefaction¨ sand with a relative density of 22% is categorized as loose sand.

Pore-pressure ratio (ru) function

The pore pressure generated during a cyclic loading is a function of the equivalent number of uniform cycles, N, for a particular loading and the number of cycles, N_L, which will cause liquefaction for a particular soil under a particular set of stress conditions. The ratio of N/NL is then related to a pore pressure parameter r_u as shown in Figure 5.8. The pore pressure function used herein is a sample function found in QUAKE/W.

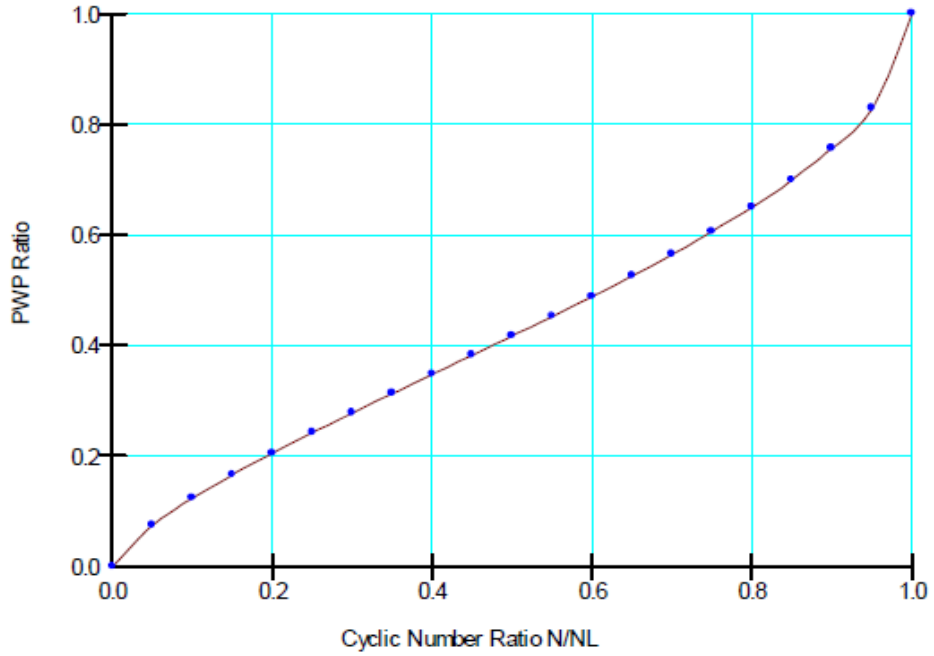

Figure 5-8 Cyclic number ratio N/N_L Vs pore pressure ratio r_u, QUAKE/W 2007 engineering book

Figure 5.8 is based on the equation; $r_u = \frac{1}{2} + \frac{1}{\pi} sin^{-1}\left[2\left(\frac{N}{N_L}\right)^{\frac{1}{\alpha}} - 1\right]$

It is possible to have various functions by changing the value of α which depends on soil property and test condition. α=0.7 is used herein which is an average value of the upper and lower boundary value of observed bounds of excess pore pressure generation functions. The observations done by Seed et. al. (1975) is presented in chapter 2 figure 2-7.

Cyclic number function

As discussed in the previous chapter, the concept of liquefaction is related with cyclic stress ratio, CSR and the number of cycles required to produce liquefaction. The relationship between these two factors is described by a function called Cyclic Number function. A typical function used herein and found in QUAKE/W is presented in Figure 5.9.

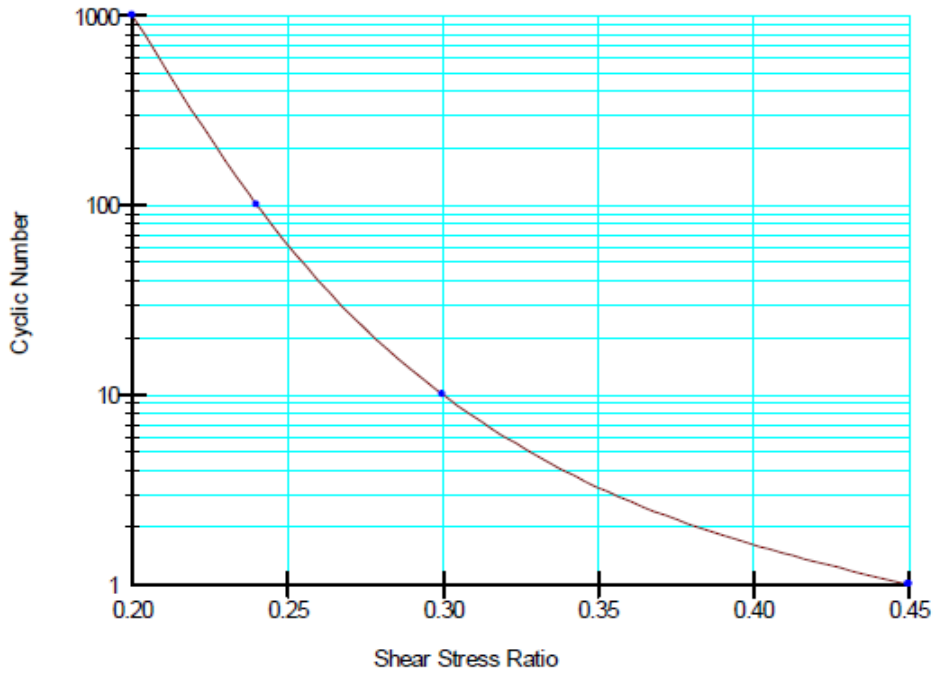

Figure 5-9 Cyclic number function, QUAKE/W 2007 engineering book

The above two functions i.e. cyclic number function and Pore-pressure ratio (r_u) function are only sample functions and can only be used for preliminary or educational purpose only. They can be used as guide as to what is required when running a dynamic analysis. They are usually obtained from cyclic laboratory test, therefore in order to get an actual result; laboratory test should be carried out.

5.2.3 Damping

Damping ratio of sand

The damping ratio of sand varies with cyclic shear strain amplitude and effective stress level and it is independent of loading frequency **(**Rollins et al. 1998). The effect of void ratio and anisotropic consolidation is negligible. Over consolidation is not important either. Sand becomes stiffer with the number of cyclic loading. The influence of vertical confining pressure, σ_v' less than 25KPa can be significant, which represent conditions in the top few meters of soils but as we get dipper the influence gets smaller (Kramer 1996).

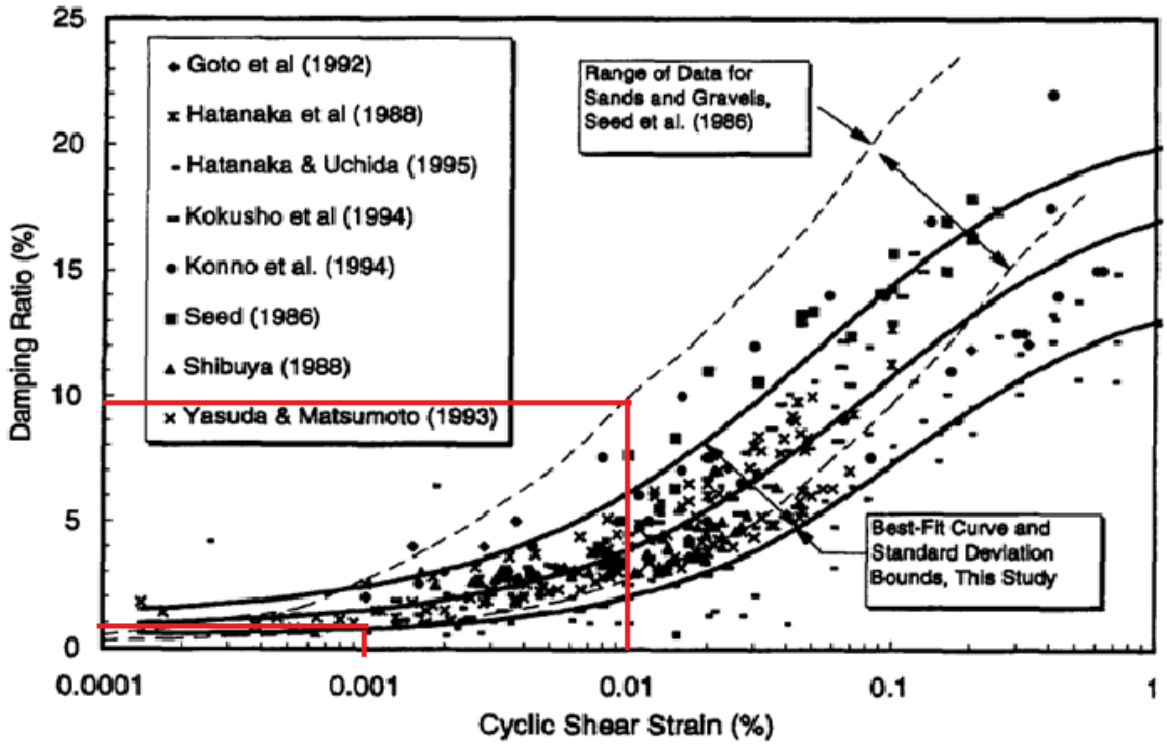

Figure 5-10 Data points defining ξ and γ relationship from different investigations, (Rollins et al. 1998)

According to the measurement taken in 1999, a cyclic shear strain of 1.0 $*10^{-3}$ % at a 50% confidence level and 4.8 $*10^{-3}$ % at a 95% confidence level was reported (NGI report). The red marked region on figure 5.10 is done by taking 1.0 $*10^{-3}$ % of shear strain as a lower bound and 1.0 $*10^{-2}$ % as an upper bound. For the analysis herein, a damping ratio between 1% and 10% is considered. The maximum damping ratio for sandy soil is 33.3 %(Isshibashi and Zhang, 1993) and a result using this value is also presented.

Damping ratio of clay

The damping ratio of clay is not affected by loading frequency and effective stress. The effect of consolidation time seems less important (Kramer 1996). Like sand, the damping ratio varies with the number of loading cycle. Unlike sand, clay becomes softer with the number of cyclic loading and this is because the bonding between clay particles is destroyed and the effective stress is

decreased due to the excess pore pressure generated. The damping ratio is also significantly affected by plasticity index, I_p

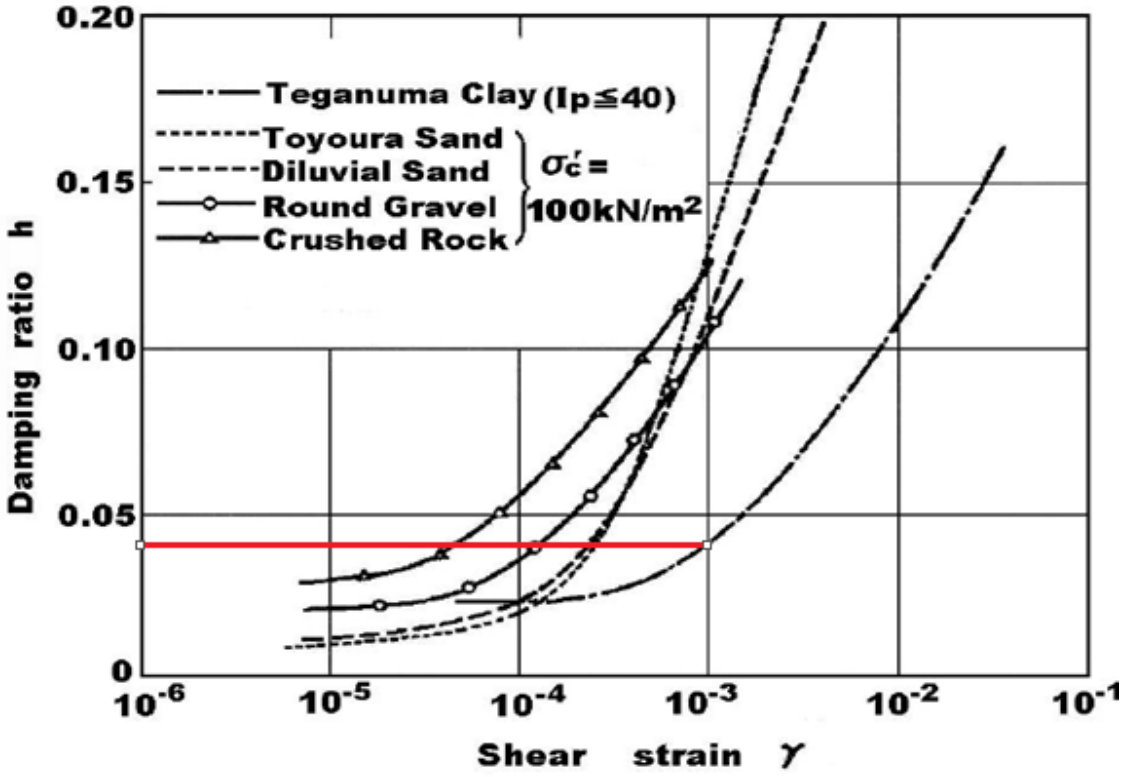

Figure 5-11 Damping ratio of clay, sand, and gravel, (from Towhata 2008)

As can be seen from figure 5.11, damping ratio of clay is smaller than other coarser materials. This is probably because clay is more continuous than sand and gravel. Based on the investigation done in 1999 the reported cyclic shear strain is 10^{-3} %. The red line in figure 5.11 shows the corresponding damping ratio used herein.

5.2.4 Vibration Record

In 1999 there was an investigation carried out by Statens Vegvesen and NGI at Finneidfjord to see if the blasting for the tunnel construction in 1996 has caused the landslide. During this investigation it was possible to measure 3 different time histories shown in the figures below. Figure 5.12, 5.13, and 5.14 shows blast vibration data in terms of velocity Vs time from 1150kg, 150kg and 350kg of dynamite respectively. The one in figure 5.12, i.e. the 1150kg dynamite, was

for the purpose of road cut as part of a road construction at the time of investigation. The other two were for the sole purpose of the investigation. The frequency is about 20Hz which is common for blasting and it has a pick particle velocity of 8mm/s. The distance between the measurement point and the blast location varies between 60m to 175m.

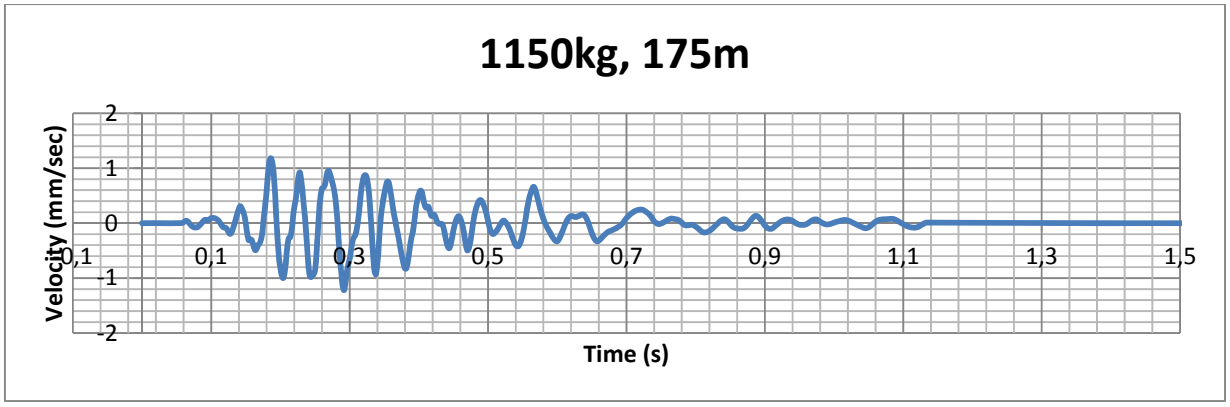

Figure 5-12 Blast vibration from 1150kg Dynamite, (NGI, 1999)

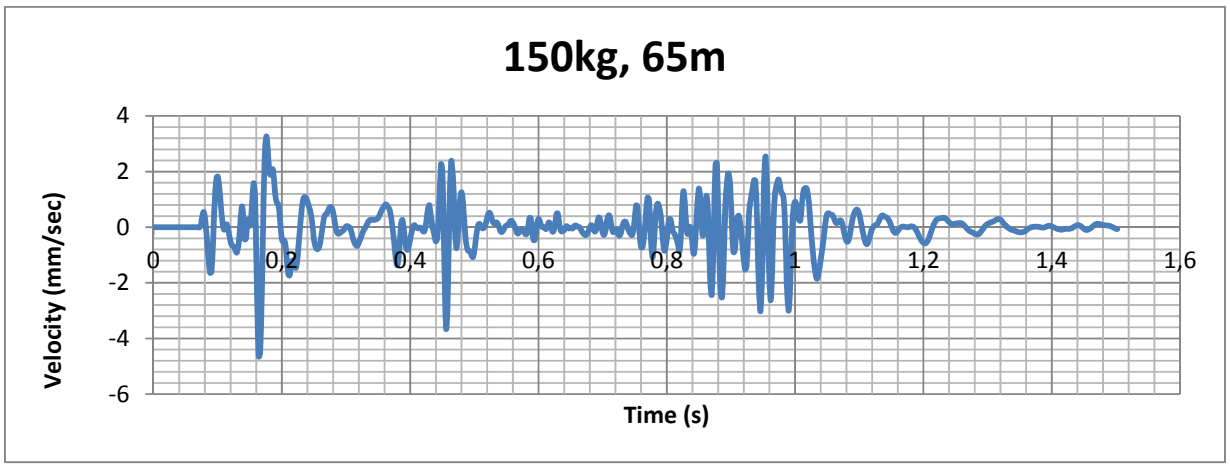

Figure 5-13 Blast vibration from 150kg Dynamite, (NGI, 1999)

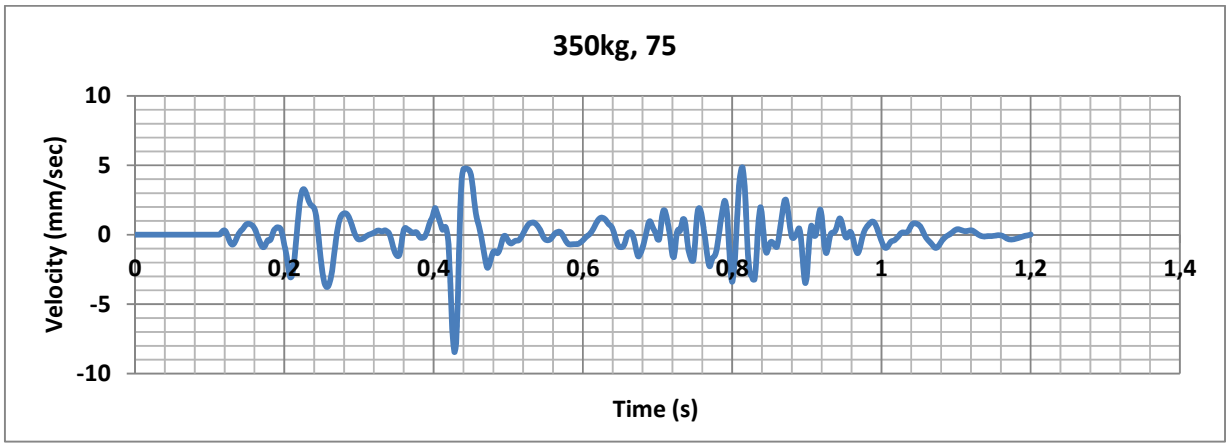

Figure 5-14 Blast vibration from 350kg Dynamite, (NGI, 1999)

Statens vegvesen, (1999) has reported that the amount of dynamite used at the time when the slide occurred in 1996 was 150kg. From the vibration data we have the one shown on figure 5.13 is thought to represent the real condition. One of the advantages of using QUAKE/W is, it lets the user to provide vibration measurement from an earthquake or blasting as a loading for the dynamic analysis.

Table 5-1 Material properties used for dynamic and slope stability analysis

Material	Property	Symbol	Value	Unit
Sand	Unit weight	ρ	17	KN/m^3
	Angle of friction	ϕ	30	[^{o}] degree
	Relative density	D_r	22	%
	Shear modulus	G_{max}	22.5	MPa
	Poisson's ratio	υ	0.3	[-]
	Damping ratio	ξ	1-10	%
Clay	Unit weight	ρ	19	KN/m^3
	Cohesion	c	2.5	KPa/m
	Plasticity index	I_P	6	[-]
	Liquidity index	I_L	2.5	[-]
	Shear modulus	G_{max}	25.13	MPa
	Poisson's ratio	υ	0.3	[-]
	Damping ratio	ξ	4	%
Bed rock	Unit weight	ρ	20	KN/m^3
	Shear modulus	G_{max}	100	MPa
	Poisson's ratio	υ	0.3	[-]
	Damping ratio	ξ	1	%

Table 5.1 shows most of the material data used for the analysis results to be presented in the next sections.

5.3 Dynamic Analysis Result

Three types of cases are analyzed using the above mentioned inputs on QUAKE/W. Two cases to see the effect of damping by introducing the clay layer on top of the bed rock on one model and without this layer on the other are considered. One additional case was considered to see the effect of geometry on the generation of excess pore pressure.

The results obtained are presented below. It should be noted that the excess pore pressure generated and the liquefaction conditions are the main aim here. The stability condition due to the generated excess pore pressure is analyzed with SLOPE/W and will be presented later in this chapter.

5.3.1 Effect of Damping

The effect of damping is analyzed using three different values of damping ratio for the sand layer and the results are presented in figures 5-15 to 5-18.

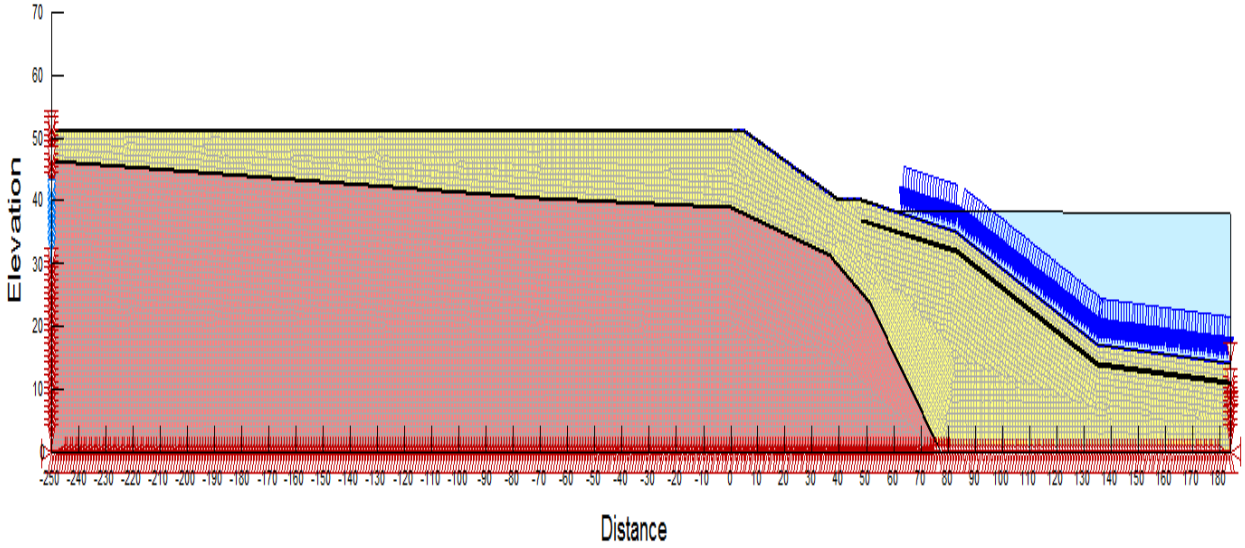

Figure 5-15 Model with clay on top of the bed rock.

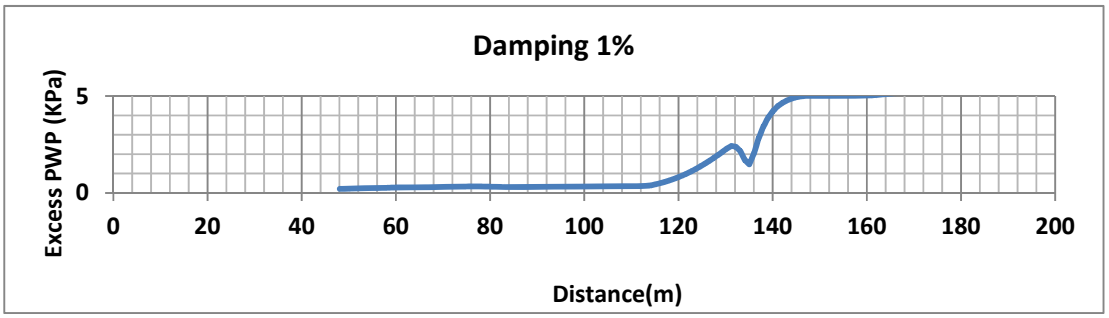

Figure 5-16 Damping ratio of sand, 1%

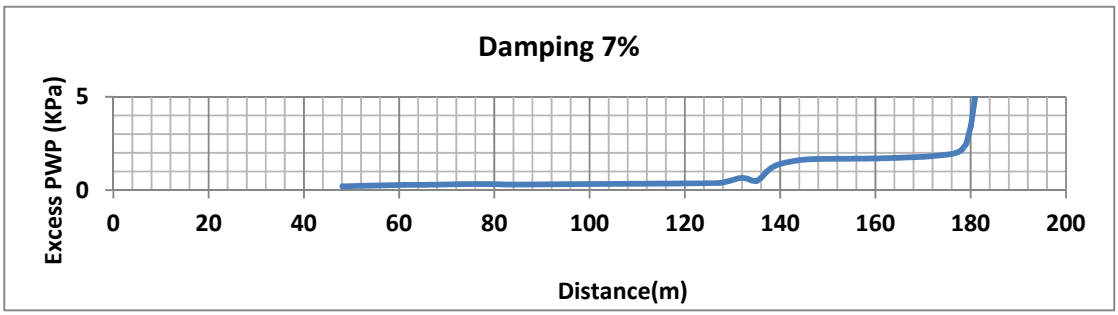

Figure 5-17 Damping ratio of sand, 7%

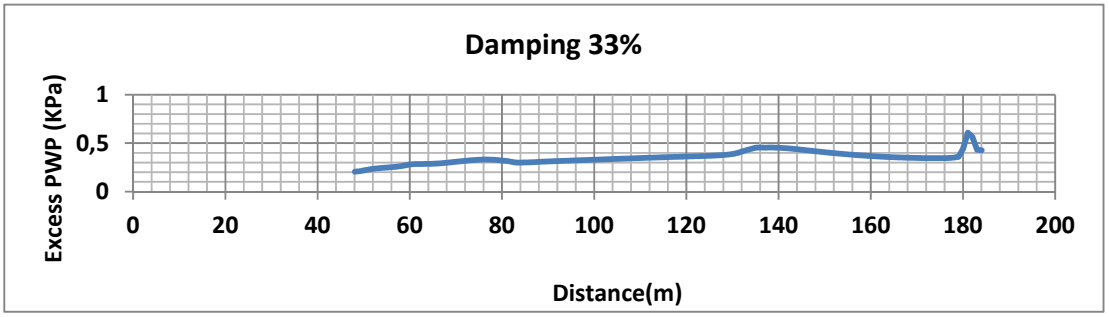

Figure 5-18 Damping ratio of sand, 33%

The extent of the clay layer on top of the bed rock, depth wise, is not exactly known. According to the geological map shown on figure 5.1, the location where the clay material and where the bed rock are clearly distinguished. Therefore to take into consideration, even if not exactly known, the fact that there is a couple of meters of soil material on top of the bed rock, the model shown on figure 5-15 is created.

Figure 5-15 shows the model and loading condition for the dynamic analysis with the clay layer on top of the bed rock. The curves on figure 5-16 to 5-18 show the excess pore pressure distribution along the sand layer. The distribution curves show that excess PWP is low around the top of the slope where the sand layer begins and gets higher around the toe. An average of 4kPa, 1.5kPa and 0.4kPa of excess PWP is generated taking 1%, 7% and 33% damping ratio of sand respectively. The main focus herein is the excess pore water pressure generated in the sand layer. Therefore the presented curves are solely for the excess PWP generated in the sand layer.

5.3.2 Effect of Geometry

In this section the effect of geometry is analyzed. For this purpose a model without the clay layer on top of the bed rock is considered. This is done in order to see both the effect of geometry and the absence of the clay layer together. The location where the clay layer begins is shown on figure 5.1. Two models are considered here. Figure 5-19 represent the profile where the clay layer starts 40m away from the shore and figure 5-20 represents the profile where the clay layer starts and the shore are located at the same place.

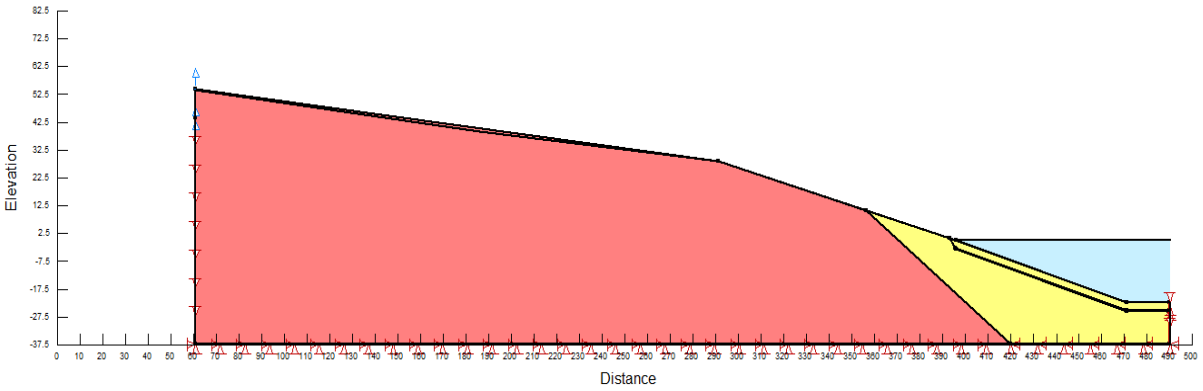

Figure 5-19 Clay region ends 40m away from the shore

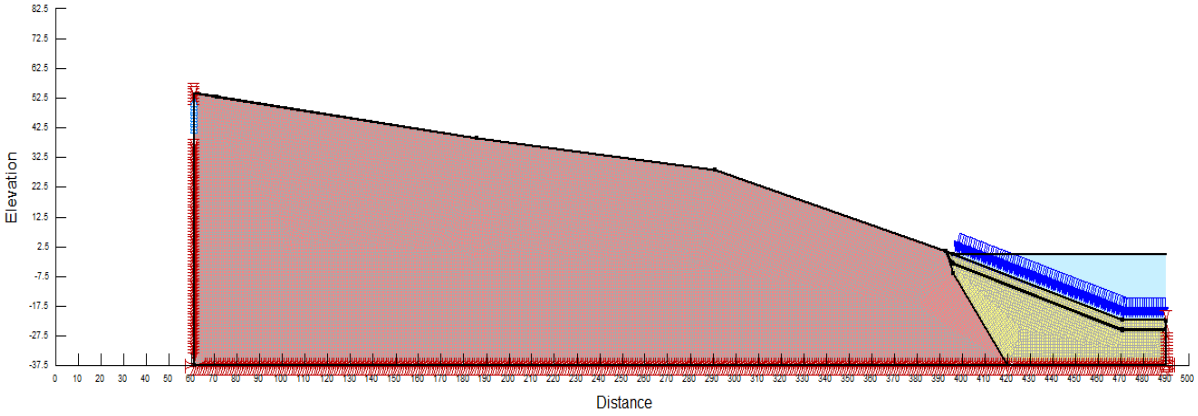

Figure 5-20 Clay region ends at the shore

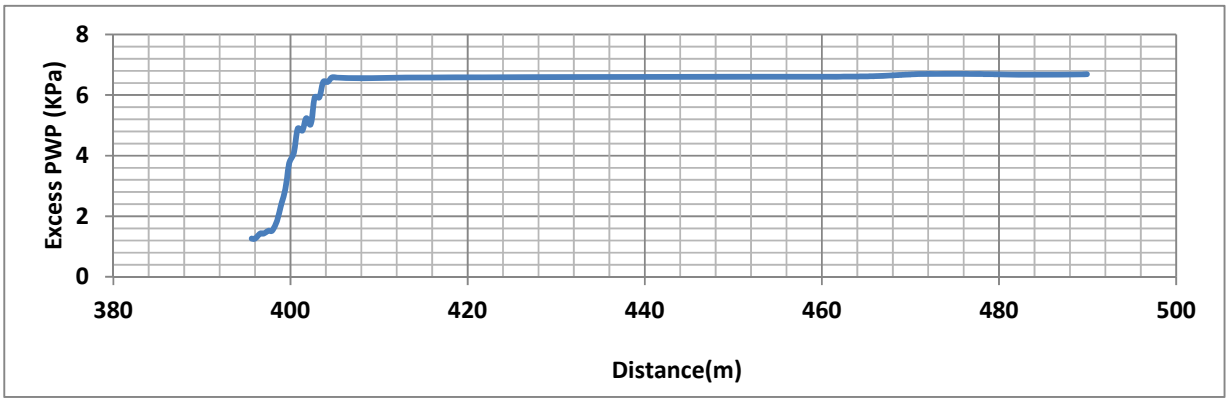

Figure 5-21 Typical excess pore pressure diagram

The result from this section analysis is shown on figure 5-21. Even though two analyses are carried out the results are almost the same. Therefore showing one representative curve is sufficient. An average of 6kPa excess PWP is generated. The distribution of the excess PWP is almost uniform throughout the sand layer. These analyses show that the effect of geometry i.e. the location where the clay region starts has less significance, but the presence of the clay layer on top of the bed rock plays a great role in taking the energy from the blasting. The effect of changing the damping ratio of the sand layer is also checked but the result is same as the one shown on figure 5.21.

Therefor from the above discussed cases, given the specified inputs, an excess PWP of 0.4kPa to 6kPa is believed to be generated due to the blasting.

5.3.3 Liquefaction Analysis Result

Liquefaction analysis result from QUAKE/W and analytical analysis is presented in this section.

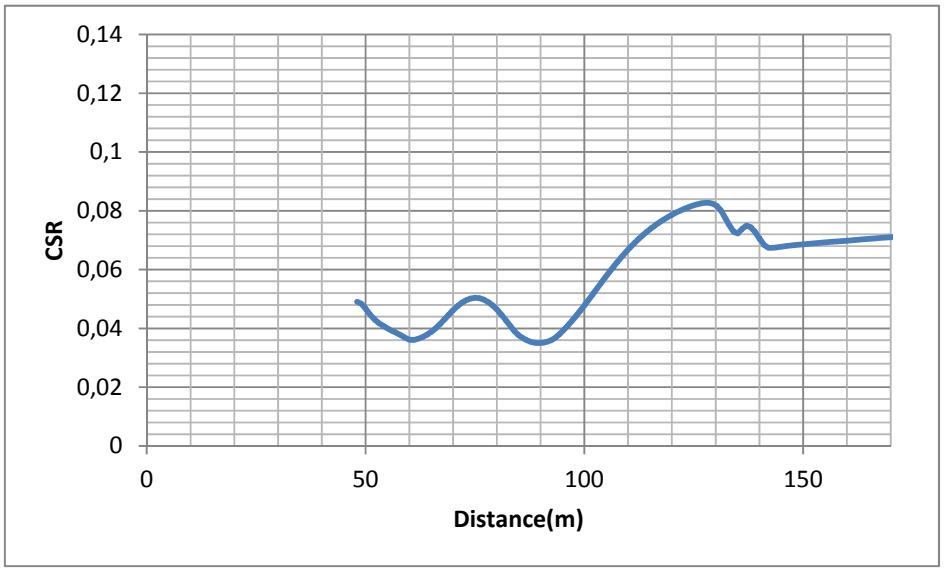

Figure 5-22 Typical cyclic stress ratio Vs Distance curve

Figure 5.22 shows a typical cyclic stress situation in the sand layer taken from the model shown on figure 5-15. It was discussed in chapter 2 that cyclic stress ratio is one of the input for the calculation of safety factor against liquefaction. For a pick acceleration of approximately 0.05g, from the vibration data presented earlier, an average CSR of 0.07 is obtained from QUAKE/W. Using the empirical relations discussed in the literature, the following results are obtained;

$$\mathrm{CSR} = \left(\frac{\tau_{av}}{\sigma'_{vo}}\right) = 0.65\left(\frac{a_{max}}{g}\right)\left(\frac{\sigma_{vo}}{\sigma'_{vo}}\right) r_d$$

$$\mathrm{CSR} = \left(\frac{\tau_{av}}{\sigma'_{vo}}\right) = 0.65\left(\frac{0.05g}{g}\right)\left(\frac{52}{27}\right) 0.976$$

$$\mathrm{CSR} = 0.061$$

The result obtained using the empirical relation and QUAKE/W are almost the same.

As for the cyclic resistance ratio, $CRR_{7.5}$, a calculation based on CPTU data is given in the appendix and it was calculated to be 0.05. The empirical relation used for the calculation is developed for an earthquake of magnitude 7.5 and since the magnitude of the blasting is less

than magnitude 7.5 a scaling factor is required. The factors given in table 2.2, chapter2, are only for magnitude of 7.5 to 5.5. Assuming the lower boundary value on the table, i.e 5.5, a scaling factor of 2.86 for a PI<20% is taken. With this an equivalent value of CRR=0.143 is calculated. This value could be even be greater if a scaling factor for a lesser magnitude was available. Table 2.2 shows that scaling factor gets higher as the magnitude gets lower. It is also possible to calculate $CRR_{7.5}$ using the measured shear wave velocity;

$$CRR_{7.5} = 0.22\left(\frac{V_{s1}}{100}\right) + 2.8\left(\frac{1}{(V_{slc} - V_{s1})} - \frac{1}{V_{slc}}\right) \qquad 5\text{-}1$$

$$CRR_{7.5} = 0.22\left(\frac{115\text{m/s}}{100}\right) + 2.8\left(\frac{1}{(210\text{m/s} - 115\text{m/s})} - \frac{1}{210\text{m/s}}\right) = 0.045$$

The safety factors against liquefaction will be;

$$\text{FS} = \frac{\text{CRR}}{\text{CSR}}$$

$$\text{FS} = \frac{0.143}{0.061} = 2.3$$

The calculated factor of safety shows that the sand layer is far from liquefying with the amount of blasting carried out. From this section result i.e. with the generated excess PWP a slope stability analysis result is presented in the next section.

5.4 Slope Stability Analysis Results

Once the FEM analysis is finished, the results can be used for the next step that is the slope stability analysis. Being part of the geotechnical integrated suit, GeoStudio, SLOPE/W is able to use the finite element computed pore-water pressure and stress in the stability analysis

The dynamic analysis shows that liquefaction is not a major treat or not a treat at all. Therefore, while working with the slope stability the excess pore pressure will be the main focus. SLOPE/W has a various ways of specifying the pore-water pressure condition. From all the options, specifying using R_u coefficient is found to be more appealing. The method is chosen based on the fact that there is an existing excess pore pressure mentioned in the existing excess PWP

sectio and it allows combining the calculated and the existing and applying it for the stability calculation.

The pore-water pressure ratio R_u is coefficient that relates the pore-water pressure to the overburden stress and it is given by:

$$R_u = \frac{u}{\sigma'} \qquad 5\text{-}2$$

Where: u = pore water pressure

σ' = effective vertical over burden stress

The coefficient can vary throughout the slope. Therefore it's recommended to use a better option while dealing with a real project. For an educational purpose taking an average condition can be tolerated. Saying this, the different slope stability analyses carried out using the excess pore pressure from the dynamic analysis and from the field measured pore pressure are presented below.

5.4.1 Initial Condition

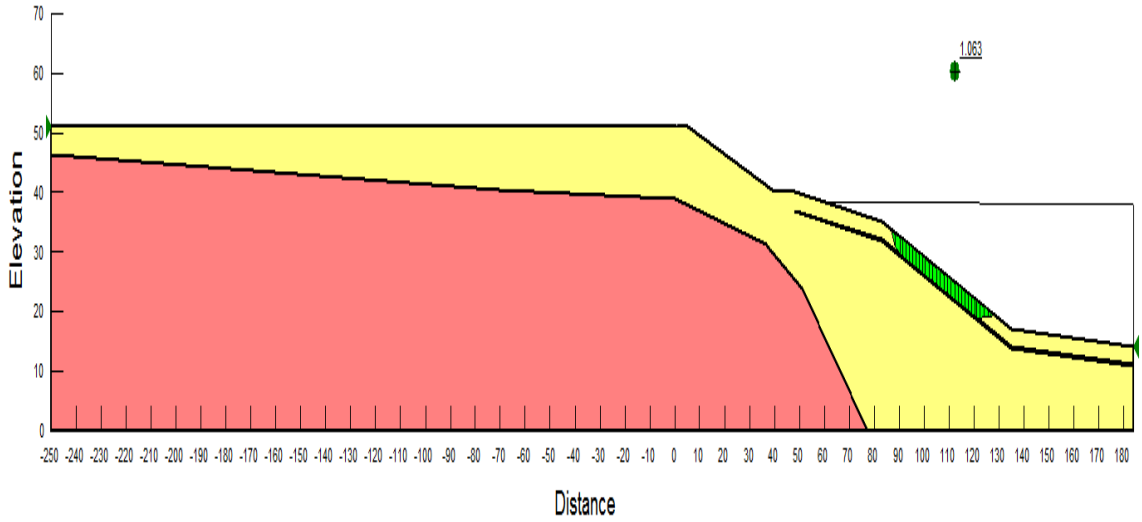

Figure 5-23 Initial condition

Figure 5-23 is the result obtained before applying the blast loading. The measured excess PWP is considered and a factor of safety 1.063 is calculated. This result shows the stability condition of the slope prior to blasting which is quite low.

5.4.2 Effect of Damping

This section presents the slope stability analysis result using the excess PWP generated in section 5.3.1 i.e. excess PWP calculated by varying the damping ration of the sand with the clay layer on top of the bed rock. The measures excess PWP is also included.

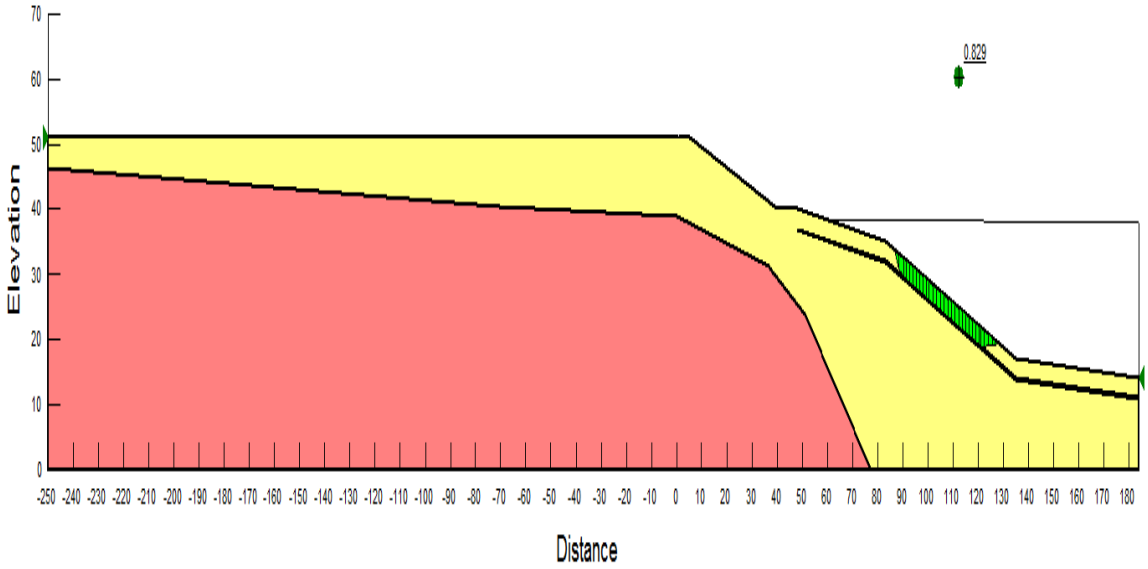

Figure 5-24 Factor of safety for 1% damping ratio

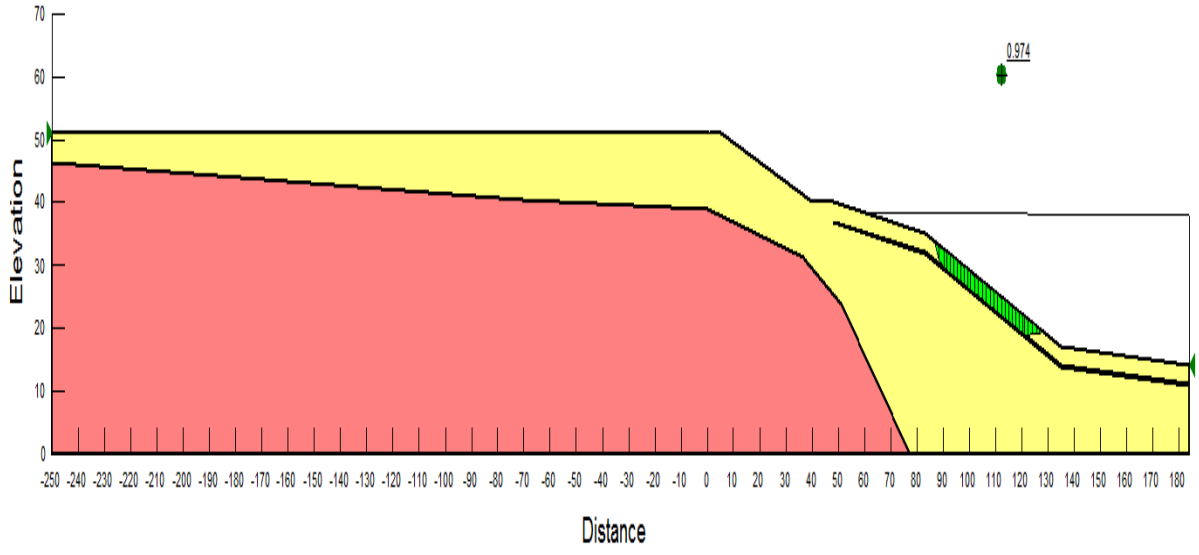

Figure 5-25 Factor of safety for 7% damping ratio

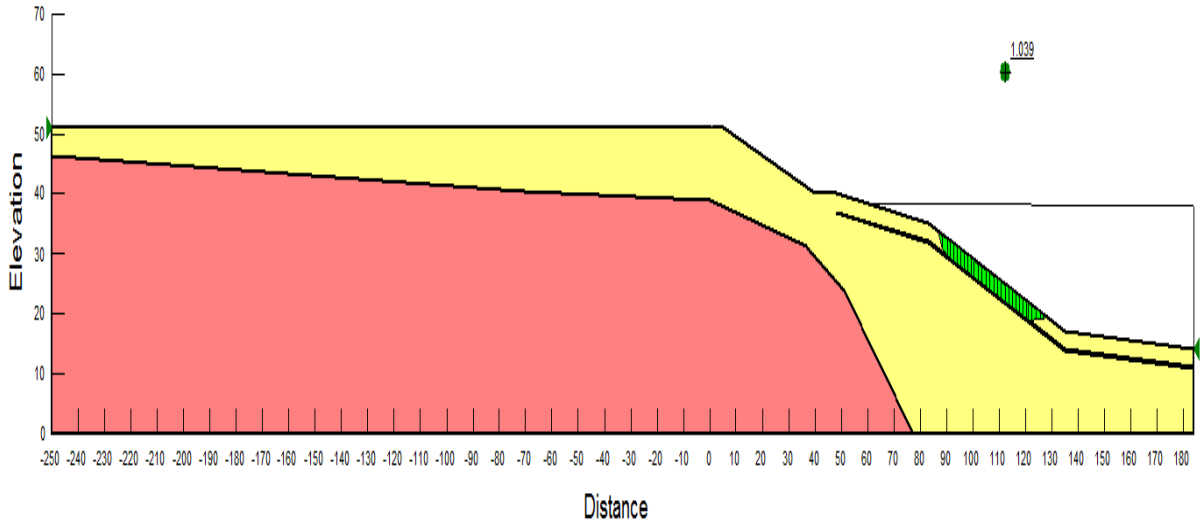

Figure 5-26 Factor of safety for 33% damping ratio

Figure 5-24, 5-25 and 5-26 shows the factor of safety calculated for 1%, 7% and 33% damping ratio respectively. In the same order a factor of safety of 0.829, 0.974 and 1.039 is obtained. The results show how sensitive the slope is since it was on the verge of failure even before the blasting.

5.4.3 Effect of Geometry

This section presents the slope stability analysis result using the excess PWP generated in section 5.3.2 i.e. excess PWP calculated by varying the geometry of the model without the clay layer on top of the bed rock. The measures excess PWP is also included. As discussed in the dynamic analysis section, the effect of changing the geometry, i.e. changing the location where the clay layer starts, is not significant. This is also true for the stability analysis there for presenting one representative result is sufficient. Figure 5.27 show the result from this analysis.

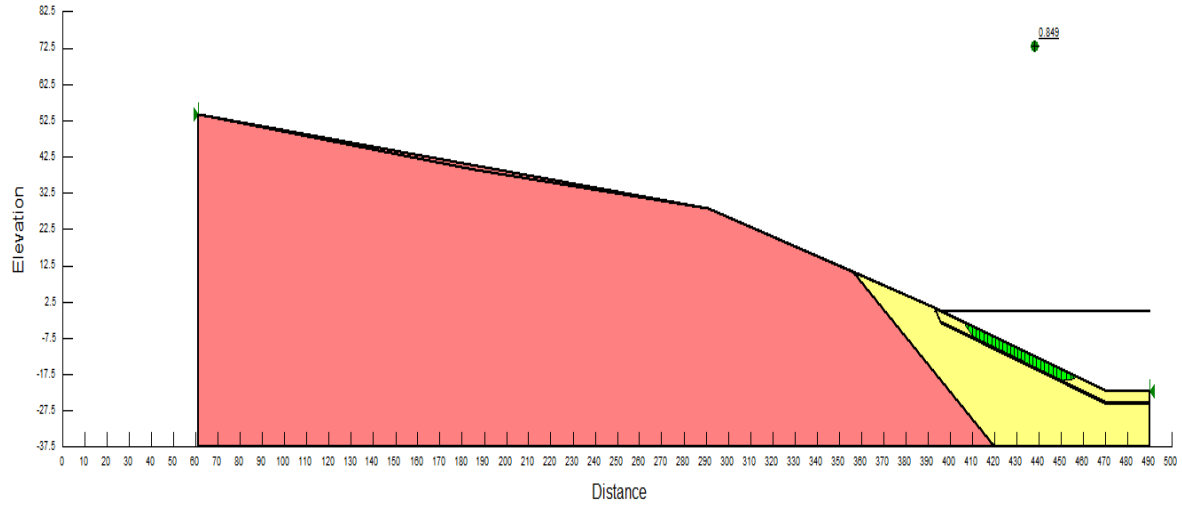

Figure 5-27 Factor of safety without considering the clay layer on the bed rock

A factor of safety of 0.849 is obtained from this analysis.

The loose sand layer is found approximately 3m below the sea bed. Assuming that the material above the sand layer is only clay, the effective vertical overburden stress is calculated as:

σ'=γ'*H

= 9KN/m^3 * 3m= 27kPa

27kPa is used to calculate the R_u coefficient used for each analysis. A summary of the calculated R_u with the corresponding calculated factor of safety is presented in table 5.2.

Table 5-2 R_u coefficient and calculated factor of safety

Case	Dynamic PWP	Total PWP	$R_u = \frac{u}{\sigma'}$	Factor of safety
Initial condition	-	8	0.296	1.063
ξ=1%	4	12	0.44	0.829
ξ=7%	1.5	9.5	0.35	0.974
ξ=33%	0.4	8.4	0.311	1.039
w/o clay layer	6	14	0.518	0.849

- The total excess pore pressure is calculated by adding the measured excess pore pressure to the dynamic PWP.

Chapter 5: Results and Interpretation

6. Discussion

6.1 Introduction

The main aim of this thesis was to study the role of the blasting for the 1996 Finneidfjord landslide. The area, since the catastrophic incidence, has been treated as a natural laboratory and different researchers have been working on different aspects to try and understand how the slide might have been triggered. Different field works and laboratory investigations have been carried out to characterize the event bed. All these investigation agree on the fact that a very distinct mechanically weak layer is the event bed and it is characterized as loose thin sand layer sandwiched between two impermeable clay layers. To narrow down the project and make it more specific, the effect of the vibration from the blasting on the sand layer is studied in this study. The sand layer is chosen based on the thinking that shear strain due to vibration propagation in sand, especially in a very loose sand can be potentially a problem at a shear strain level less than 10^{-2}%.

Loose sands have the tendency to contract when subjected to a cyclic loading and if the sand is fully saturated, there will be a generation of excess pore water pressure due to the fact that the sand grains will try to occupy the void. If the generated excess pore pressure is not dissipated in time the intergranular contact will be lost and the soil will not be able to take the normal and shear stress coming to it. In such condition where the effective stress becomes zero the soil is said to be liquefied.

Using the field investigation data and some empirical relations suggested by different intellects the liquefaction potential of the sand layer is analyzed. Utilizing a finite element method software QUAKE/W (2007) and an experimental vibration data the amount of excess pore pressure generated in the sand layer is calculated. Using the result from the dynamic analysis and a reading from a piezometer, a slope stability analysis using a limit equilibrium method software SLOPE/W (2007) was carried out.

In this chapter summary of results, important study findings and limitations are discussed.

6.2 Summary of Results and Important Findings

The results and important findings can be classified based on the analysis carried out; dynamic and slope stability analysis.

6.2.1 Summary of the Dynamic Analysis

Two categories of analysis were carried out using QUAKE/W; 1: to see the effect of damping, and 2: to see the effect of geometry.

- The analysis with the clay layer on top of the bed rock is done by fixing the damping ratio of the clay material based on the reported cyclic shear strain in 1999 and considering different damping ratios of the sand layer. Three different analyses with a damping ratios ranging from 1% to 33% are carried out. An average value of 4KPa from the 1%, 1.5KPa from the 7% and 0.4KPa from the 33% damping ratio is calculated. Though the difference may not be really big, for a naturally weak layer as the one under consideration, an excess pore pressure of such a value could be potentially an addition to triggering a land slide. Previous studies (L'Heureux, 2012) have mentioned that an additional stress of 4-8kPa could cause a failure.

- The analysis done without having the clay layer on top of the bed rock gave an excess pore pressure of around 6KPa. The effect of varying the damping ratio of the sand layer was checked but it didn't have much difference on the result. This shows the contribution of the clay material on top of the bed rock in taking some portion of the energy from the vibration and knowing the exact depth of this layer could lead to a more refined result. The other possible reason for getting this value is the fact that the bed rock is a more continuous material therefore it transmits the energy with a minimum damping.

- The two analyses done to see the effect of geometry i.e. distance between shoreline and end of the clay region didn't have much difference in the excess pore pressure calculated. The maximum difference measured from a GPS map was around 40m and this is quite small compared to the scale of the analysis.

- Relative density interpreted from the CPTu data, refer the appendix for the interpretation, indicates that the layer under study is a loose sand and based on the correlation between the tip resistance Vs. pre-failure effective stress, shown on figure 2-17 in the literature study indicates that it's a contractive sand which is susceptible to compaction under cyclic loading.

- It was possible to analyze the liquefaction potential of the sand layer from the empirical relation mentioned in the literature study and from the cyclic stress ratio output of QUAKE/W. The CSR obtained from both empirical and numerical analysis were almost the same, approximately 0.07 of CSR. As for the cyclic resistance ratio, CRR an empirical relation was used, refer the appendix for the calculation, and the relation available was developed for an earthquake 7.5 in magnitude. The scaling factor given in table 2.2 is only up to magnitude of 5.5. Though it can be presumed that the blasting under consideration is not as high as magnitude 5.5 earthquake, using it as a reference can tell if there is a risk of liquefaction. Applying a scaling factor of 2.86 for a PI<20%, a CRR of 0.143 is obtained, giving a factor of safety of 0.143/0.07=2.04. The scaling factor increases as the magnitude decreases therefore for a lesser magnitude, like the one in this study, the FOS against liquefaction will also increase. This shows that liquefaction was not the triggering mechanism for the 1996 Finneidfjord landslide.

- The results from the dynamic analysis are excess pore pressure right after the blast. The amount of reduction, if any, in the pressure after going through consolidation is not seen herein. The reduction might not be considerable since the layers above and below the sand layer are low permeable clay layers but still having a consolidation analysis could refine the result.

6.2.2 Summary of the Slope Stability Analysis

Based on the results from the dynamic analysis and the piezometric reading, five types of analysis were carried out.

- The piezometric reading around the slide scar showed an excess pore pressure of 8KPa. Using this value, the initial stability condition is analyzed and a factor of safety of 1.06 was obtained. This shows the fact that the slope was already on the verge of failure even before the vibration load come to the picture.

- Slope stability analysis based on the result of the dynamic analysis varying the damping ratio plus the piezometric reading was carried out. A safety factor of 0.829 from the 1%, 0.974 from the 7% and 1.039 from the 33% damping ratio analysis were obtained. This can be a testament for the fact that if the natural stability of a slope is on the verge of failure a small increase in the excess pore pressure could cause failure.

- One can guess without saying from the above discussions that the 6KPa from the analysis without the clay layer on top of the bed rock could easily cause a decrease in the effective stress and result in slope instability. This result shows the contribution of the soil layer on top of the bed rock and the fact that rock transfers the energy from the blasting with a minimum decrease since rock structure is quite continuous compared to clay.

- The calculated excess PWP lie in the range where previous studies showed that it could cause a failure. That is between 4 to 8kPa.

- Researches around the study area show that the mechanically weak layer is continuous around the region and has been an event bed for various landslides. Therefore it is wise to investigate the effect of different anthropological activities before proceeding with any project.

6.3 Limitations

- Running cyclic laboratory tests could have improved the reliability of the results obtained since cyclic number function and Pore-pressure Ratio (r_u) function are usually obtained from this test.

- Multiple blast points may be more effective in generating excess pore pressure and knowing the number of blasting carried out the day the slide took place and the time interval could improve the analysis result.

- The measured excess pore pressure is a onetime data i.e. the PWP condition in a different season is not considered. Knowing this could lead to a conclusion which bases the seasonal condition.

Chapter 6: Discussion

7. Conclusion, Recommendation and Future work

7.1 Conclusion

After the aftermath of the catastrophic occurrence at Finneidfjord in 1996, the area has been developed as a natural laboratory. Different investigations and researches have been carried out for the better understanding of the cause of the landslide and general stability of slopes with a mechanically weak layer. This study is part of this ongoing research with the aim of understanding the effect of anthropological activity at the time of the incidence. Based on some vibration datas taken for the purpose of investigation and some field and laboratory test results, a numerical analysis and some analytical studies were carried out and based on the results the following conclusions are given;

- Analyzing the liquefaction potential was one of the aims of the study and the result from the numerical and analytical analysis shows that liquefaction was not the cause for the landslide.

- As for the generated excess pore water pressure, results of the numerical analysis gave an excess pore water pressure ranging from 0.4KPa to 6KPa varying some parameters. Referring to the result from the slope stability analysis, the generated excess pore water pressure could potentially trigger a land slide. But it is not the conclusion of this study that the blasting prior to the landslide in 1996 at Finneidfjord caused the incidence, at least not until all the necessary improvements mentioned in the limitations and in the future work section are applied.

- A vibration with a pick particle velocity of 8mm/s could potentially have a role in void redistribution of a loose sand, as in the sand herein.

7.2 Recommendation

Dissipating excess pore pressure caused by an undrained cyclic loading could increase the shearing resistance of granular materials. The greater the dissipation of the excess pore water pressure the greater will be the increase in the strength (K.Yasuhara et.al. 2009). For layer incorporating low permeable materials, as the case under study, that impedes drainage, a water film and or void redistribution may cause complete loss of strength of the soil directly beneath that layer. Therefore installing a mechanism like vertical drains can mitigate the distractive effect of low permeable layer by dissipating the excess pore water pressure.

For blasting carried out near shore, it is wise; first to investigate if there are such weak layers as the one under study and measure the excess PWP in the weak layer and second to calculate the maximum excess pore water pressure generated from the blasting and with this check the stability of the ground before facing any inconveniences.

7.3 Future Work

- Running cyclic laboratory tests and improving some site specific parameters like pore-pressure function (r_u) function and cyclic number function could add to the understanding of the amount of excess pore pressure generated during the blasting.

- Carryout consolidation analysis to see how much time it would take for the excess pore pressure to dissipate.

- Researches done in different areas in Norway concerning near shore landslides share the same type of event bed as the study area. Which in turn imply that these types of weak layers should be investigated more and some remedial actions should be taken since they are prone to failure due any kind small triggering actions.

References

References

Alois Steiner, Jean-Sebastian L'Heureux, Achim Kopf, Maarten Vanneste, Oddvar Longva et al. (2012) An in-situ free-fall piezocone penetrometer for characterizing soft and sensitive clays at Finneidfjord, northern Norway. In: Yamada Y et al (eds) Submarine mass movement and their consequences, 31:99-109

Carmine P. Polito, Russell A. Green, Jongwon Lee (2008) Pore pressure generation models for sands and silty soils subjected to cyclic loading. Journal of Geotechnical and Geoenvironmental Engineering 134(10):1490-1500

Dynamic Modeling with QUAKE/W 2007 (2009) An engineering methodology fourth edition. Manual

E.C. Morgan, M. Vanneste, O. Longva, I. Lecomte, B. McAdoo, L. Baise (2010) Evaluating gas-generated pore pressure with seismic reflection data in a landslide-prone area: an example from Finneidfjord, Norway. In: Yamada Y et al (eds) Submarine mass movement and their consequences, 28:399-410

Gregersen O. (1999), Kvikkleireskredet i Finneidfjord 20 juni 1996. NGI Report

Groot M.B. et. al. (2006) Physics of liquefaction phenomena around marine structures. Waterway, port, coastal, and ocean engineering. 10.1061/(ASCE)0733-950x(2006) 132:4(227)

ICG report (2012)

Ikuo Towhata, Geotechnical earthquake engineering, Springer Series in Geomechanics and Geoengineering, 2008, Part 2, 180-216, DOI: 10.1007/978-3-540-35783-4_10.

Isao Isshibashi, Xinjian Zhang (1993), Unified dynamic shear moduli and damping ratios of sand and clay. Soils and Foundations 33(1):182-191

Janbu N., Raset i Finneidfjord-20. juni 1996. Unpublished export's report prepared for the county sheriff of Nordland. Report number 1, revision 1, 1996.

Jean-Sebastian L'Heureux et al. (2010) Ny kunnskap om skredmekanisme langs norske fjorder: Exampler fra Trondheimsfjorden og Finneidfjord. Geoteknikkdagen, pp 20.1-20.15

References

Jean-Sebastian L'Heureux, Oddvar Longva, Alois Steiner, Louise Hansen, Mark E. Vardy, Maarten Vanneste et al. (2011), Identification of weak layer and their role for the stability of slopes at Finneidfjord, Northern Norway. In: Yamada Y et al (eds) Submarine mass movement and their consequences, 31:321-330

K. Yasuhara, S. Murakami (2009) Effect of drainage on improving post-cyclic behavior of non-plastic silt. Proceeding of the 17th international conference of soil mechanics and geotechnical engineering, pp. 171-174

Kramer, S.L., 1996. Geotechnical Earthquake Engineering, Prentice Hall, New York.

Kyle M. Rollins, Mark D. Evans, Nathan B. Diehl, William D. Daily III (1998) Shear modulus and damping relationships for gravels. Journal of Geotechnical and Geoenvironmental Engineering 124(5):396-405

Longva O, Janbu N, Blikra LH, Bøe R (2003) The 1996 Finneidfjord slide; seafloor failure and slide dynamics. In: Locat J, Mienert J (eds), Submarine mass movement and their consequences, 531-538. Kluwer Academics Publishers.

M. B. de Groot, M. D. Bolton, P Meijers, A. C. Palmer, R. Sandven, A. Sawicki, et al. (2006) Physics of Liquefaction Phenomena around Marine Structures. Journal of Waterway Port Coastal and Ocean Engineering 132(4):227-243

Maarten Vanneste, Jean-Sebastian L'Heureux, Nicole Baeten, Jo Brendryen, Mark E. Vardy, Alois Steiner, et al. (2012) Shallow landslides and their dynamics in coastal and deep-water environments, Norway. In: Yamada Y et al (eds) Submarine mass movement and their consequences, 31:29-41

Mark E. Vardy, Jean-Sebastian L'Heureux, Oddvar Longva, Maarten Vanneste, Alois Steiner, Carl Fredrik Forsberg, et al. () Multidisciplinary investigation of a shallow near-shore landslide, Finneidfjord, Norway.

NGI report (1999)

Olsen L., Sveian H., Bergstrom B., 2001. Rapid adjustment of the Western part of the Scandinavian Ice Sheet during the Mid and Late Wiechselian: A new model. Norsk Geologisk Tidsskrift 81, 93-118.

P. K. Robertson, K.L. Cabal (2010) Guide to Cone Penetration Testing for Geotechnical Engineering. Fourth edition

References

P. K. Robertson, R.G. Campanella (1983) Interpretation of cone penetration tests. Canadian geotechnical journal 20(4):78 pp

R.A. Green, J.K. Mitcheell, C.P. Polito (2000) An energy-based pore pressure generation model for cohesionless soils. Proceedings of the John Booker memorial symposium, Sydney, New South Wales, Australia, November 16-17, 2000

Russel A. Green, James K. Mitchell (2004) Energy-Based Evaluation and Remediation of Liquefiable Soils. Geotechnical engineering for transportation projects, pp. 1961-1970

Scott A. Ashford et. al., (2004) Blast-Induced Liquefaction for Full-Scale Foundation Testing. In: Journal of Geotechnical and Geoenvironmental Engineering ASCE, pp. 798-806

Scott M. Olson, Timothy D. Stark (2003) Yield Strength Ratio and Liquefaction Analysis of Slops and Embankments. Journal of Geotechnical and Geoenvironmental Engineering 129(8):727-737

Stability Modeling with SLOPE/W 2007 (2008) An engineering methodology fourth edition. Manual

T.L.Youd, I.M.Idriss (2001) Liquefaction resistance of soils: summery report from the 1996 NCEER and 1998 NCEER/NSF workshops on evaluation of liquefaction resistance of soils. Journal of Geotechnical and Geoenvironmental Engineering 127(4):297-313

Takaji Kokusho (2003) Current state of research on flow failure considering void redistribution in liquefied deposits. Soil Dynamics and Earthquake Engineering 23 (2003): 585-603

Takeji Kokusho, Katsuhisa Fujita (2002) Site Investigations for Involvement of Water Films in Lateral Flow in Liquefied Ground. Journal of Geotechnical and Geoenvironmental Engineering 128(11):917-925

References

Appendices

Parameter calculation from CPTu data.

Relative density, Dr, Baldi et al. 1986

$$D_r = \frac{1}{C_2} ln \frac{Q_{cn}}{C_o}$$

$$Q_{cn} = \frac{q_c}{P_a} \Big/ \left(\frac{\sigma'_{vo}}{P_a}\right)^{0.5}$$

C_o=15.7

C_2=2.41

P_a=ref. Pressure 100Kpa

$$Q_{cn} = \frac{381.7KPa}{100KPa} \Big/ \left(\frac{21.36KPa}{100KPa}\right)^{0.5}$$

$$Q_{cn} = 8.26$$

$$D_r = \frac{1}{2.41} ln \frac{8.26}{15.7}$$

$$D_r = 22\%$$

Angle of friction, Robertson and Campanella, 1983

$$tan\varphi = \frac{1}{2.68}\left[log\left(\frac{q_c}{\sigma'_{vo}}\right) + 0.29\right]$$

$$tan\varphi = \frac{1}{2.68}\left[log\left(\frac{381.7KPa}{21.358KPa}\right) + 0.29\right]$$

$$tan\varphi = 0.575$$

$$\varphi = 30^o$$

Appendices

Calculation of $CRR_{7.5}$ from CPTu data

As mentioned in section 3.2.2

$$\mathrm{CRR}_{7.5} = 93\left[\frac{(\mathrm{Q_{tn,cs}})}{1000}\right]^3 + 0.08$$

If $50 \leq Q_{tn,cs} \leq 160$

$$\mathrm{CRR}_{7.5} = 0.833\left[\frac{(\mathrm{Q_{tn,cs}})}{1000}\right]^3 + 0.05$$

If $Q_{tn,cs} < 50$

$$(\mathbf{Q_{tn}})_{\mathbf{cs}} = \mathbf{K_c Q_{tn}}$$

$$Q_{tn} = \left(\frac{q_c - \sigma_{vo}}{\sigma'_{vo}}\right)$$

$$Q_{tn} = \left(\frac{381.7KPa - 52.1KPa}{27KPa}\right)$$

$$Q_{tn} = 12.21$$

$K_c = 1$ if $I_c \leq 1.64$

$K_c = 5.581I_c^3 - 0.403I_c^4 - 21.63I_c^2 + 33.75I_c - 17.88$ if $I_c > 1.64$

$$I_c = [(3.47 - logQ_{tn})^2 + (logF + 1.22)^2]^{0.5}$$

$$F = \frac{fs}{[(q_c - \sigma_{vo})]}\text{X100\%}$$

$$F = \frac{8KPa}{[(381.7KPa - 52.1KPa)]}\text{X100\%}$$

$$F = 2.43\%$$

$$I_c = [(3.47 - log12.21)^2 + (log2.43 + 1.22)^2]^{0.5}$$

$$I_c = 2.873$$

For if $I_c > 1.64$, K_c will be

$K_c = 5.581(2.87)^3 - 0.403(2.87)^4 - 21.63(2.87)^2 + 33.75(2.87) - 17.88$

$K_c = 5.45$

$$(\mathbf{Q_{tn}})_{\mathbf{cs}} = 5.45 * 12.21 = 66.54$$

for $50 \leq Q_{tn,cs} \leq 160$

$$\mathbf{CRR_{7.5}} = \mathbf{0.833}\left[\frac{(\mathbf{Q_{tn,cs}})}{\mathbf{1000}}\right]^{\mathbf{3}} + \mathbf{0.05}$$

$$\mathbf{CRR_{7.5}} = \mathbf{0.833}\left[\frac{(66.54)}{\mathbf{1000}}\right]^{\mathbf{3}} + \mathbf{0.05}$$

$$\mathbf{CRR_{7.5}} = 0.05$$

Since the calculated cyclic resistance ratio is for an earth quake of magnitude of 7.5 richter scale, it should be multiplied by a factor given in table 2.2 in chapter 2. But still the available data is only for magnitude of 7.5 to 5.5 and the blasting we do not have this high magnitude. Assuming the boundary value on the list, i.e 5.5, a scaling factor of 2.86 for a PI<20% is taken and the corresponding CRR will be;

$$\mathrm{CRR} = CRR_{7.5} * \mathrm{Cm}$$

$$\mathrm{CRR} = 0.05 * 2.86 = 0.143$$

Appendices

MATLAB Code used to change the measured vibration data file, *.sgy to *.txt file and plot curves.

```
% Example script that plots and calibrate from different channels from

% one seyfile

clear

clc

% The file to be processed :

filePath = 'D:\*\';

calPath = 'D:\*\';

segyFile = [filePath '*.sgy'];

outFile = ['*.txt'];

% Import the data :

[Data,SegyTraceHeaders,SegyHeader]=ReadSegy(segyFile,'revision','1','endian','b');

% The calibration factors :

calFact = load([calPath 'CAL1.DAT']);

calInt = 4096;      % Conversion from binary data to real

% Info about the measurement setup from report

% 1-3 : velocity hus1 / pos1 z,x, and y direction

% 4-6 : velocity hus2 / pos2 z,x, and y  direction

% 7 : velocity hus2 / pos2 z direction

% 22-23 vertical velocity on rock

% Calibrate data

Trigger = real(Data(:,1))*calFact(1)/calInt;

pos1x = real(Data(:,2))*calFact(2)/calInt;
```

```
pos1y = real(Data(:,3))*calFact(3)/calInt;

pos1z = real(Data(:,4))*calFact(4)/calInt;

pos2x = real(Data(:,5))*calFact(5)/calInt;

pos2y = real(Data(:,6))*calFact(6)/calInt;

pos2z = real(Data(:,7))*calFact(7)/calInt;

rock1 = real(Data(:,22))*calFact(22)/calInt;

rock2 = real(Data(:,23))*calFact(23)/calInt;

% Save calibrated ascii files

outData = [SegyHeader.time', Trigger, pos1x, pos1y, pos1z, pos2x, ...

pos2y, pos2z, rock1, rock2];

save(outFile,'outData','-ascii');

% Trigger

figure

hold on

grid on

set(gca,'fontsize',16,'gridlinestyle','-')

plot(SegyHeader.time, Trigger,'b')

xlabel('Time [s]','fontsize',16);

ylabel('Trigger velocity [mm/s]','fontsize',16);

% plot the first location

figure

hold on

grid on

set(gca,'fontsize',16,'gridlinestyle','-')
```

```
plot(SegyHeader.time, pos1x,'r')
plot(SegyHeader.time, pos1y,'g')
plot(SegyHeader.time, pos1z,'b')
xlabel('Time [s]','fontsize',16);
ylabel('Velocity [mm/s]','fontsize',16);
legend('x-dir','y-dir','z-dir');
% Second location
figure
hold on
grid on
set(gca,'fontsize',16,'gridlinestyle','-')
plot(SegyHeader.time, pos2x,'r')
plot(SegyHeader.time, pos2y,'g')
plot(SegyHeader.time, pos2z,'b')
xlabel('Time [s]','fontsize',16);
ylabel('Velocity [mm/s]','fontsize',16);
legend('x-dir','y-dir','z-dir');
% On rock
figure
hold on
grid on
set(gca,'fontsize',16,'gridlinestyle','-')
plot(SegyHeader.time, rock1,'b')
plot(SegyHeader.time, rock1,'r')
```

Appendices

```
xlabel('Time [s]','fontsize',16);

ylabel('Velocity [mm/s]','fontsize',16);

legend('z-dir, A','z-dir, B');
```

Peak particle velocity Vs time data (NGI, 1999)

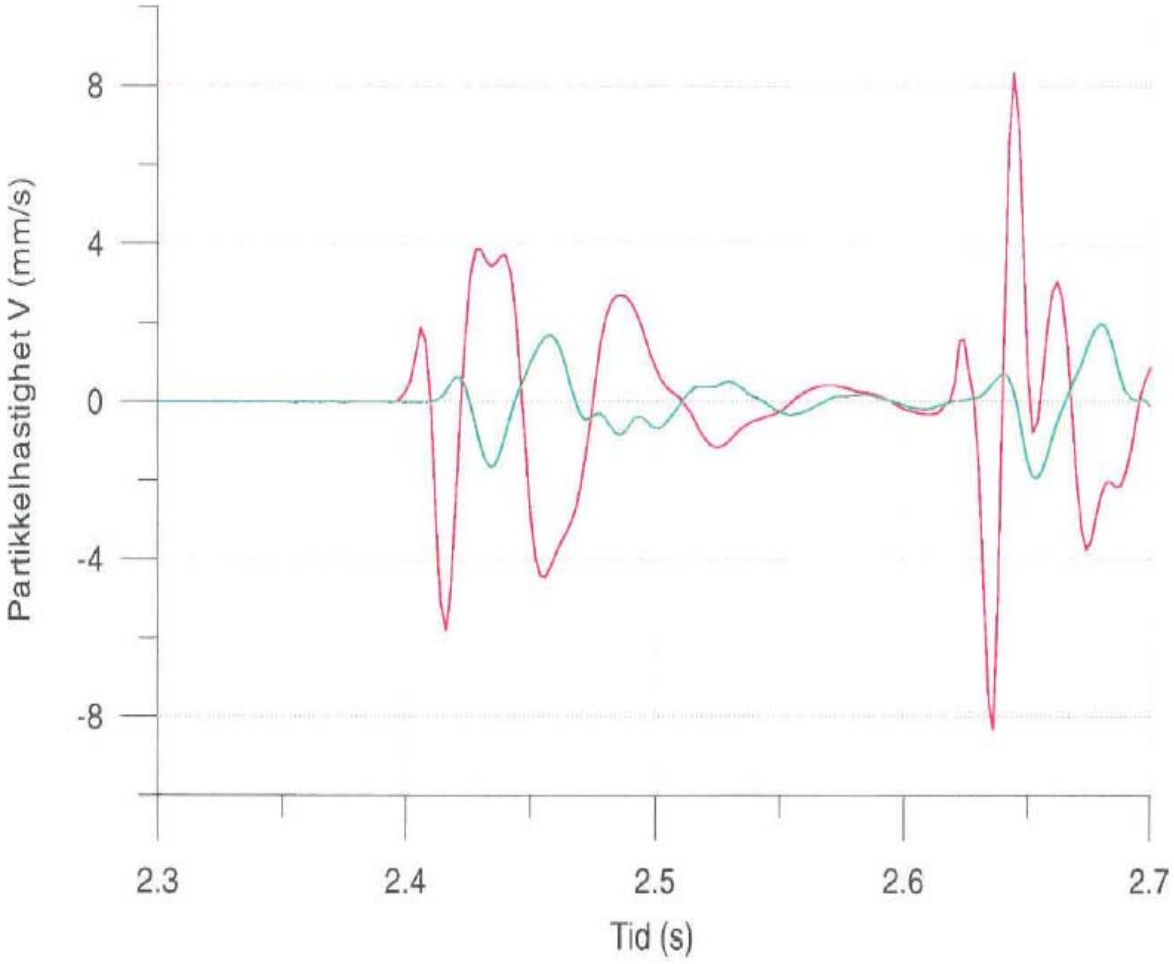

Appendices

Shear wave velocity from the different blasting (NGI, 1999)